FABRICATION OF SiC/MAGNESIUM ALLOY COMPOSITE VIA FRICTION STIR PROCESSING

by

Ahmad Z. Naser

A Thesis Presented to the Faculty of the
American University of Sharjah
College of Engineering
in Partial Fulfillment
of the Requirements
for the Degree of

Master of Science in
Mechanical Engineering

Sharjah, United Arab Emirates

January 2016

Approval Signatures

We, the undersigned, approve the Master's Thesis of Ahmad Z. Naser.

Thesis Title: Fabrication of SiC/Magnesium Alloy Composite via Friction Stir Processing.

Signature	**Date of Signature** (dd/mm/yyyy)
_____	_____
Dr. Basil Darras Associate Professor, Department of Mechanical Engineering Thesis Advisor	
_____	_____
Dr. Lotfi Romdhane Professor, Department of Mechanical Engineering Thesis Committee Member	
_____	_____
Dr. Farid Abed Associate Professor, Department of Civil Engineering Thesis Committee Member	
_____	_____
Dr. Mamoun Abdel-Hafez Head, Department of Mechanical Engineering	
_____	_____
Dr. Mohamed El-Tarhuni Associate Dean, College of Engineering	
_____	_____
Dr. Leland Blank Dean, College of Engineering	
_____	_____
Dr. Khaled Assaleh Interim Vice Provost for Research and Graduate Studies	

Acknowledgements

In the name of *Allah* the most beneficent, the most merciful.

Firstly, I am most grateful to *Allah the Almighty* for giving me the power, will, and determination to carry on and finish this scientific research. I also would like to express my sincere gratitude to my advisor Dr. Basil Darras for his continuous support of my Master study and related research, for his patience, motivation, and wide knowledge. His guidance helped me throughout all the time of research and writing of my thesis. Besides my advisor, I would like to express my thanks to Dr. Hana Sulieman for her help and support in the modeling part. Moreover, I would like to thank the rest of my thesis committee: Dr. Lotfi Romdhane and Dr. Farid Abed, for their insightful comments that motivated me to widen my research from various perspectives. Furthermore, I would like to express my warm thanks to Dr. Fathia Saleh and Eng. Salman Pervaiz, who provided me with technical support, aided me in using lab equipment, and gave me access to the laboratory and research facilities. Without their valuable support it would not be possible to progress in this research. I am also grateful to Mr. Ricardo De Jesus and Mr. Ronald Almirez for their precious help throughout the experimental work. My sincere thanks also goes to the Department of Mechanical Engineering at the American University of Sharjah for supplying machines and equipment used to accomplish this research. Last but not least, I would like to use this opportunity to express my gratitude to my friends and my family: my parents and to my brothers and sister for supporting me during the writing of this thesis and throughout my life.

Dedication

To my beloved Mother, who brought me life and joy, for her prayers to me.
To my Father, the first to teach me.
Without them none of my success would be possible.

Abstract

One of the most interesting improvements in the history of materials is composites manufacturing. Because of their ability to improve different mechanical properties of some metals, nanoparticles have been given much attention in the composites community. After the successful use and popularity of Friction Stir Welding (FSW) in many applications worldwide, its latest modification into Friction Stir Processing (FSP) has recently been given a considerable amount of attention. FSP can be considered today as one of the most successful alternatives for fabricating metal matrix composite. In this investigation, a Silicon Carbide (SiC)/magnesium alloy composite was fabricated using FSP. Different combinations of tool rotational and translational speeds (RS and TS) were used throughout the study. The effect of such combination on the thermal profile, micro-hardness, and microstructure was studied and compared. Furthermore, a Response-Surface Methodology was used to develop a model to predict the micro-hardness for FSPed specimens using different combinations of process parameters. FSP of Mg AZ 31B as well as Mg/SiC composite was successfully accomplished using different combinations of tool rotational and translational speeds. Micro-hardness results showed excellent agreement with both the thermal and microstructural analysis. Micro-hardness results of the Mg/SiC composite showed a significant amount of improvement. The developed micro-hardness model was very accurate in predicting the micro-hardness values.

Table of Contents

List of Figures

List of Tables

Chapter 1: Introduction

1.1 Problem Statement

Finding a material with particular properties is considered an important concern in many manufacturing and industrial applications, precisely in the automobile and aerospace industries. Hence, there is always a need for designing specific materials with desired properties. There are many processing techniques that can help in producing a material with relatively small grain size that guarantees ductility and strength. Furthermore, one of the challenging problems in the aerospace and automobile industries is the formability of light alloys at room temperature. Hence, new processing methods such as FSP are being studied and under development to achieve this goal and to overcome these challenges. FSP is a material fabrication method that uses a high amount of energy to locally manipulate the microstructure of materials in the solid state. During FSP, a tool with a special design is usually plunged into the work piece resulting in an extreme plastic deformation through stirring action. This action will result in a defect free, fine grain, and dynamically recrystallized microstructure. One of the challenges that prevents the widespread use of light weight alloys in aerospace industries is the difficulty of producing ultrafine grain sheet metals. Most of the conventional grain refinement methods include thermo-mechanical processing. However, this type of processing is time consuming, costly, and not environmentally friendly due to the excess use of energy. As a result, alternative processes for obtaining ultrafine grain is required in the industry. Lately, a new process which was implemented using the mechanism of FSW has been developed. FSP can be positively used to obtain homogenized structure and ultrafine grain.

1.2 Significance of FSP

According to Zweben, the construction of complex and huge structures is well adapted in many manufacturing processes for composites. This can guarantee merging of different parts which can save manufacturing costs from the economical point of view. Composites are multifunctional materials with unique mechanical and physical properties. These properties can be subjected to different changes in order to satisfy the requirements of a single application. Hence, the unique properties of composites can offer various design opportunities which are not available with conventional un-

reinforced materials. Particle-reinforced metal matrix composites (MMCs) which can be made using molten metal processing or the powder metallurgy (P/M) route have many advantages. Some of these advantages include higher strength and modulus. During P/M processing, both the kind of reinforcement in addition to the matrix's composition can be subjected to variation within little limitations. In the P/M route, a homogenous mixture between the matrix alloy and the reinforcement particles is achieved as a result of blending both together. FSP which is considered today as the recent modification of FSW, proved to be an effective technique for guarantying a fine grain size of around 0.5 to 5 μm and an extra-fine grain size of about 30 to 180 nm. These results were reported for both Friction Stir Processed (FSPed) aluminum and magnesium alloys inside the dynamically recrystallized zone [1-11].

FSP is widely used today in many manufactured parts such as critical and diesel engine components, due to its ability in guarantying better mechanical properties. Due to its ease and effectiveness in fabricating different materials, today FSP is considered as a quite attractive process for adoption. FSP has been widely used in the modification of microstructure for various aerospace aluminum alloys. The aim of such modification is to achieve high fatigue, strength, and fracture resistant aluminum materials. According to Sun, N. et al. metal matrix composites processed using FSP have three main advantages in comparison to other processing techniques. First, FSP strengthens the material by a local fabrication of the composite layer. Second, it can be implemented to repair localized defects. Third, the porosity caused by the evolution of gases in addition to other unwanted reactions inside the matrix are mitigated [12-13].

1.3 Objectives

The purpose of this work was to use FSP in order to fabricate a Mg/SiC composite. The main aim of this fabrication was to be able to achieve better micro-hardness, homogenous microstructure, and fine grain size. This was accomplished by studying the effects of input parameters on such properties. The input parameters include tool rotational and translational speeds. Moreover, other samples were processed using friction stir without any addition of silicon carbide and the results were compared. All the results were then compared with the properties of the base material. This was important in order to understand the effectiveness and enhancements the SiC has/ has not on the micro-hardness.

The objectives of this investigation were achieved according to the following tasks:

1- Perform FSP of Magnesium AZ 31 samples using various tool rotational and translational speeds. The processing was accomplished without any addition of SiC. The thermal profile of these samples was recorded throughout the process.
2- Carry out FSP of Magnesium AZ 31 samples in order to fabricate silicon carbide/magnesium composite. The thermal profile of these samples was recorded throughout the process.
3- Perform micro-hardness tests for the first and second tasks and compare the results.
4- Investigate the microstructure of the friction stir processed samples by taking microscopic images.
5- Use Response Surface Methodology to develop a quadratic model for the micro-hardness of FSPed specimens with different process parameters.

1.4 Research Methodology

The first step in any successful project is a good literature review. Hence, a detailed literature review was done and previous works examining the same topic were studied. The main aim of this project was to come up with a quantitative method that can compare the two cases of FSP. The first case was FSP without the addition of any powder particles, while the second case was processing with the use of specific powder particles. In both cases, the magnesium AZ 31B alloy was used as the raw material. However, in the second case, silicon carbide particles that have a size of 250 µm were used as a reinforcement in order to come up with the Mg/SiC composite. In order for such a quantitative study to be accomplished, practical experiments were designed and carried out using various tool rotational and translational speeds. Moreover, in both cases, the thermal profiles were recorded throughout the process. Next, the micro-hardness values and the microstructure of the different trials were obtained. Response-Surface Methodology (RSM) was used to obtain a quadratic model for the micro-hardness for FSPed workpieces under different working parameters. Then, optimization for the response was conducted. The methodology was accomplished using some software such as: MATLAB,

Microsoft Excel, PowerSight manager, PicoLog Recorder, and IRSee. A summary of this work methodology is shown in Figure 1.1.

1.5 Thesis Outline

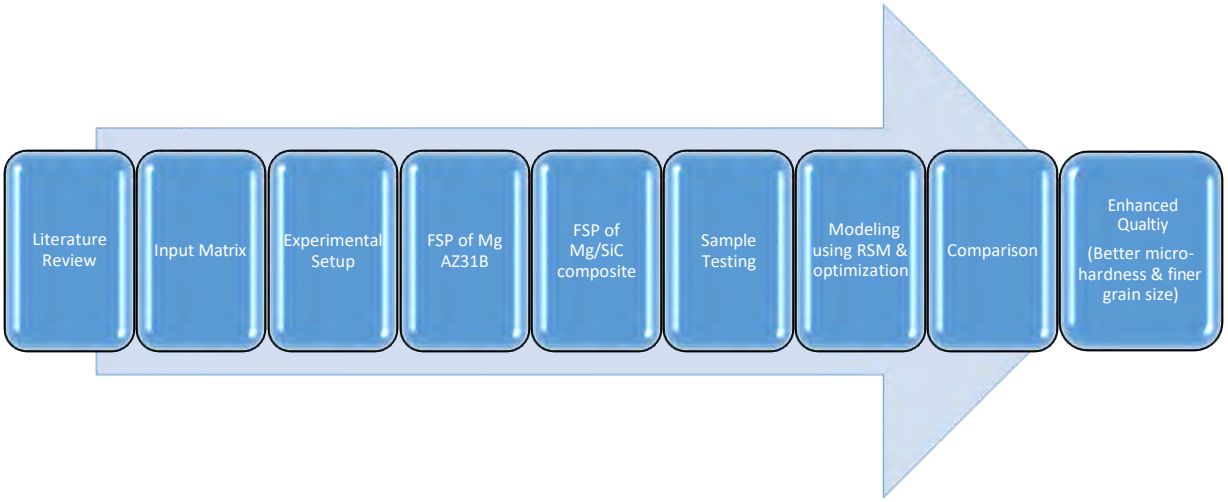

Figure 1.1: Summary of the methodology to be followed

The framework of the thesis is as shown below:

- Chapter 1: Contains the thesis introduction which includes the problem statement, significance of FSP, objectives, and a summary of the methodology.
- Chapter 2: Includes a background about FSW, FSP and a review of the literature.
- Chapter 3: Covers material selection, experimental setup, process parameters as well as results of FSP, FSP of Mg/SiC composite, and defective specimens.
- Chapter 4: Contains the thermal analysis, discussion of the effects of both rotational and translational speeds on temperature profile, microstructural and grain size analysis. It also contains the micro-hardness results.
- Chapter 5: Illustrates the use of Response Surface Methodology to come up with a quadratic model to predict the hardness of FSP. A check of the adequacy in addition to a verification of the developed model is introduced. Furthermore, an optimization of the micro-hardness is also included. Contour and 3D response plots are also provided and discussed.
- Chapter 6: Includes conclusions of the findings and suggestions for future work.

Chapter 2: Background

Today, FSP is considered an advanced tool which can produce surface composites by using second phase particles as a reinforcement. During FSP such phase particles will be broken into almost fine and equiaxed particles. Usually these particles are uniformly distributed inside the matrix. Moreover, grain refinement is obtained as a result of the dynamic recrystallization caused by FSP throughout the process. Friction stir processing was established based on the principle of friction stir welding (FSW); hence, a detailed analysis of the mechanism of FSW is needed in order to know how FSP works.

Friction stir welding, which was initially invented in the United Kingdom in 1991 by the Welding Institute, can be described as a simple solid-state welding process. In this process, a non-consumable rotating tool with a special pin and shoulder is used as illustrated in Figure 2.1. The tool is inserted into the abutting edges of two or more materials resulting in good joints as the tool continues to apply force and pass through the joint line. The rotating tool helps in heating the specimen, moving the material to make the joint, and in containing the high temperature metal under the shoulder of the tool. The friction between the shoulder and the pin of the rotating tool in addition to the plastic deformation that the specimen experiences throughout the process are the main reasons behind the production of heat within the specimen. The produced heat, in addition to the rotation and translation movement of the tool, help in softening the portion of the material around the pin and in moving the material to the back of the pin. Meantime, the shoulder of the tool helps in restricting the flow of metal to a specific level that is equivalent to the shoulder position [5, 14-16]. As a result of the different geometrical structures on the tool, the material around the tool pin can experience a complex movement with various changes in temperature, strain, and strain rate [17]. Hence, the resulting microstructure of the nugget zone is not homogenous. The microstructure can clearly reveal these differences in thermo-mechanical properties. Regardless of this inhomogeneity in the local microstructural level, one of the most important advantages of friction stir welding is the fine grain, fully recrystallized microstructure produced in the nugget as a result of extreme plastic deformation at high temperature. The fine grain microstructure helps in producing superb fatigue and mechanical properties [18-22]. FSP follows the same mechanism as FSW except the

tool will be positioned to make one pass along one complete piece of material, hence, no welding is applied.

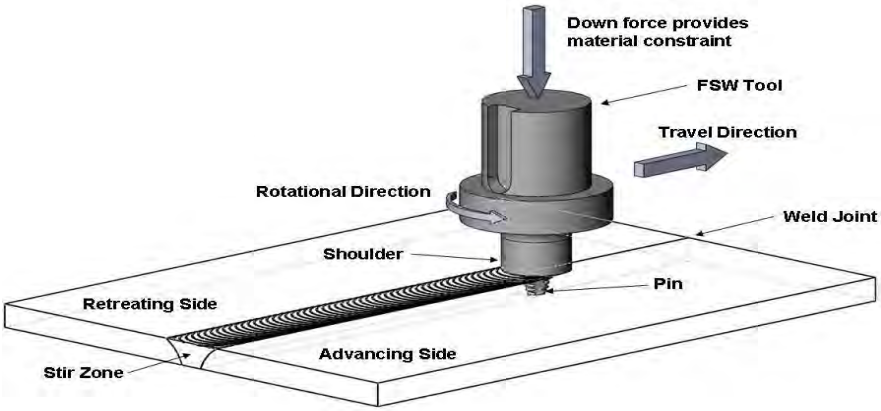

Figure 2.1: FSW mechanism [23]

Moreover, FSW improves formability and can guarantee excellent super plasticity. As per any new technologies, a new nomenclature should be used in order to be able to describe observations in a precision way. In friction stir welding, new scientific terms are required to describe the resultant weld microstructure in an accurate way. Threadgill made the first attempt in successfully classifying the microstructure of any Friction Stir (FS) welded work piece according to a specific system. The system divides the weld zone into four different regions: the un-affected material or parent metal, heat-affected zone, thermo-mechanically affected zone (TMAZ), and the weld nugget. Each of the four zones is shown in Figure 2.2. The unaffected material illustrated by the symbol A, is the portion of the material that is far from the weld and has not experienced any deformation. Although the material at this region can experience a thermal cycle from the weld, the heat inside this zone has no significant effect on the material in terms of its mechanical properties or microstructure. The portion of the material which lay on the heat affected zone, which is illustrated by the symbol B, is closer to the center of the weld. In this zone, the material experiences a modification in the microstructure and mechanical properties due to the thermal cycle. The material included inside this zone experiences no plastic deformation. In the TMAZ zone which is shown by the symbol C, the heat resulting from the welding process will have an effect on the material. Furthermore, in this zone the material will be subjected to plastic deformation caused by the FSW rotating tool. Significant plastic strain can be obtained inside this zone without recrystallization in the case of FSW of aluminum alloys. A discrete boundary separating the plasticity deformed zones of the TMAZ from the fully recrystallized zone (weld nugget) usually existed. Finally, the completely

recrystallized zone is called the weld nugget or stir zone (identified by the symbol D) which refers to the area which was occupied by the tool pin [24].

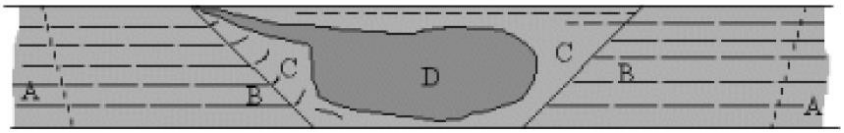

Figure 2.2: A transverse section of a FS welded material [24]

FSW is classified today as one of the most important improvements in the metal joining industry. Furthermore, it is considered to be an environmental friendly technology due to the non-existence of harmful emissions and shielding gases during the process. FSW is classified as an energy efficient welding technique since it uses less energy and non-consumable flux in comparison with all other traditional welding processes. FSW uses only 2.5 percent of the energy needed in any laser welding [16]. Since there is no melting in this welding technique due to the absence of filler metal, many alloys can be welded together without worrying about composition compatibility or solidification cracking highly linked with fusion welding. In addition, different alloys and composites can be welded with the same ease [25–27]. In contrast to traditional frictional welding, a technique which can be used to weld only a small axisymmetric parts [28], friction stir welding is applicable with a variety of geometric structural shapes and sorts of joints. Both the butt and lap joints are the most two convenient types of joints for friction stir welding. In the butt joint, two metal plates having the same thickness are positioned on a backing plate and then fixed tightly. The existence of the backing plate is crucial in order to prevent the normal forces associated with friction stir welding and the two plates. Throughout the process, the lateral forces can experience a significant increase; hence, additional attention is needed to make sure that the two plates inside the butt configuration are still fixed without separation. The FSW rotating tool is then subjected to the joint line and then guided to pass along this line. Meanwhile, the shoulder of the rotating tool is maintained in close contact with respect to the surface of the two plates. Both the penetration depth and the position of the tool can be controlled using the control of the applied normal force or the position control [29].

Stanfield [30] discussed how FSW can produce free of defects and high-strength bonds by using frictional heating combined with forging pressure. The FSW is a process that transforms metal’s state from solid into plastic-like while a rotating pin tool is used

to soften and forge the bond. Jon Street, the welding and manufacturing lead in the Material and Processes Laboratory at the Marshall Center said: “State-of-the-art friction stir welding will continue to be a critical technology as we continue to learn how to build more efficient space vehicles with less expensive materials.” The FSW process was used for the first time by Marshall Engineers who utilized it on the external tanks of the orange space shuttle since it reduced the manufacturing cost, increased the reliability, and lowered the number of defects. FSW is considered today as a common technique in the manufacturing of external tanks of the heavy lift launch vehicle manufactured by the National Aeronautics and Space Administration (NASA), taking into the account some aspects including cost and reliability. In addition, the Boeing Company is currently developing a space launch system core that will store liquids including cryogenic liquid hydrogen and liquid oxygen to feed the RS-25 engines. FSW has much potential for many advantages such as higher strength metals and higher efficiency. Furthermore, FSW is considered safer and more environmentally friendly than any traditional welding technique.

In his article [31], Hancock discussed the use of aluminum friction welding which uses the pressure and the connection between the material and the spinning pin to make friction energy that heats the material. After the material cools, the result will be a welded part similar to the original material. This is because the tool of the friction stir makes it easy for both materials to construct bonds at the molecular level by driving both edges toward each other. The article pointed out that this welding technique was used by MAZDA Motor Corporation to construct the bonnet and doors of the RX-8 sports car as shown in Figure 2.3. The car manufacturer confirms that the welding technique saves money and energy and is the preferable technique for welding aluminum. The new spot joining technique depends on a welding gun to fix the parts with the help of extra welding tools. Heat is generated as a result of the applied forces throughout the spinning of the tool. Mazda manufacturers were able to reduce the energy consumption in aluminum welding to 99 per cent while in steel welding to 80 per cent, cut the equipment investment by 40 percent, and maintain a clean welding environment.

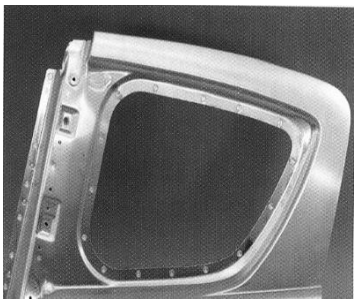

Figure 2.3: MAZDA RX-8 rear doors [31]

Lakshminarayanan et al. [32] talked about the effect of several welding processes such as FS, Gas Tungsten Arc Welding (GTAW), and Gas Metal Arc Welding (GMAW) techniques on the AA6061 aluminum mechanical properties. FSW is a solid phase welding process used for welding metals and alloys that cannot be welded by traditional welding techniques. The effect of these three welding processes on the mechanical properties was understood after conducting different welding experiments using each technique. Tensile properties such as tensile strength, yield strength, and percentage of elongation were obtained and evaluated. In addition, the microstructure was tested at different locations for each aluminum alloy joint. The results showed that the aluminum welds resulting from FSW had the best mechanical properties compared to the other two techniques as suggested by Table 2-1.

Table 2-1: Tensile properties of welded joints [32]

Joint Type	Yield strength (MPa)	Ultimate tensile strength (MPa)	Elongation (%)	Weld region hardness (VHN)
GMAW	141	163	8.4	58
GTAW	188	211	11.8	70
FSW	224	248	14.2	85

Liua et al. [33] defined FSW as a new process which can weld heat-treatable aluminum alloys and produce high quality and low cost aluminum joints. This is because this process uses no consumable filler material and can eliminate cracks and porosity. Furthermore, the tensile properties and welding parameters relationships were studied to determine the optimum welding parameters. The evaluation of the experimental results showed that the joints fracture locations and tensile test were

affected by the FSW parameters such as welding speed, rotation speed, and revolutionary pitch.

Taban and Kaluc [34] studied the mechanical properties and the microstructure of various welding processes including Metal Inert Gas (MIG), Tungsten Inert Gas (TIG) and FS. The raw material used was 5086-H32 aluminum alloy. After conducting the experiments, the welded joints were evaluated by performing micro-structural tests utilizing a light optical microscope which tested the fracture and hardness of the welded joints. The results showed that FSW welded joints had superior mechanical properties when compared to other welding techniques such as MIG and TIG.

Wang et al. [35] used FSP to produce aluminum metal matrix composite using silicon carbide powder. In their experiments, they used plates which were made of 5A06Al as the raw material to be investigated. To be able to use the powder, a groove with a 1 mm depth and 0.5 mm width was produced. Then, the groove was filled with the powder before initiating the process. The FSP was carried out using a rotational speed of 1180 rpm and a translational speed of 95 mm/min. The SiC powder successfully covered all the distance along 1.5mm far from the pin's edge and the distribution of the metal matrix composite at 2mm depth was approximately 2.5 mm. The results of the experiment insured an increase of about 10% in the micro-hardness value of the metal matrix composite reinforced with SiC compared to the micro-hardness of the raw material which was about 88 HV.

Lim et al. [36] used multi-walled carbon nanotubes to produce a reinforced aluminum alloy composite using FSP. A groove with 0.3 mm × 2.3 mm was made to be able to insert the multi-walled nanotubes. After this, the groove was covered with a sheet made from Al 6111–T4 alloy with a thickness of 1.1 mm. Al 7075–T6 alloy was the chosen material for the lower plate with a thickness of about 6.35 mm. The integrated nanotubes had a length of 10 to 20 micrometers and an outer diameter of 30 to 50 nanometers. The tool used in the FS process had a pin diameter of 4 mm and a length of 2.2 mm. During the process, a translational speed of 2.5 mm/s along with different rotational speeds ranging between 1500 to 2500 rpm were used. It was shown that when the rotational speed was 1500 rpm and the shoulder penetration depth was raised to about 0.24 mm, there were no resulting voids in the stir zone. Results from a transmission electron microscope alongside a scanning electron microscope both

confirmed that the nanotubes were fixed inside the region of the aluminum alloy stir zone. Moreover, results confirmed that the structure of the nanotubes was retained. However, some results provided proof that some nanotubes were cracked throughout the process of friction stir. Results suggested that increasing both the rotational speed and the shoulder penetration depth of the tool will guarantee a better distribution of the carbon nanotubes inside the aluminum alloy matrix. At the end, using multiple passes was proposed as one way in order to improve the distribution of the carbon nanotubes inside the metal composite matrix.

Ke et al. [37] presented a work that was based on using friction stir processing to produce an Al–Ni intermetallic composite. They used aluminum as the raw material and nickel powder to reinforce the composite. In order to add the powder, two holes in a row were created with a 2.5 mm diameter and a 3 mm depth each. The FSP was done using a tool that had an 8.5 mm screw thread probe. A rotational speed of 1500 rpm with a tilt angle of about 3° for the tool and a translational speed of 23.5 mm/min were used. In order to improve the interaction between the aluminum and the nickel powder, three friction stir passes were carried out, and heat treatment at a temperature of 550°C for six hours was applied. The results obtained showed high bonding between the particles and the composite matrix, and the final result was an Al–Ni intermetallic composite that was free of defects with AL_3Ni and Al_3Ni_2 noticed in the FS processed zone. The three passes of FSP positively affected the refinement of the grain and the hardening of the Al_3Ni_2 particles. Thus, this guaranteed a good increase in the micro-hardness of the Al- Al_3Ni composites.

Dixit et al. [38] analyzed the mechanical properties of friction stir processed Al 1100–NiTi composite. NiTi powder which contained a particle size ranging between 2 to 193 μm were filled into 1.6 mm diameter 76 mm length, and 0.9 mm depth holes. After that, the specimens were friction stir processed using an tool rotational speed of 1000 rpm and a translational speed of 25 mm/min. Three samples were prepared. The first one was only applied to FSP. The other samples were exposed to cold rolling and then to heating and annealing at a temperature of 85°C for a time period of 15 minutes. The results of this analysis showed that friction stir processing can be successfully implemented to make composites. The microscopic results showed that the powder particles were distributed in a uniform manner and had a good bond with the matrix. The modeled and the experimental data proved that there was an improvement in the

mechanical properties for the resulting FSPed composite. Furthermore, the results showed a significant increase in terms of the micro-hardness values.

Analysis for silicon carbide reinforced AZ91composite was carried out by Asadi et al. [39]. Silicon carbide powder with a particle size of 5 μm in diameter was added to the surface layer of the 5 mm thickness prepared composite. A FSP tool having a length of 2.5 mm, and 5 mm diameter was used. Different rotational speeds ranged from 710 to 1400 rpm with translational speeds ranging from 12.5 to 80 mm/min were tested. The tool tilt angle varied from 2.5° to 4°. Using the scanning and optical electron microscopes, both the microstructure and the distribution of the silicon carbide particles were studied. A micro-hardness test was carried out starting from 1 mm away from the upper edge of different cross sections of the processed specimens. All the tested cross sections were subjected to a load of 200 g for approximately 15 seconds. The result of the analysis showed that a decrease in the grain size can be achieved by increasing the translational speed and at the same time decreasing the rotational speed. The size of the grains was significantly dropped from 150 to 7.17 μm while the hardness value increased from 63 to 96 HV in the stir zone.

Mahmoud et al. [40] analyzed the mechanical properties of Al-1050-H24 plates. The 5 mm thickness plates were reinforced using different ratios of SiC and Al_2O_3 powders. The results of the experimental data showed that the powder particles were uniformly distributed along the FSPed stir zone. The distribution was free of any significant defects. Moreover, the average micro-hardness values of the tested composite were recorded. The micro-hardness values increased to approximately 60 HV using a 100% SiC powder. However, the micro-hardness values deceased whenever the relative ratio of the Al_2O_3 powder particles increased. At the end, it was proven that the addition of SiC and Al_2O_3 powders helped in a significant way to improve the mechanical characteristics of the Al matrix and at the same time decrease the wear volume loss.

Alidokht et al. [41] investigated the microstructure of aluminum alloy A356 plates reinforced by a 99.5% pure silicon carbide powder which contained particles of a size of 30-μm and a 99% pure MoS_2 powder with a particle size of about 5-μm. Friction stir processing was carried out using a fixed rotational speed of about 1600 rpm and a translational speed of 50 mm/min. A groove with a width of 0.6 mm and a depth of 3.5 mm was manufactured, and the two powders were inserted. The results

from the hardness tests proved that the FSPed specimens which were reinforced using the two types of powder recorded higher micro-hardness values compared to as-received specimens.

Morisada et al. [42] used multi-walled carbon nanotubes with a length of 250 nm and a diameter of 50 nm as a reinforcement to the 6 mm thickness plates made from AZ31. A groove with a width of 1 mm and a depth of 2 mm was made in order to be filled with the multi-walled carbon nanotubes. After that, FSP was carried out using a tool with a length of 1.8 mm and a probe diameter of 4 mm. The FSPed surface composite was studied using an optical microscope. The results showed that the distribution of the multi-walled carbon nanotubes was dependent on the translational speed of the tool. The best distribution of the nanotubes was recorded for the case of 1500 rpm and 25 mm/min translational speed. Moreover, the addition of the nanotubes helped in improving the micro-hardness values of the resulting composite. The highest micro-hardness value for a FSPed sample without the carbon nanotubes reinforcement was about 55 HV. However, this value increased to about 78 HV after the addition of nanotubes. Furthermore, the results showed some grain refinement. Grains with a size less than 500 nm could be obtained easily.

Both the mechanical characteristics in addition to the microstructures of Al 6082 7 mm thickness plates reinforced by small size Al_2O_3 powder particles that had a 50 nm average diameter were studied by Zarghani et al. [43]. A tool consisting of a steel pin of 5 mm diameter with a length of 4 mm was used to accomplish the FSP. In their experimental investigation, they used a tool rotational speed of 1000 rpm and a translational speed of 135 mm/min. A groove that had a width of 1 mm and a depth of 4 mm was made and the Al_2O_3 powder was inserted. A different number of passes were applied to different samples. The number of passes varied from one to four and different passes with and without the powder were also applied. The different samples were subjected to ambient air cooling whenever one pass was finished. Comparing the composite layer's surfaces, the Al_2O_3 powder particles in the case of three passes were distributed in a better way than the case where only one FSP pass was applied. However, there were few zones where the aggregated particles of the Al_2O_3 powder existed. The best distribution of the small particles of the used powder was obtained in the case where four passes were applied. As stated by other researchers [44, 45], it was suggested that dynamic recrystallization was the main reason behind the refinement of

the grains during the process of friction stir. Using friction stir for processing 6082 Al matrix reinforced with the Al_2O_3 powder proved to be an effective way to decrease the grain size of particles less than 300 nm. After this, a micro-hardness test was carried out along the center line of the FSPed cross sections. The results showed an increase in the micro-hardness values of about three time more than the values of the as received aluminum alloy. The highest micro-hardness value was achieved in the case when four passes of FSP were applied.

Yang et al. [46] carried out an analysis of AA6061 samples that were reinforced using 99.9% pure and 50 nm size Al_2O_3 powder particles. FSP was used to create the reinforced composite matrix. A drill was used to create different holes inside the samples under consideration. The holes had a 2 mm diameter and depth. After that, the Al_2O_3 powder particles were inserted into the holes. FSP started with a tool rotational speed of 480 rpm and a translational speed of about 203.2 mm/min. A different number of passes was created and different axial forces were applied. The axial forces varied from 13.23 to 22.05 kN. After subjecting the FSPed samples into an optical microscope, the results showed that both the value of the axial force in addition to the number of passes had an effect on the formation of the composite. Moreover, it was found that as the number of passes increased, the aluminum matrix composite zone was extremely bonded to the aluminum alloy and the powder particles were uniformly distributed within the matrix. The results from the micro-hardness test showed that the zones of aluminum matrix composite had the highest Vickers micro-hardness values. This was due to the refined size of the grain via dynamic recrystallization. However, the minimum micro-hardness values were inside the heat-affected zone.

Sharifitabar et al. [47] studied the mechanical properties of 5052-H32 rolled aluminum plate that was reinforced using nano-size Al_2O_3 powder particles. The plate had a thickness of 4 mm and FS was used to process the composite. A groove that had a width of 1 mm and a depth of 2 mm was machined in order for the Al_2O_3 powder particles to be filled in. After that, FSP was initiated using a tool rotational speed of 1600 rpm, a translational speed of 16 mm/min, and a tilt angle of about 5°. A different number of passes ranging from one to four were created. The results showed that the best distribution of the powder particles was achieved in the case when four passes were done. In that case, the results showed that the powder particles were separated from each other and were within a uniform distribution. Furthermore, the results showed that

grains of the matrix were refined after friction stir processing was applied. The average grain size of the base material was about 25-μm whereas it decreased to about 3.7 to 5.8 μm after FSP. The results proved that as the number of passes increased, the grain size decreased. At the same time, it was shown that the minimum grain size was achieved by using multiple-passes of FSP. The grain size in that case ranged between 5 and to 0.94 μm.

Mazaheri et al. [48] used FSP to come up with A356/Al_2O_3 surface composite. A356 samples that had dimensions of 10 mm×50 mm×250 mm were mixed with the powder particles of Al_2O_3. Micro and nano sizes of the particles of Al_2O_3 powder were used. During the FSP, the used tool rotational speed was about 1600 rpm, the translational speed was 200 mm/min, and the tilt angle was about 2°. The results of the investigation showed that layers of the composite at the surface turned out to be well bonded to the used alloy. There were no defects found along the layers of the composite at the surface. A micro-hardness test was carried out using a Vickers indenter with a load of 100 g and a dwell time of 5 seconds. After this, the hardness profile of different cross sections taken from the friction stir processed samples was studied. The results showed that the average micro-hardness values of the prepared composite using the two different sizes of the Al_2O_3 powder increased to about 90 and 110 HV which were higher than the micro-hardness value of the as-received sample. Finally, it was shown that as the size of Al_2O_3 powder particles decreased, the value of the micro-hardness increased significantly.

Hsu et al. [49] studied the mechanical behavior of Al–Al3Ti composite prepared using friction stir processing. The used aluminum powder (denoted Al–5Ti, Al–10Ti, and Al–15Ti) was mixed with titanium powder ranging from 5 to 15 %. During FSP, the tool rotational speed was set to 700 and 1400 rpm, whereas the translational speed was set to 45 mm/min. Different numbers of FSP passes were applied. For multiple FSP passes, the sample was subjected to cooling before the next pass was applied. After analyzing the FSPed samples via X-ray Diffraction (XRD), it was shown that the titanium particles reacted with the aluminum particles to produce Al_3Ti. However, some titanium particles remained without a reaction after four FSP passes were applied. Furthermore, the microstructure of the processed samples was studied using the backscattered electron image. Results showed that the grain size was decreased from 40 μm to about 1–5 μm. The micro-hardness value of the Al_3Ti was

about 200 HV. Results suggested that the FSP parameters had a significant effect on the size of the particles. The size of the particles seemed to increase as the tool rotational speed increased. This was due to the higher temperature obtained at higher tool rotational speed.

Zhang et al. [50] used FSP to produce Al_3Ti and Al_2O_3 aluminum composite. Two pure powders were used in this investigation. Commercially available aluminum and TiO_2 powders were used. During the process, four FSP passes were applied in the air and an extra two passes were applied under water. Results showed that after four FSP passes, a reaction between the two used powders existed. The reaction resulted in producing a small quantity of TiO in addition to Al_3Ti, and α-Al_2O_3. The average grain sizes were about 1,285 and 602 nm for the FSPed samples in air and water respectively. The results proved that the rapid cooling significantly forced the growth of recrystallized grains due to rapid cooling.

Bauri et al. [51] studied the effect of friction stir processing on the mechanical properties and microstructure of Al–TiC composite. In order to form the TiC particles, K_2TiF_6 salt and a 50 μm size of graphite powder were used. FSP was started using a tool rotational speed of 1000 rpm and a translational speed of 60 mm/min. Electron Back Scatter Diffraction (EBSD) and a field emission gun were used to study the metallurgical properties of the FS processed samples. Moreover, micro-hardness test were used to study the mechanical characterization. Results showed that the TiC particles were uniformly distributed inside the matrix after only two FSP passes. The average grain size for the FSPed samples after one pass was found to be 9 μm, whereas it was found to be 4 μm in the case when two FSP passes were applied. The grain size for as-received material was about 48 μm. Furthermore, results showed that the micro-hardness values increased after friction stir processing. The micro-hardness values for a single and double FSP pass were 48 and 58 HV respectively compared with 38 HV of the as-received sample. This improvement in hardness along the composite was due to the better uniform distribution of particles after FSP.

Tewari et al. [52] analyzed the change in silicon carbide particles orientation after friction stir processing was applied. The raw material used was aluminum A6061. In order to be able to study the microstructure of the SiC/ A6061 composite materials, high resolution and large area images using the scanning electron microscope were

obtained. The silicon carbide particles were found to have an average aspect ratio that varied in the range from 1.6 to 1.8. In addition, the powder particles had an anisotropic shape. After analyzing the orientation of the particles, it was found that the SiC powder particles preferred to be placed in a specific orientation after friction stir processing was applied. The orientation of the particles was in a parallel direction to the extrusion direction. The axis of the extrusion was vertical. However, this particles' preferred direction of alignment could be modified during the passage of the FSP tool. After analyzing the microstructural data it was found that different modifications took place during the process of FS. Some of these modifications include a decrease in the levels of microstructural heterogeneity and anisotropy. Moreover, a re-alignment of the SiC powder particles was also a significant modification present.

Asadi et al. [53] successfully used FSP to study the effects of the number of FSP passes in addition to the type of powder particle on the mechanical properties of a magnesium composite. The raw material under investigation was an AZ91 magnesium alloy. The raw material had an average grain size of about 150 μm. SiC and Al_2O_3 powder particles were both used to reinforce the raw material. The particles' average diameter in the used powder was about 30 nm and both powders were almost 99.98 % pure. A groove which had a depth of 1.2 mm and a width of 0.8 mm was machined on the AZ91 samples. A fixed tool rotational speed of about 900 rpm and a translational speed of 63 mm/min were used during the FSP. It was noticed that during the process of FS different combined alumina particles were present throughout some points inside the composite matrix. This resulted in the creation of alumina clusters which were distributed in a uniform way inside the stir zone. On the other hand, the results proved that the distribution of silicon carbide powder particles was not uniform; nevertheless, the particles did not stick to each other. Results from the experimental investigation showed that the average grain size of the particles in the stir zone increased as the number of FSP increased. The average Vickers hardness of the raw sample was about 63 HV. However, this hardness value experienced an increase in a range of 90 to 115 HV in the samples where the silicon carbide powder was added. However, the hardness value increased after two FSP passes to about 105 HV in the case where the Al_2O_3 powder was added. Finally, it was observed that as the number of FSP passes increased, the grains became very fine and uniformly distributed. This resulted in improving both the percentage elongation and the strength compared to a single FSP pass.

Chapter 3: Experimental Setup

3.1 Material Selection

The raw material that was used throughout this investigation was commercial Mg alloy AZ31B in the form of a 5 mm thick sheet, whereas the particles used as reinforcement were SiC particles. Chemical compositions of AZ31 and SiC particles are shown in Tables 3-1 and Table 3-2. The compositions were obtained using Energy Dispersive X-Ray Spectroscopy (EDS) as shown in Figure 3.1 and 3.2 respectively. The chemical composition for AZ 31B magnesium alloy obtained using the EDS approach is within a good agreement with the one reported in the literature by Xiaofei et al. [54]. Magnesium is considered to be the lightest metal on earth. It is lighter than steel by about 78% and aluminum by almost 35%. If a good design is to be considered, magnesium can be used as a great alternative to steel and aluminum since it guarantees a weight reduction. Magnesium alloys feature high specific strength, low density, excellent machinability, hot formability, and good electromagnetic shielding characteristics. Most of the successfully manufactured magnesium parts in today's industry are cast-components. However, without the use of magnesium in sheet metal forming, the significant reduction in weight in many applications will not be achieved. AZ 31B magnesium alloy is used widely in a variety of applications such as automobile, aerospace, electronic, and sports industries. This magnesium alloy offers good mechanical properties and is commercially available in the form of a sheet. AZ 31 magnesium alloy is the most commonly used commercial magnesium alloy [13, 55-59].

Table 3-1: Chemical composition of Mg AZ 31B (wt%)

Mg	**Al**	**Zn**	**Mn**	**Na**	**Si**
Balance	2.8	1.6	0.4	0.3	0.1

Table 3-2: Chemical composition of SiC particles (wt%)

Si	**C**	**Pb**	**Ni**	**Al**	**Na**
Balance	37.1	0.4	0.1	0.1	0.1

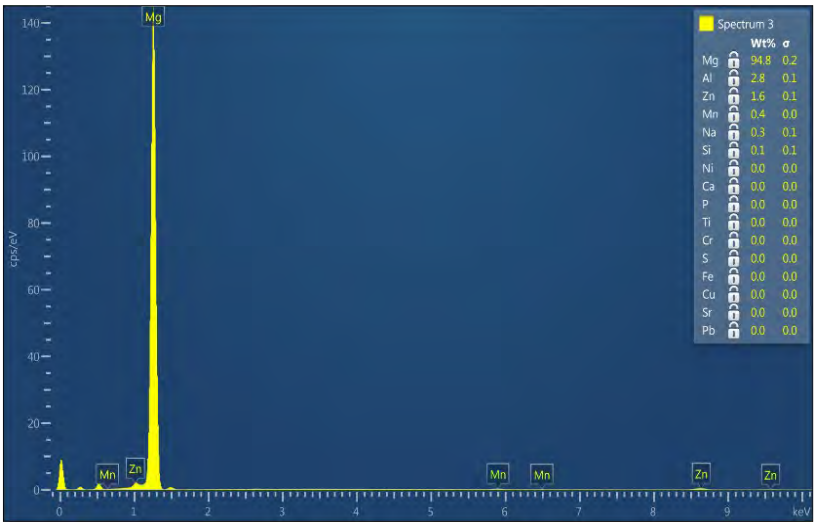

Figure 3.1: EDS analysis of the used Mg AZ31B

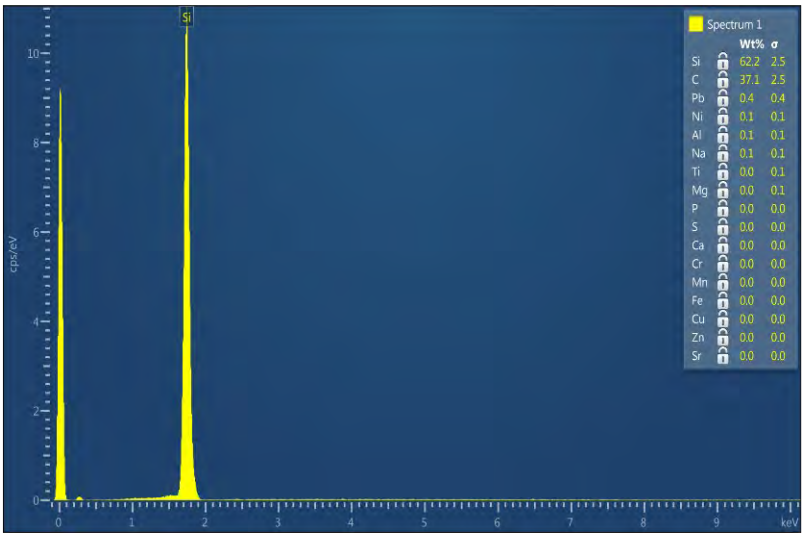

Figure 3.2: EDS analysis of the used SiC

3.2 Experimental Setup of FSP

The raw material that was used throughout the whole investigation was magnesium AZ 31B alloy. Different samples each having a length of 130 mm, a width of 60 mm, and a thickness of 5 mm were manufactured. Then, a groove with a width of 2 mm and a depth of 0.5 mm was made along the center line of the specimen. A sample of the dimensions of the working specimens alongside a sample of the working specimens are shown in Figures 3.3 and 3.4 respectively. A total number of three holes each with a diameter of 1.5 mm were made alongside each

specimen as illustrated in Figure 3.4. The purpose behind such holes was to be able to place the thermocouples during the process. Two cases of FSP were carried out. First, FSP without any addition of SiC. Then, silicon carbide particles with a size of 250 µm were inserted in order to fill the groove. After that, FSP was initiated using different sets of tool rotational and translational speeds. In both cases, two samples for each FSP condition were made. FSP was accomplished using a tool that had a 15 mm diameter shoulder, a pin which had a 5 mm diameter and 4 mm length, as shown in Figure 3.5. The tool was mounted on the vertical CNC milling machine. Before starting the process, the work piece with a groove was fixed in its place in the CNC machine. In order to insure a stable process, the specimen was fixed in its place using screws at different locations. Then, using the setup available in the CNC machine, the location of the specimen was adjusted using the three axes x, y, and z**.** After that and by using the drilling tool available in the CNC machine, an initial hole with a small depth was created to indicate the start of the processed length. SiC particles filled in the groove as illustrated in Figure 3.6. K-type thermocouples were inserted inside the three holes alongside the specimen in order to obtain the thermal profile for each FSP condition. The locations of the thermocouples were adjusted with one placed near the start of the process, while the others were placed close to the middle and end of the processed length. The locations of the three thermocouples are shown in Figure 3.6. The thermocouples were connected to a computer and their data were transferred via Bluetooth. A software called PicoLog Recorder was used to get the temperature data. Furthermore, an ULIRvision TI-395 infrared camera was fixed at a specific angle and then was used to capture/record thermal images/videos during the process as shown in Figure 3.7. Such data was used in the thermal analysis. Next, different working samples were subjected to FSP with and without SiC under different tool rotational speeds and translational speeds. Finally, FSP was accomplished resulting in a defect-free pass which had a full length of 80 mm. as illustrated in Figure 3.8. The complete experimental setup is shown in Figure 3.9.

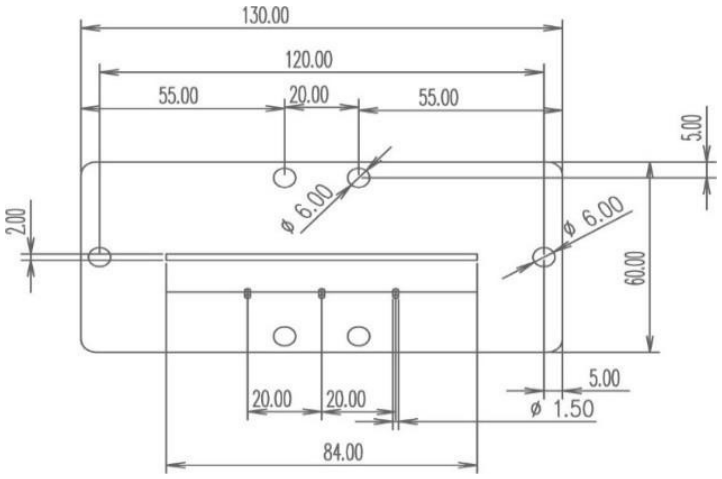

Figure 3.3: Dimensions in mm of a sample work piece

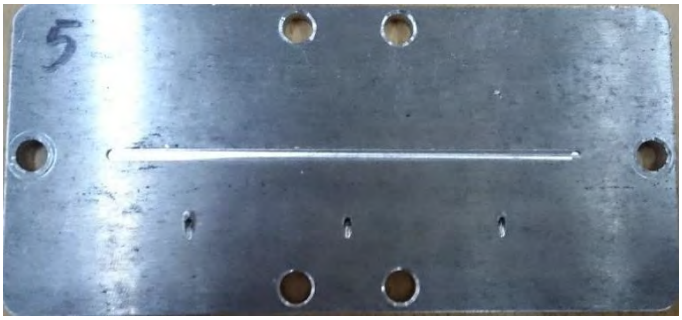

Figure 3.4: A sample work piece with three holes

Figure 3.5: FSP tool

Figure 3.6: A fixed work piece filled with SiC particles

Figure 3.7: The ULIRvision TI-395 infrared camera

Figure 3.8: An 80 mm FSP pass

Figure 3.9: The complete experimental setup

3.3 Experimental Procedure of Microstructural Analysis

The optical microscope shown in Figure 3.10 was used to capture different microstructure images for all the FSP conditions. All samples had to go through polishing and grinding processes. The grinding machine shown in Figure 3.11 was used. A polished specimen alongside an unpolished one are shown in Figure 3.12. Furthermore, diamond paste of 1 µm size was applied to the samples. A piece of cotton filled with a chemical etchant (1% oxalic acid in water) was subjected to the sample under interest. The sample was next washed with distilled water before it was subjected to acetone and again washed with distilled water. The same process was repeated if necessary. Samples were kept inside a desiccator. Microstructural images at 2.5 mm from the top were taken and grain size was analyzed.

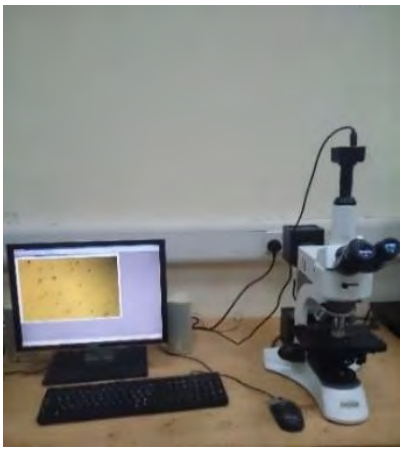

Figure 3.10: Optical microscope

Figure 3.11: Grinding machine

Figure 3.12: A polished alongside an un-polished micro-hardness specimens

3.4 Experimental Procedure of Micro-hardness

The QV-1000 DM digital micro-hardness tester shown in Figure 3.13 was used to conduct Vickers micro-hardness. The original processed specimens were cut into smaller pieces that had dimensions of 20×10 mm as shown in Figure 3.14. The micro-hardness specimens were then placed into molds where they were subjected to both ClaroCit Powder and ClaroCit Liquid chemicals as shown in Figure 3.15. After that, the micro-hardness specimens took the shape of the molds and they became easier to hold while testing. Before starting the test, it was necessary to grind and polish the

micro-hardness specimens. Next, the test was started using a load of 9.807 N and a dwell time of 10 seconds as illustrated in Figure 3.16. Different hardness readings were taken along the center line of each micro-hardness specimen. To be more precise, three different through-thickness positions along the center line of each FSPed specimen were investigated. Micro-hardness values for 25%, 50% and 75% through-thickness positions measured from the top edge were taken. At the end, the average value of three to five readings was considered for every position. On the other hand, micro-hardness values for through-thickness positions of 10%, 16%, 50% and 75% measured from the top edge were considered in the case of FSP with SiC. Again, for every through-thickness position the average micro-hardness of three to five readings was considered. Finally, five readings to the right and left of the center line of through-thickness position of 10% were taken with an increment of 0.4 mm away from the center line.

Figure 3.13: QV-1000DM digital micro-hardness tester

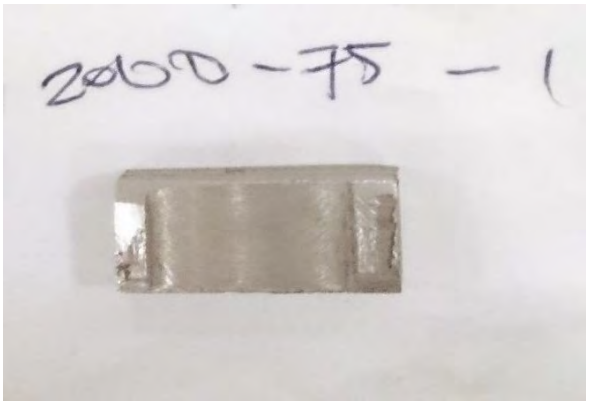

Figure 3.14: A Micro-hardness test specimen

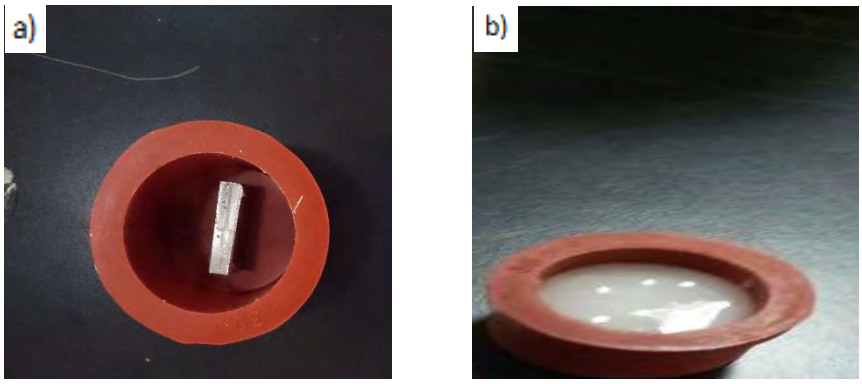

Figure 3.15 a) Test specimen inside a mold b) Test specimen subjected to chemicals

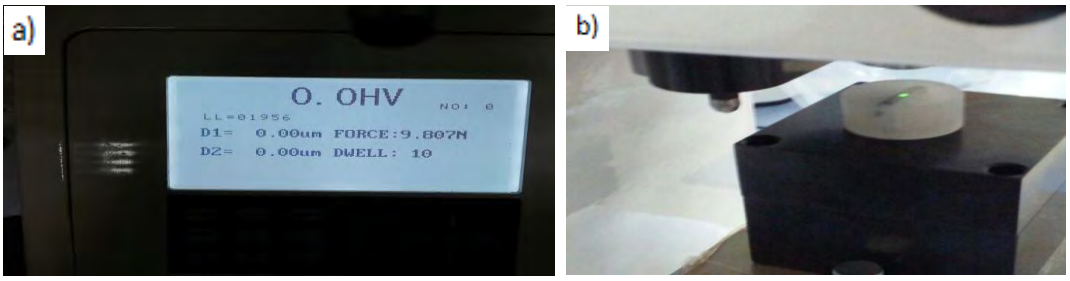

Figure 3.16-a) Micro-hardness test settings b) Micro-hardness specimen under testing

3.5 Process Parameters

The complete tool rotational and translational speed values that were used throughout this investigation are shown in the input matrix in Table 3-3. These values were chosen after different experiments that included the use of different RS and TS; however, the chosen values turned out to give FSP passes that were free of defects. According to Darras [60] different alloys have various working limits of RS and TS for which they can produce crack free FSP passes. However, it is always essential to control both the rotational and translational speeds carefully in order to produce enough heat to soften the material and enough stirring to cause severe plastic deformation without overheating or melting. Figures (3.17-3.20) show defective free FSPed specimens for both conditions: 800 rpm, 75 mm/min, and 1200 rpm, 100 mm/min with and without SiC. Each FSP condition was repeated another time and again crack free specimens were obtained. The complete FSPed specimens can be found in Appendix A. Figure 3.21 shows a Scanning Electron Microscope (SEM) image for the SiC particles. Figure 3.22 represents an SEM image of the Mg/ SiC composite. To make sure of the existence of the particles within the composite, EDS analysis of the SiC particles inside the Mg/

SiC composite was done as shown in Figure 3.23 and the result was compared with the EDS of the base material. The EDS analysis of the Mg/SiC composite showed a significant amount of silicon and carbon in contrast to the EDS analysis of the base material. Moreover, the distribution of the SiC particles within the composite was not uniform. According to Asadi et al. [39] a more uniform distribution of particles can be accomplished by increasing the number of FSP passes. In their study, Zarghani et al. [43] were able to obtain the best distribution of Al_2O_3 powder particles after four FSP passes. The shape of the SiC particles was changed due to the stirring of the tool. This worked on breaking the sharp edges of the bigger particles and rounding them up at the same time [61]. The result was round and smaller particles.

Table 3-3: Input matrix

Tool rotational speed (rpm)	Translational speed (mm/min)
800	25,75,100,200
1200	25,75,100,200
1600	25,75,100,200
2000	25,75,100,200

Figure 3.17: FSP sample @800 rpm, and 75 mm/min

Figure 3.18: FSP (with SiC) sample @800 rpm, and 75 mm/min

Figure 3.19: FSP sample @1200 rpm, and 100 mm/min

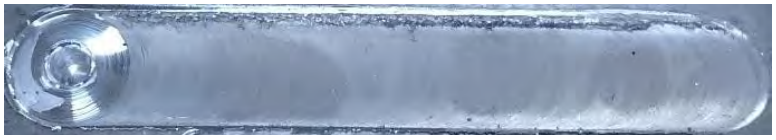

Figure 3.20: FSP (with SiC) sample @1200 rpm, and 100 mm/min

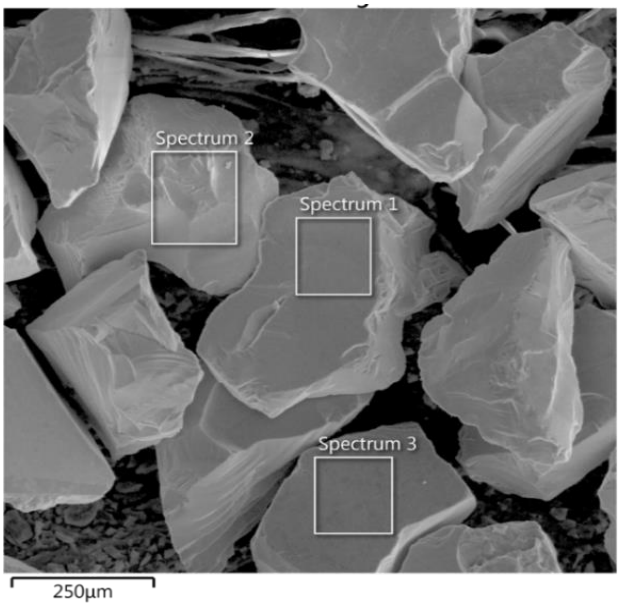

Figure 3.21: SEM image for the SiC particles

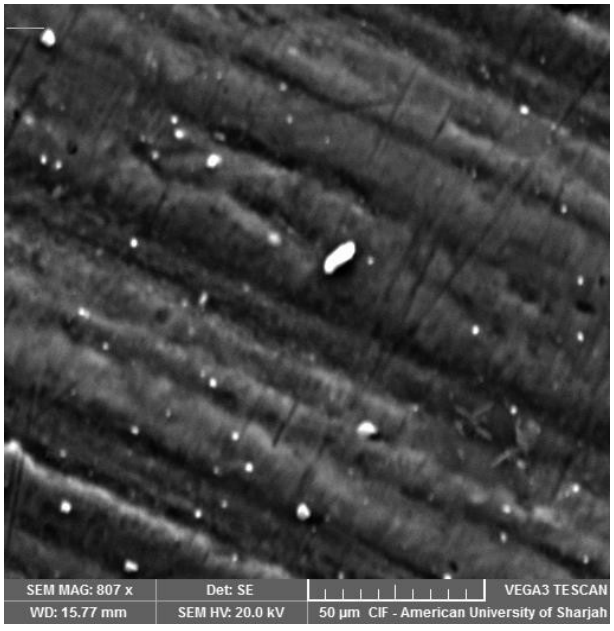

Figure 3.22: SEM image for the Mg/SiC composite

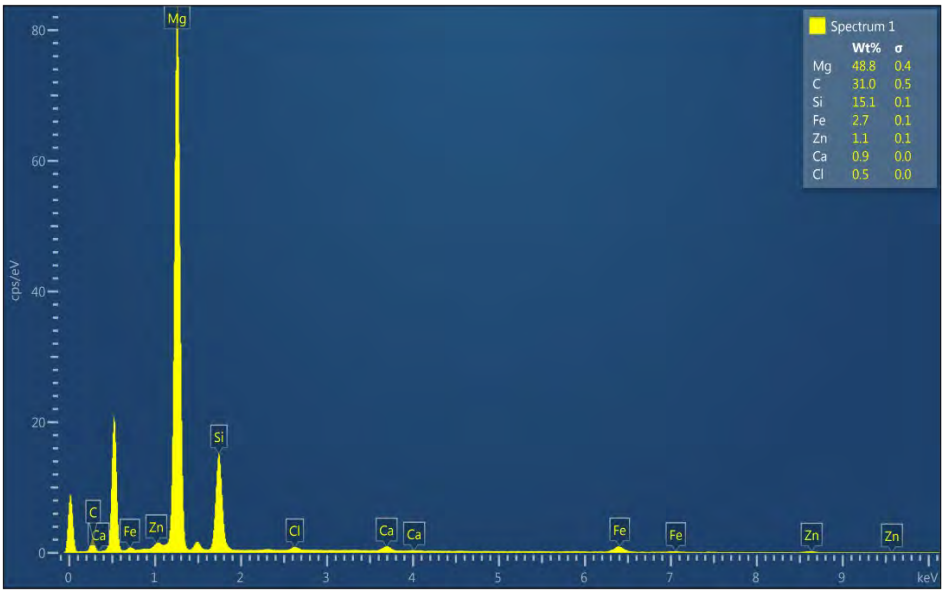

Figure 3.23: EDS analysis for the Mg/SiC composite

3.6 Defective FSP

Figures 3.24 and 3.25 show observable defects on the surface of FSPed specimens with a groove of 2 mm and 2.5 mm in depth respectively. These cracks occurred due to the fact that the FSP tool was not able to adjust a proper flow of metal nor sufficient consolidation of metal inside the friction stir processed zone [62]. Asadi [63], studied the effect of tool penetration depth on the defects formation and surface quality of AZ 91 /SiC composite via FSP. FSP was accomplished using three penetration depths of 0.1, 0.2, and 0.3 mm. When a penetration depth of 0.1 mm was used, it was observed that the processing zone was entirely defected. The FSPed surface became better when a penetration depth of 0.2 mm was used, but there was still a thorough hole and tunnelling cavity. Finally, results showed no existence of any tunnelling cavity or crack when a penetration depth of 0.3 mm was used. In addition, at this penetration depth, the FSPed surface quality was acceptable. Magnesium, which has a hexagonal closed pack structure, is considered a brittle metal and is extremely sensitive to temperature. For small penetration depths or high depth grooves, the coefficient of friction between the tool shoulder and the surface of the specimen is insufficient to produce enough heat to soften the material; hence, the brittle fracture occurs. On the contrary, when very high penetration depths or very small depth grooves were used, defects were noticed at the FSPed surface. Furthermore, results showed that a significant increase in penetration depths can lead to specimen damage. This can be explained by the fact that at very high penetration depths, the friction mode between

the specimen and the tool could change from sliding friction to sticking friction. Hence, it was essential to carry out different experiments with different groove sizes to come up with an optimum groove size that would produce defect-free FSPed specimens without damaging the FSP tool.

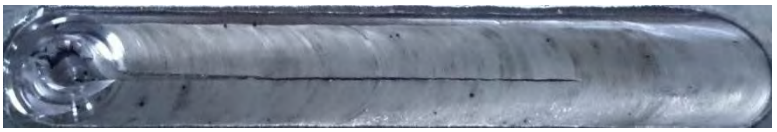

Figure 3.24: A defective FSP pass for a groove of 2mm

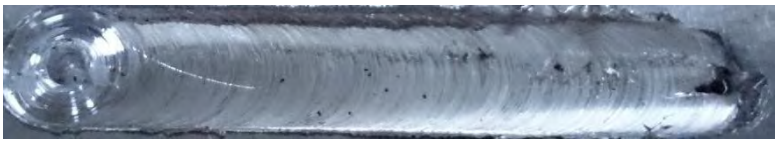

Figure 3.25: A defective FSP pass for a groove of 2.5 mm

Chapter 4: Experimental Results

4.1 Thermal Analysis

4.1.1 Thermal profiles. Figures 4.1 and 4.2 represent the temperature in three channels for FSP conditions of 1200 rpm and 75 mm/min, with and without SiC. Obviously, it can be noticed that temperature in the first channel continued to increase at the start of the process until it reached a peak value; then the temperature along the next channel started to increase until again it reached a maximum peak. When the process is near the end, the third channel experienced an increase to a peak value as well. Complete temperature profiles for all conditions can be found in Appendix B.

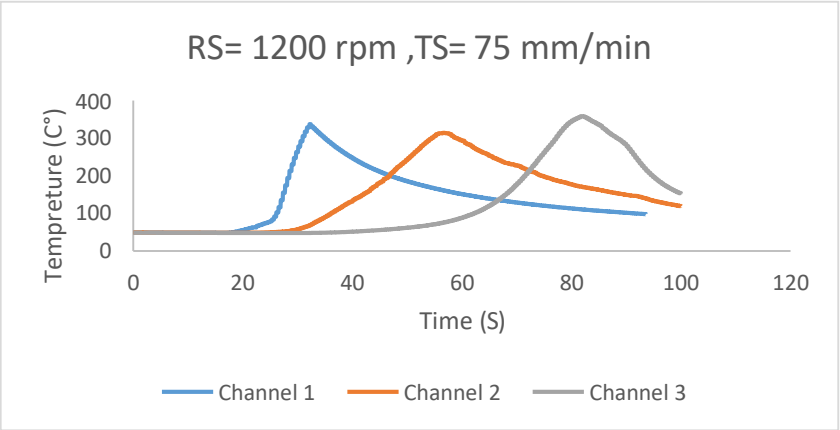

Figure 4.1: The recorded temperature @ RS=1200 rpm, TS=75 mm/min

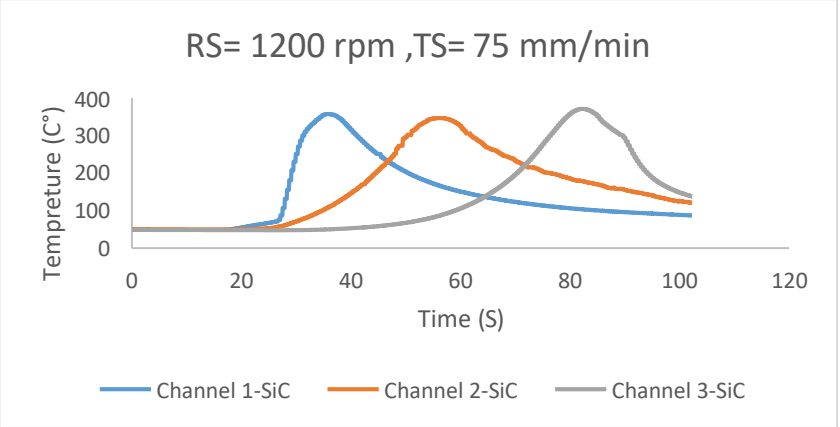

Figure 4.2: The recorded temperature @ RS=1200 rpm, TS=75 mm/min (SiC)

4.1.2 Effect of translational speed on temperature. Figures 4.3 represents the effect of translational speed on channel 1 temperature for FSP at a rotational speed of 1600 rpm. It can be noticed in either case that the change of translational speed did not

have a significant impact on the peak temperature. In general, the maximum peak temperature was always obtained at the minimum translational speed for a specific tool rotational speed. Results for other tool rotational speeds followed the same pattern. Figure 4.4 represents the effect of translational speed on channel 1 temperature for FSP with SiC at a rotational speed of 1600 rpm. Again, results for other tool rotational speeds for FSP with SiC followed the same pattern/trend. Similarly, it was found that the maximum peak temperature was always obtained at the minimum translational speed for a specific tool rotational speed. On the other hand, changing the translational speed had a significant impact on the processing time which can be represented by the width of the figures. As the translational speed increased, the width of a single graph increased; hence, the processing time also increased. From all the used values of translational speeds, it can be noticed that the slower processing time was in the case of a translational speed of 25 mm/min. Higher processing time means higher heat input and by changing the value of translational speed, a control of the amount of heat input can be achieved. This is usually important to control the grain growth throughout the process. Results of FSP with and without SiC show insignificant effect of SiC particles on the thermal profile. The complete effect of translational speeds at different rotational speeds can be found in Appendix B.

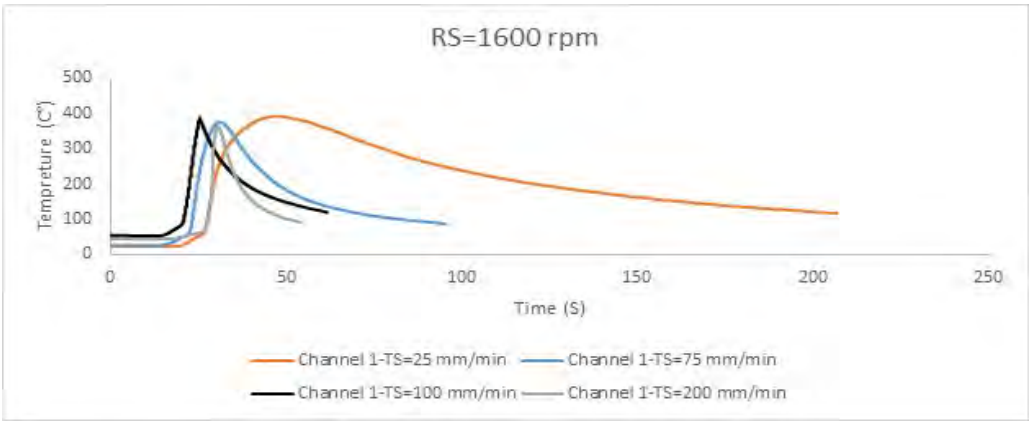

Figure 4.3: Effect of translational speed @ RS=1600 rpm

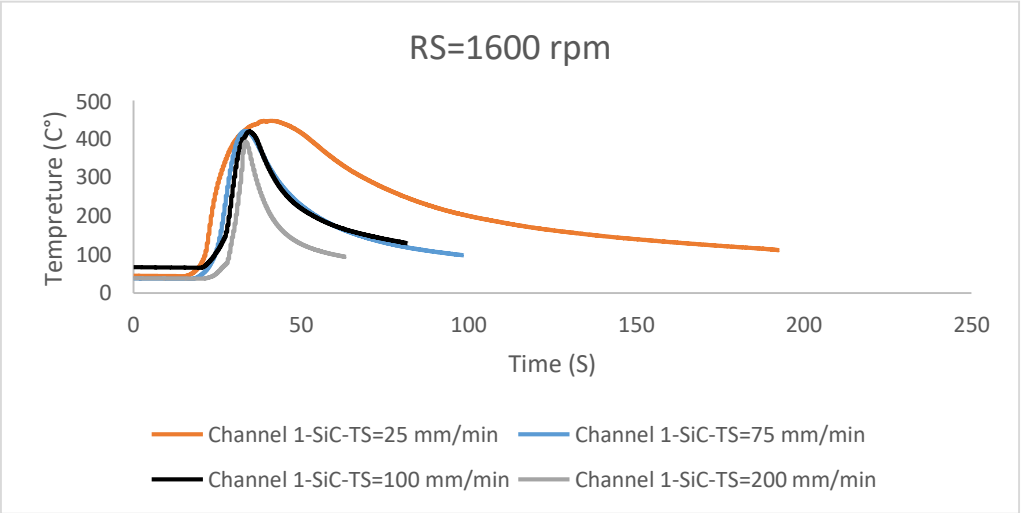

Figure 4.4: Effect of translational speed @ RS=1600 rpm with SiC

4.1.3 Effect of rotational speed on temperature. Figure 4.5 represents the effect of rotational speed on channel 1 temperature for FSP at a translational speed of 75 mm/min. Figure 4.6 shows the effect of rotational speed on channel 1 temperature for FSP with SiC at the same translational speed. It can be noticed that in either case the change of rotational speed had a significant impact on the peak temperature. In general, as the tool rotational speed increased, the value for the peak temperature increased for a specific translational speed. This could be a result of thermal conduction through the processed specimen. In all the cases, the maximum peak temperature value for each specific value of translational speed was obtained at a tool rotational speed of 2000 rpm. These results were valid for both FSP and FSP with SiC. For example, in the case of FSP without SiC and at a translational speed of 25 mm/min, the peak temperature at a rotational speed of 800 rpm was 334.93 C°; then it increased to 346.12 C° at 1200 rpm. Then, it increased even more to reach 392.6 C° and 449.02 C° at tool rotational speeds of 1600 and 2000 rpm respectively. Results for other translational speeds followed the same pattern. Results for FSP with SiC at other translational speeds followed the same pattern/trend. The complete effect of rotational speeds at different translational speeds is available in Appendix B.

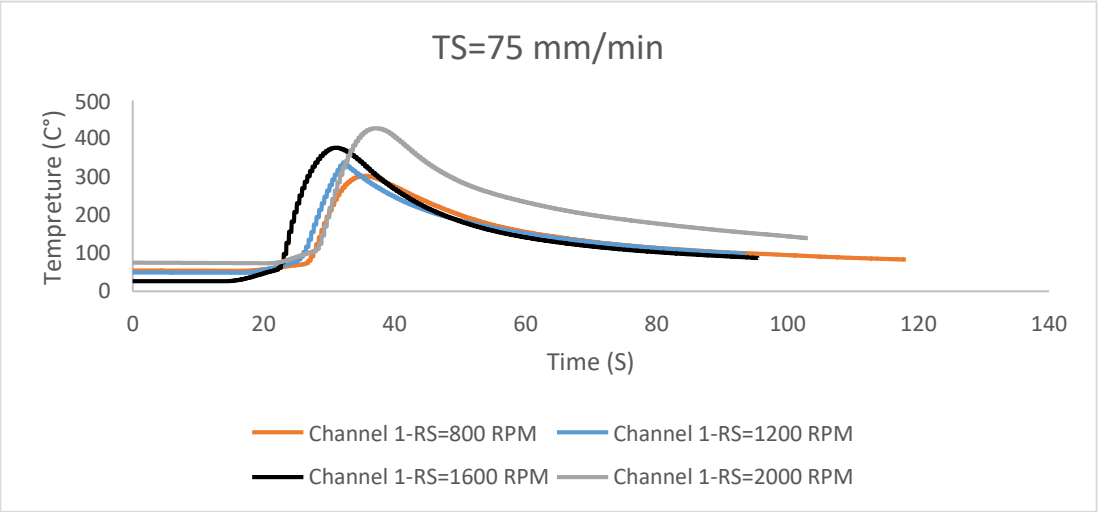

Figure 4.5: Effect of rotational speed @ TS=75 mm/min

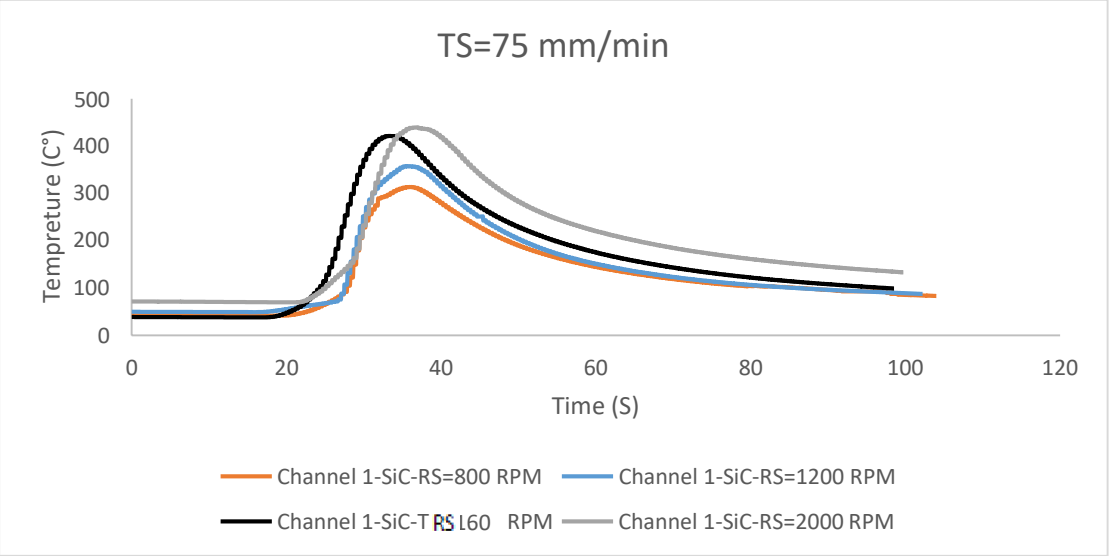

Figure 4.6: Effect of rotational speed @ TS=75 mm/min with SiC

4.2 Microstructure

Looking at the microstructural results of FSPed AZ31 Mg/SiC composite, it is clear that the results show some grain refinement; but more important, FSP was able to produce a more homogenous microstructure for some combinations of tool rotational and translational speeds. This homogenous microstructure is quite clear in all FSP conditions with 800 rpm, and in two FSP conditions of 1200 rpm which are 1200 rpm-100 mm/min, and 1200 rpm-200 mm/min. However, not all the conditions were able to give this homogenous microstructure. Non-homogenous microstructure can be seen in different conditions such as 2000 rpm-75 mm/min, 2000 rpm-100 mm/min, and 2000

rpm-200 mm/min. Figure 4.7 represents microstructural images of different FSP conditions in addition to the microstructure of the base material. Microstructural images for other conditions can be found in Appendix C. It can be seen that the as-received sheet has a fine microstructure that is not quite homogenous with an average grain size of about 13.06 µm. Moreover, the structure of the as-received consists of a combination of small and large grains while the microstructure of the FSPed samples show that almost all the grains have the same size. The results suggest that after FSP there was significant grain refinement. However, the grain structure after FSP is more homogenous and equiaxed.

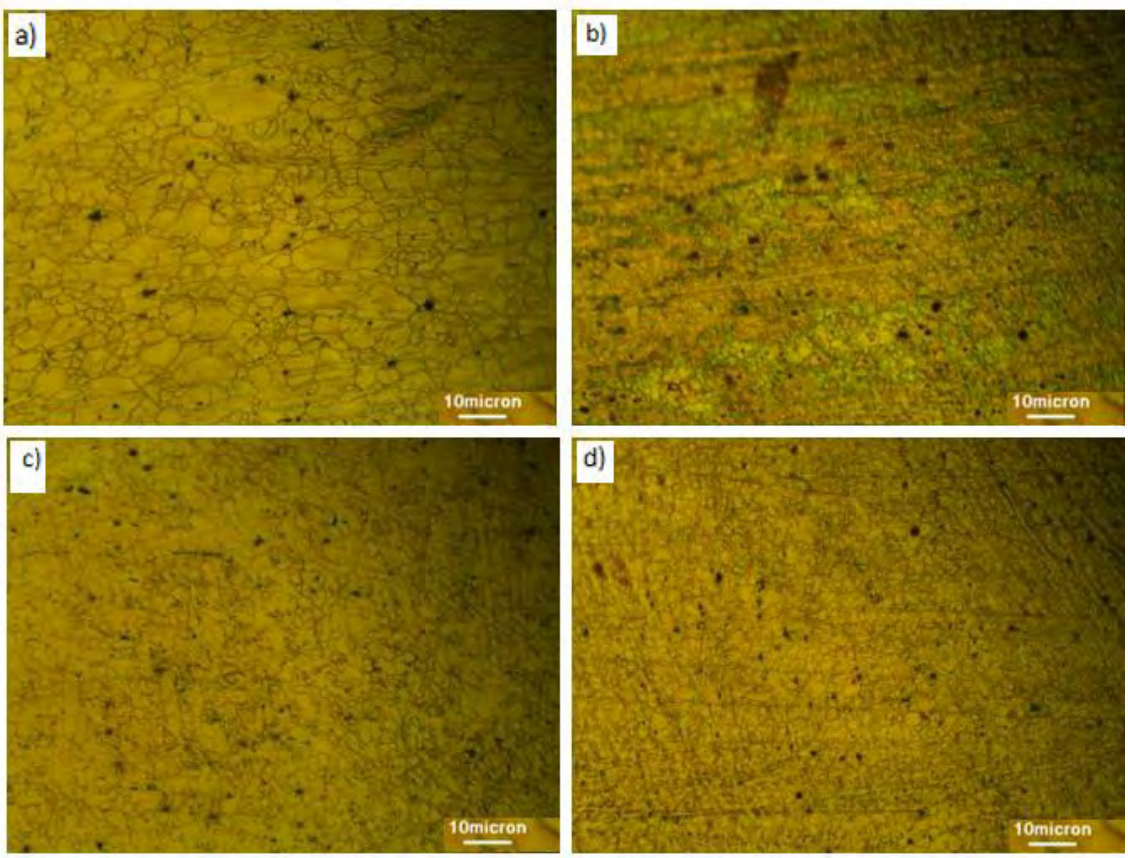

Figure 4.7: Microstructure of the a) base material, b) FSPed at 800 rpm-25 mm/min, c) FSPed at 1200 rpm-25 mm/min, d) FSPed at 1200 rpm-100 mm/min

FSP successfully refined the microstructure from an average grain size of about 13.06 µm to an average grain size of about 1.46 µm. The finer and more homogenous grain structure produced by FSP is expected to improve ductility and formability of the material at elevated temperatures, and improve its superplastic behavior. Table 1 in Appendix C introduces a summary of the average grain sizes for each FSP condition. Figure 4.8 shows the effect of rotational speed on the resulting grain size at a fixed translational speed of 25 mm/min. As the figure suggests, a decrease in the grain size

can be achieved by decreasing the rotational speeds. This can be related to the heat generation taking place throughout the process. When higher rotational speeds were used, high heat input was generated, and thus, more grain growth was developed. On the other hand, Figure 4.9 represents the effect of translational speeds on the grain size at a fixed rotational speed of 1200 rpm. It can be observed that as the translational speed increased, smaller grain size was achieved. The reason behind this is the same -- that is at lower translational speeds, longer processing time is required, and thus the processed sheet was exposed to the heat source for a longer time. This will work on giving the sheet more time and higher temperature for the grain to grow. The effect of other rotational and translational speeds on the average grain size can be found in Appendix C. One thing interesting in the results is that some combination of tool rotational and translational speeds such as 2000 rpm and 25 mm/min exhibited larger grain size than that for the as-received material can be. This shows the significance of controlling the process parameters and how this control can have a high level effect on the resulting properties. Moreover, failing to control the process parameters for every material can be significant in reversing the process to a grain coarsening process from a grain refinement process. The results agree with others related in literature such as those reported by Asadi [39], Darras [64] and Darras and Khraisheh [65]. Microstructural results are in excellent agreement with the thermal analysis.

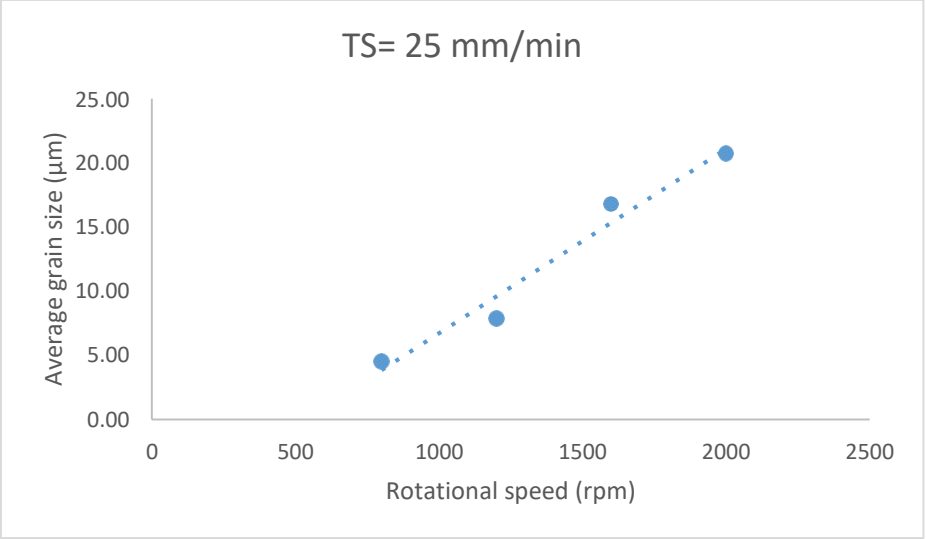

Figure 4.8: Avg. grain size @ TS=25 mm/min

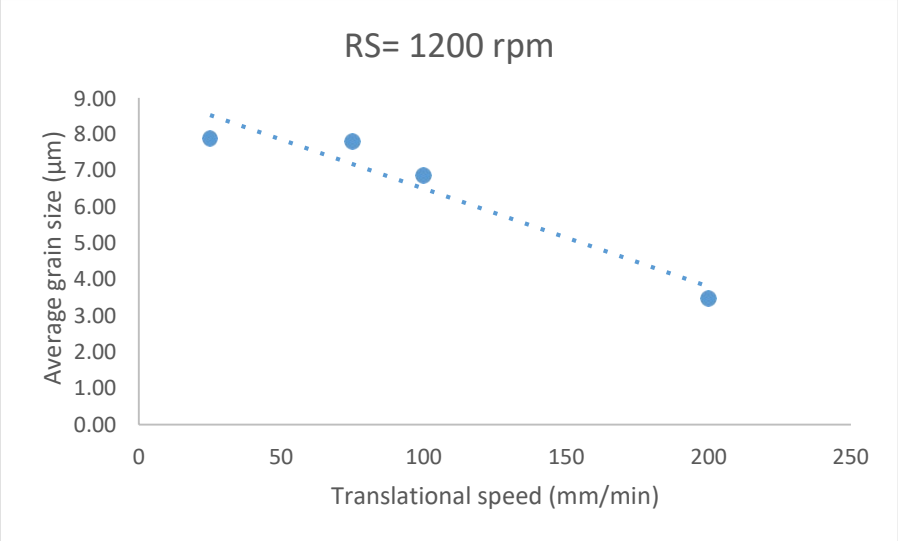

Figure 4.9 Avg. grain size @ RS=1200 rpm

4.3 Micro-hardness

4.3.1 Effect of translational speed on micro-hardness. The average micro-hardness value for 5 readings for an as-received specimen was found to be around 67.7 HV. Tables 1 and 2 in Appendix D show the average of three to five micro-hardness readings for each FSP and FSP with SiC respectively. The minimum and maximum mica-hardness values for each FSP case (with /without SiC) are highlighted in red. Figures (4.10-4.13) represent the effect of translational speed on the micro-hardness of the FSPed specimens without any addition of SiC powder. Each of the micro-hardness readings represents an average of three to five readings. Refer to the micro-hardness experimental setup for more information about the measurement of micro-hardness readings. Generally, it can be observed that as the translational speed increases, the through-thickness micro-hardness value increases. The Hall-Petch relationship states that as the grain size decreases, the hardness increases. As the translational speed increases, the FSP time decreases resulting in lower grain growth which positively affects the hardness values [60, 66]. This observation is valid when comparing the micro-hardness set of readings for a specific distance through the thickness of any FSP pass. Moreover, the results showed that the average micro-hardness values are minimum near the top edge of any micro-hardness specimens. In other words, as the through-thickness increases, the micro-hardness value increases. This is because the top surface is closer to the heat source, and this means higher temperature. This will result in more grain growth and thus lower micro-hardness values near the top edge [67,68]. For a rotational speed of 800 rpm, when the translational speed was 25 mm/min, the

average micro-hardness reading was 68.1 HV within 1.25 mm from the top edge. Then, the value increased to around 70.9 HV when the reading was taken within 2 mm from the top edge. The value increased even more to reach about 73.2 HV within 3.75 mm from the top edge. When the translational speed was increased to 75 mm/min, the micro-hardness increased to about 73.3 HV, within 1.25 mm through-thickness, 74.9 HV, and 76.3 HV within 2 mm and 3.75 mm respectively. When a translational speed of 100 mm/min was used to accomplish the friction stir processing, the micro-hardness values increased to 75.5 HV, 77.3 HV, and 78.4 HV within 1.25 mm, 2.5mm, and 3.75 mm respectively. Finally, when a translational speed of 200 mm/min was used, the average micro-hardness increased to about 76.6 HV, 78.5 HV, and 79.6 HV within 1.25 mm, 2.5mm, and 3.75 mm respectively.

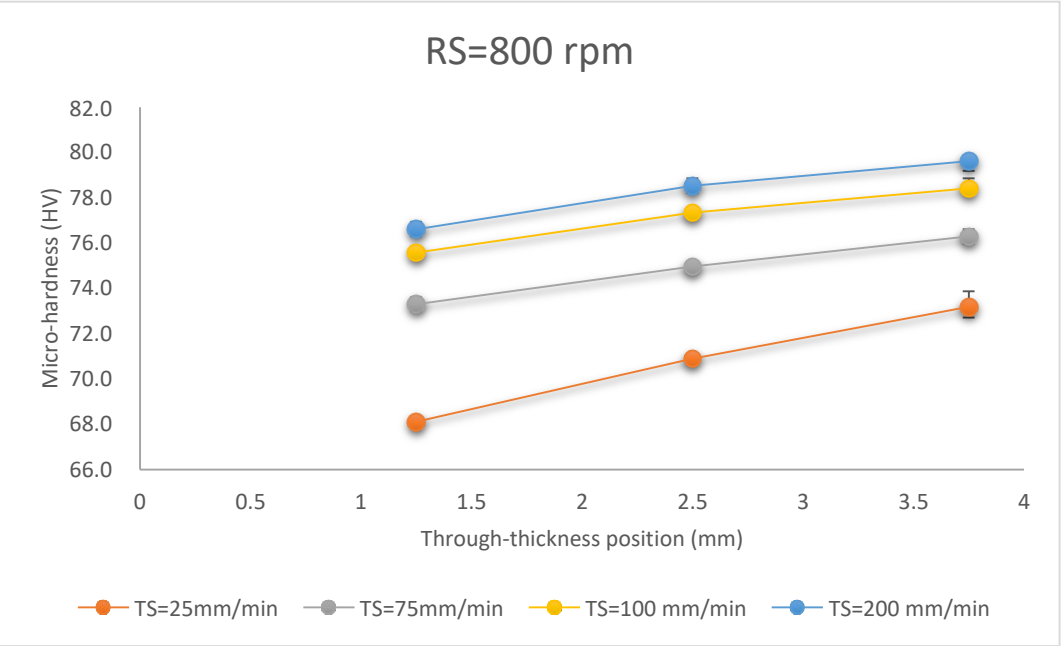

Figure 4.10: Effect of translational speed @ RS=800 rpm

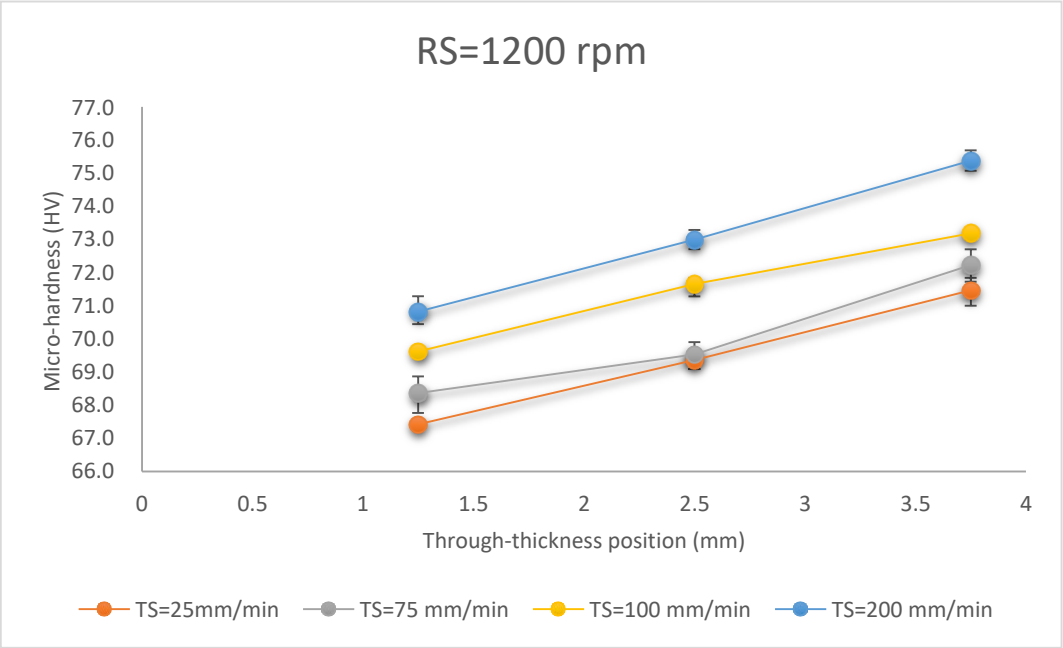

Figure 4.11: Effect of translational speed @ RS=1200 rpm

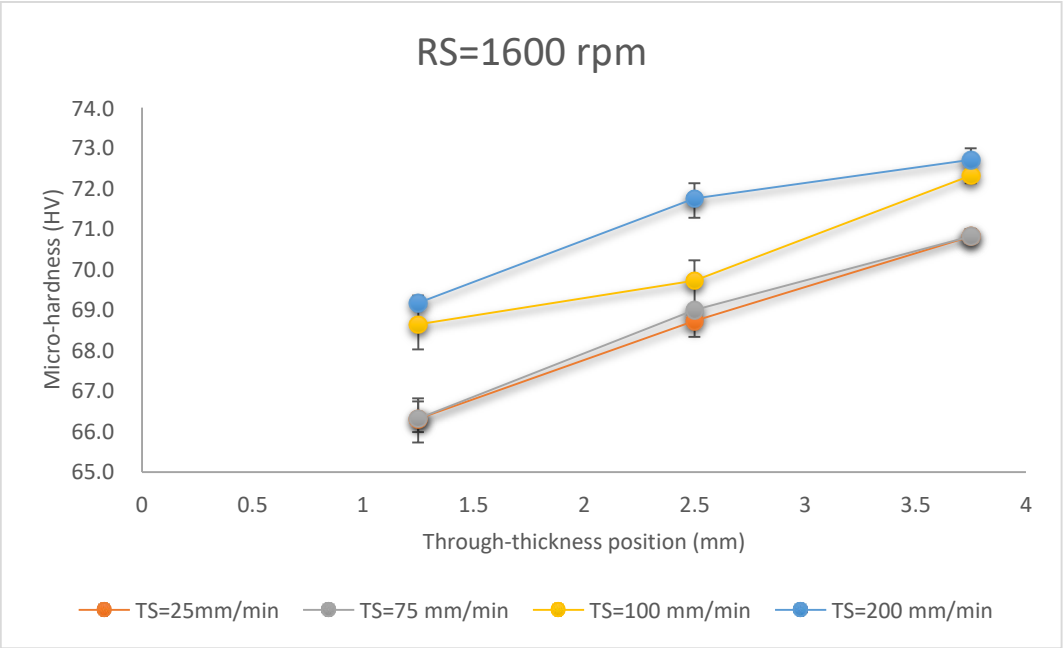

Figure 4.12: Effect of translational speed @ RS=1600 rpm

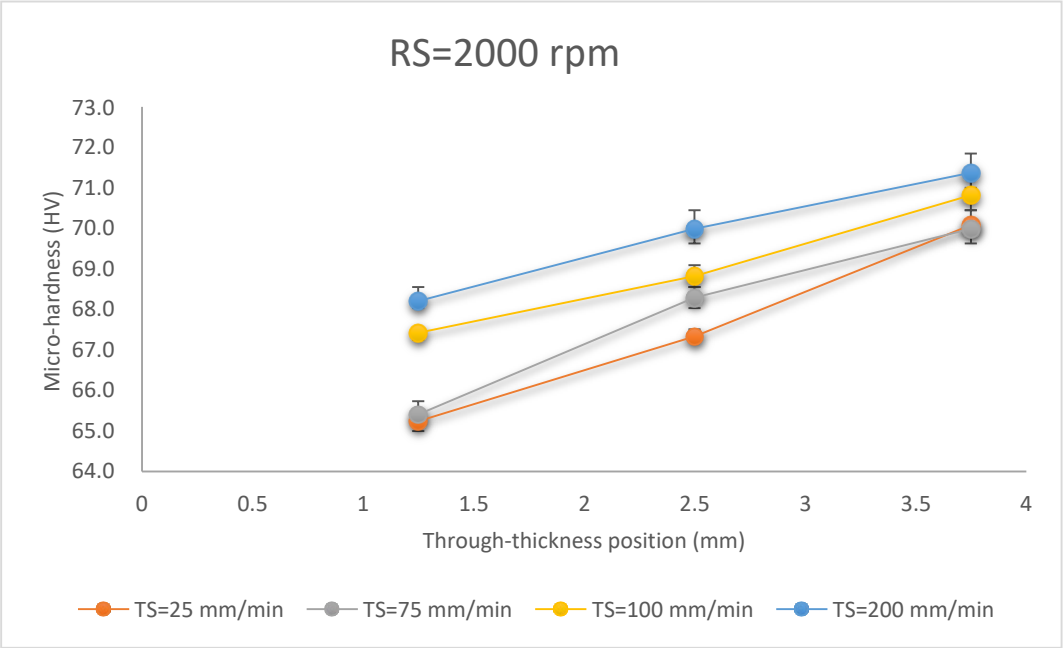

Figure 4.13: Effect of translational speed @ RS=2000 rpm

Figures (4.14-4.17) represent the effect of translational speed on the micro-hardness for FSPed specimens with the addition of SiC powder. Each micro-hardness reading represents again an average of three to five readings. Refer to the micro-hardness experimental setup for more information about the measurement of micro-hardness readings of FSP with SiC powder. Generally, it can be observed that the region that contains the SiC (which is within 0.5 mm from the top edge) has the maximum micro-hardness values. It is important to say that the values of micro-hardness within this region are affected by the amount of SiC powder inserted inside the groove during FSP. Moreover, it is affected by how much of that amount remained inside the groove during the process. However, it can be noticed that the micro-hardness values taken within 2.5 mm and 3.75 mm from the top edge were very close to those obtained with FSP only without the addition of SiC. This suggests an accuracy of the experimental work. The variation within the readings is almost negligible as can be seen from the error bars provided in the graphs. Complete micro-hardness values can be found in Table 2 provided in Appendix D.

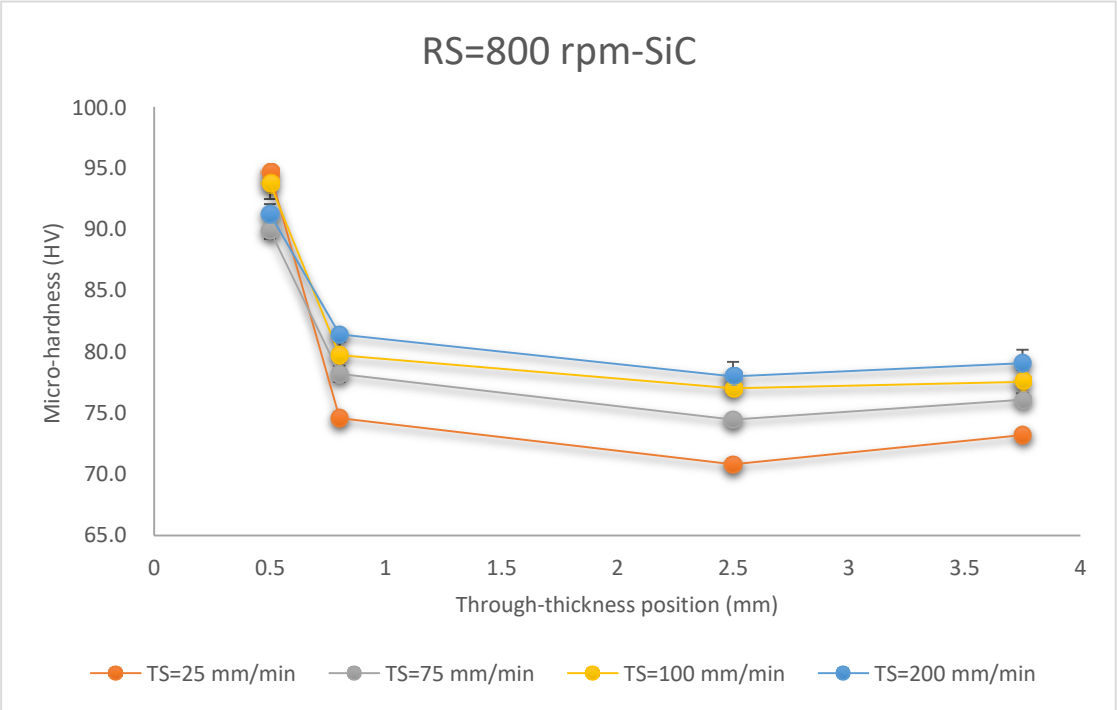

Figure 4.14: Effect of translational speed @ RS=800 rpm with SiC

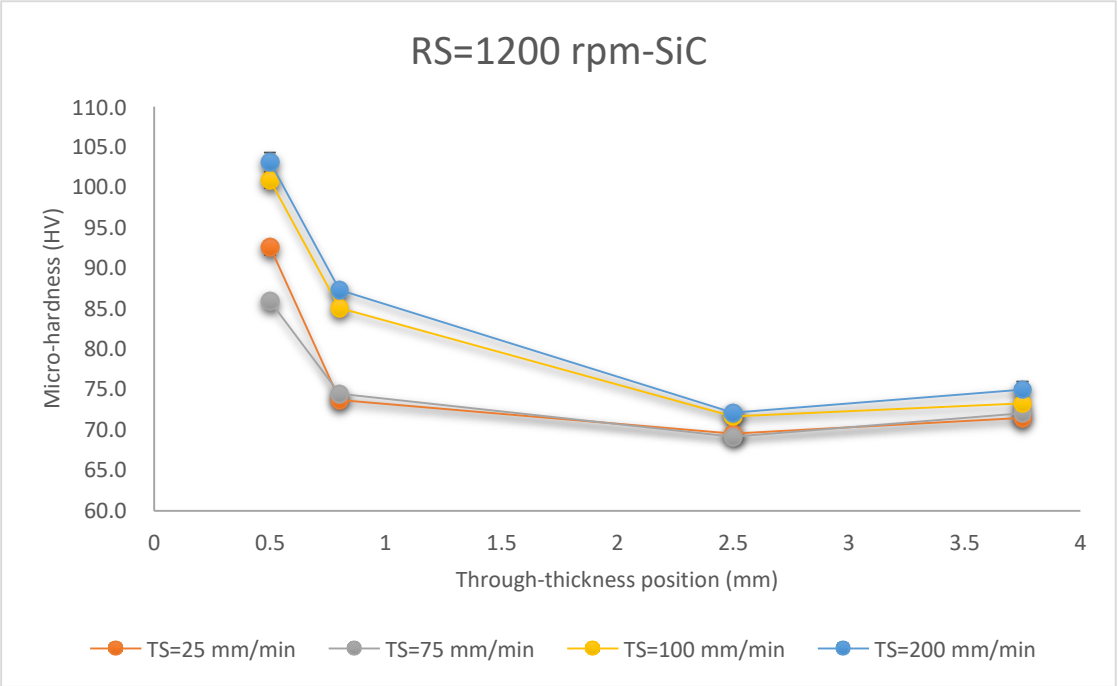

Figure 4.15: Effect of translational speed @ RS=1200 rpm with SiC

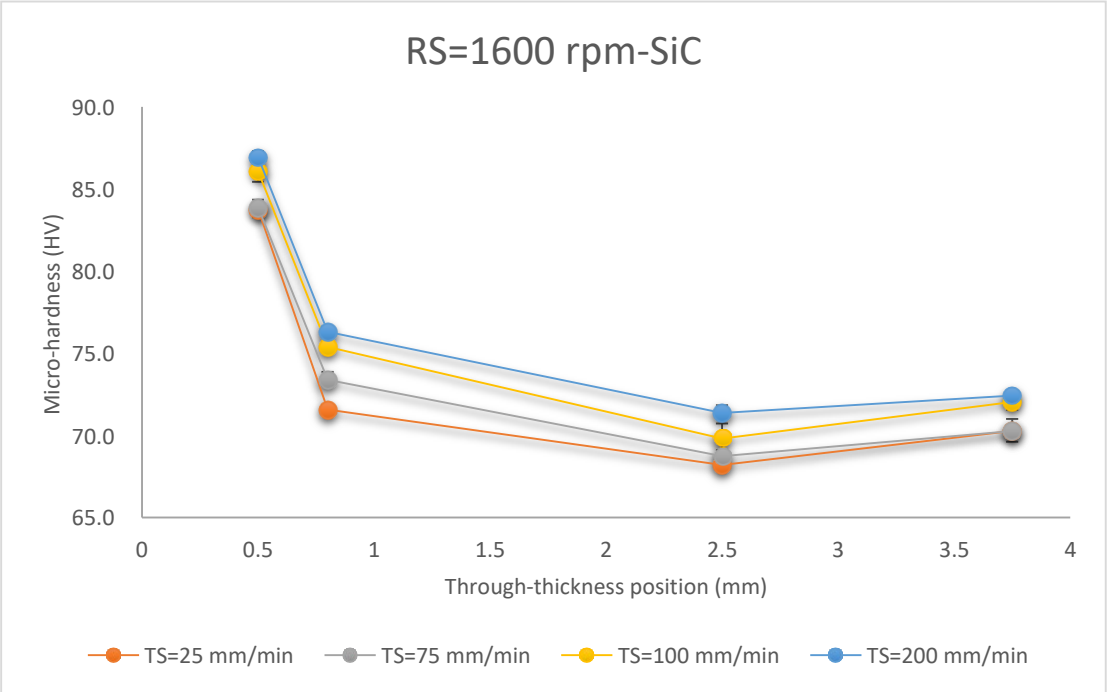

Figure 4.16: Effect of translational speed @ RS=1600 rpm with SiC

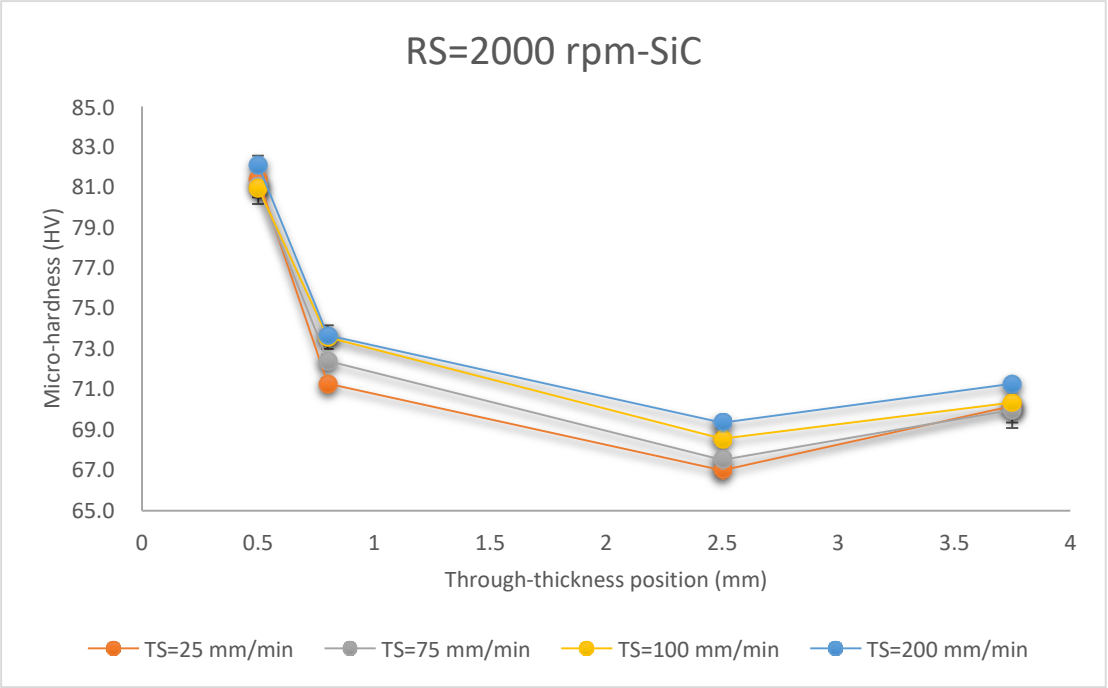

Figure 4.17: Effect of translational speed @ RS=2000 rpm with SiC

4.3.2 Effect of rotational speed on micro-hardness. Figures (4.18-4.21) represent the effect of rotational speed on micro-hardness for FSP without SiC. The Figures suggest that as the tool rotational speed increases, the micro-hardness value decreases for each translational speed. When a higher tool rotational speed was used, higher heat input was needed during FSP. This increase in the heat input resulted in higher grain

growth; hence, the micro-hardness value decreased. Following these results, it can be said at lower rotational speed, more grain refinement can be obtained [59, 64]. For example, for a translational speed of 25 mm/min, when the tool rotational speed was 1200 rpm, the micro-hardness within 1.25 mm from the top edge was 67.4 HV; then the value increased to around 69.3 HV, and 71.4 HV within 2.5mm and 3.75 mm respectively. These values were lower by 1.02%, 2.25%, and 2.45% when compared to the micro-hardness values of a tool rotational speed of 800 rpm (discussed earlier). When the FSP was done using a higher rotational speed of 1600 rpm, the average micro-hardness values were 66.3 HV, 68.7 HV, and 70.8 HV within 1.25 mm, 2.5mm, and 3.75 mm respectively. Finally, when a tool rotational speed of 2000 rpm was used, the micro-hardness values were the minimum in the case of a translational speed of 25 mm/min. The values obtained were 65.2 HV, 67.3 HV, and 70.1 HV within 1.25 mm, 2.5mm, and 3.75 mm respectively. The minimum hardness value was obtained at a rotational speed of 2000 rpm and translational speeds of 25 and 75 mm/min. The maximum hardness value was obtained at a rotational speed of 800 rpm and a translational speed of 200 mm/min.

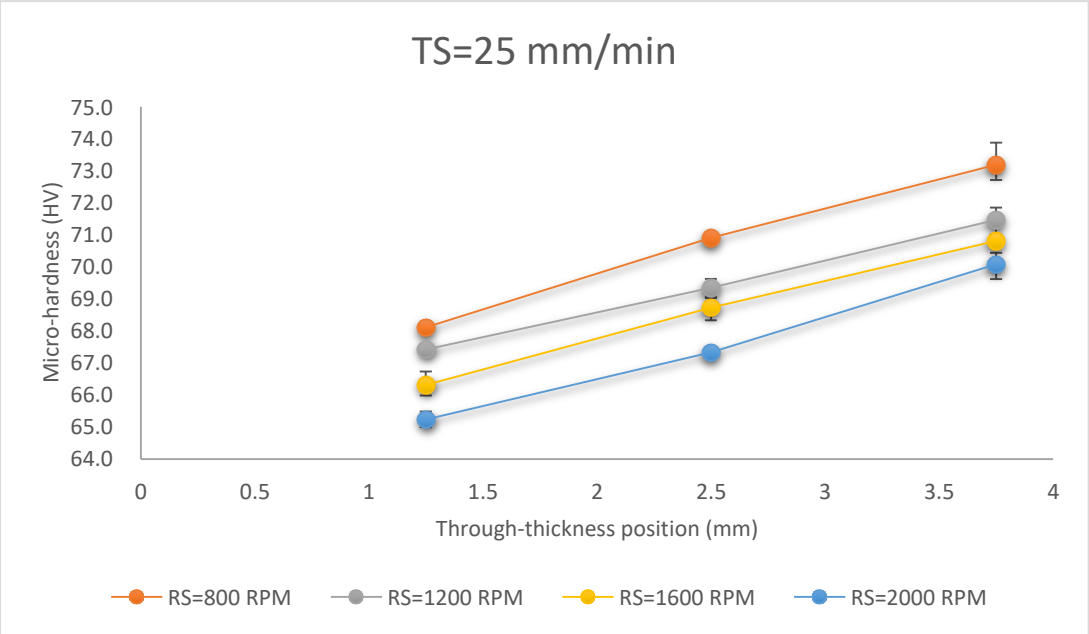

Figure 4.18: Effect of rotational speed @ TS=25 mm/min

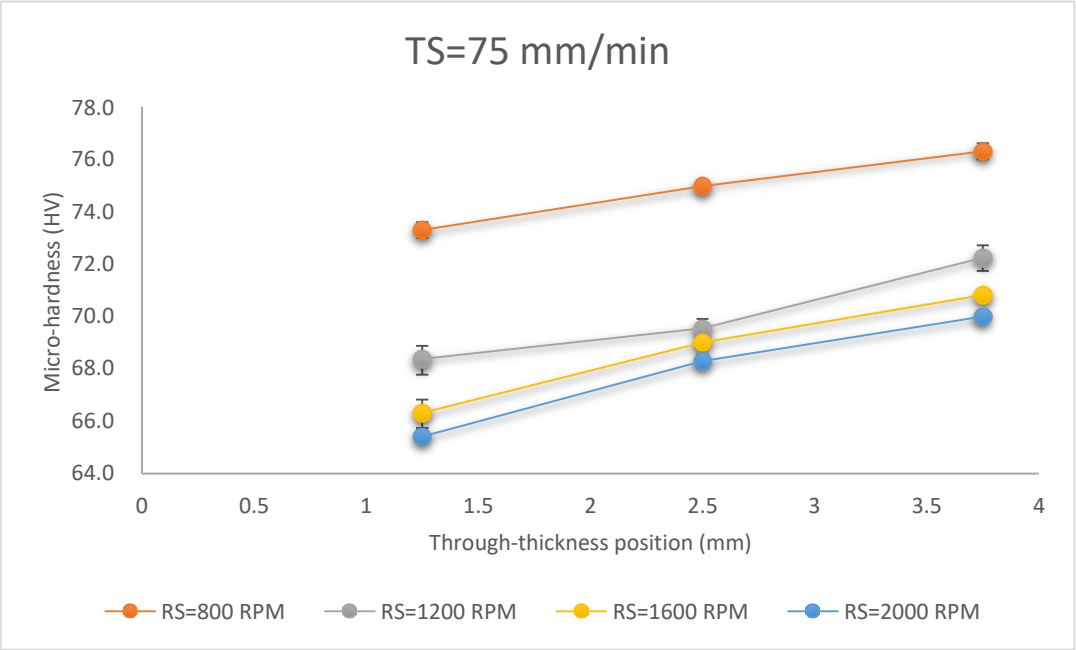

Figure 4.19: Effect of rotational speed @ TS=75 mm/min

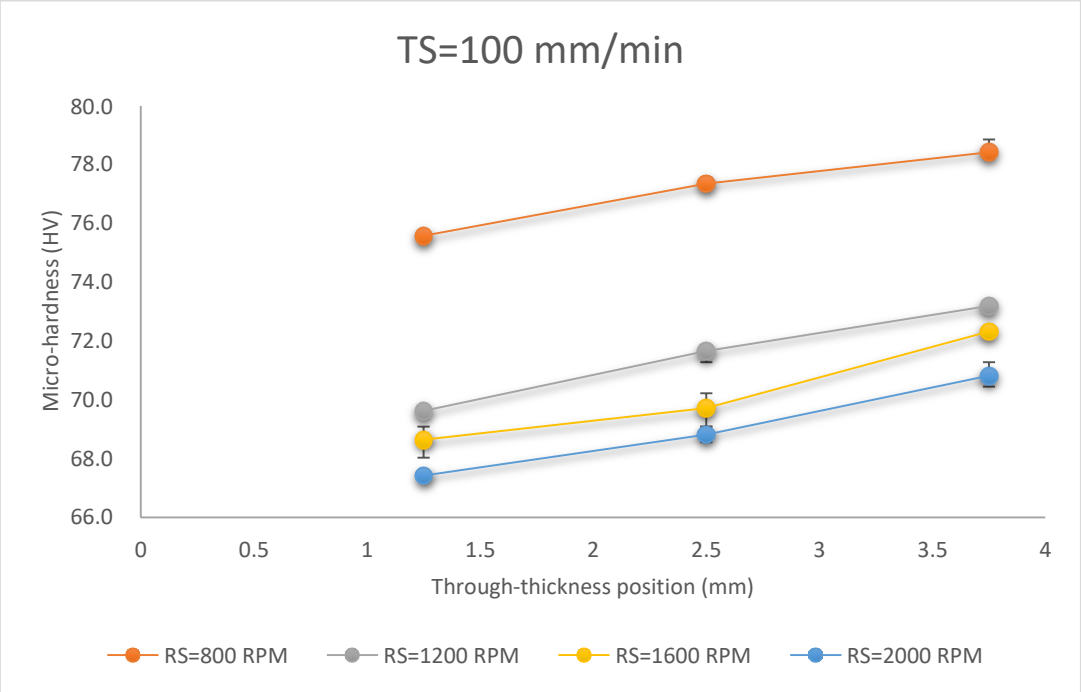

Figure 4.20: Effect of rotational speed @ TS=100 mm/min

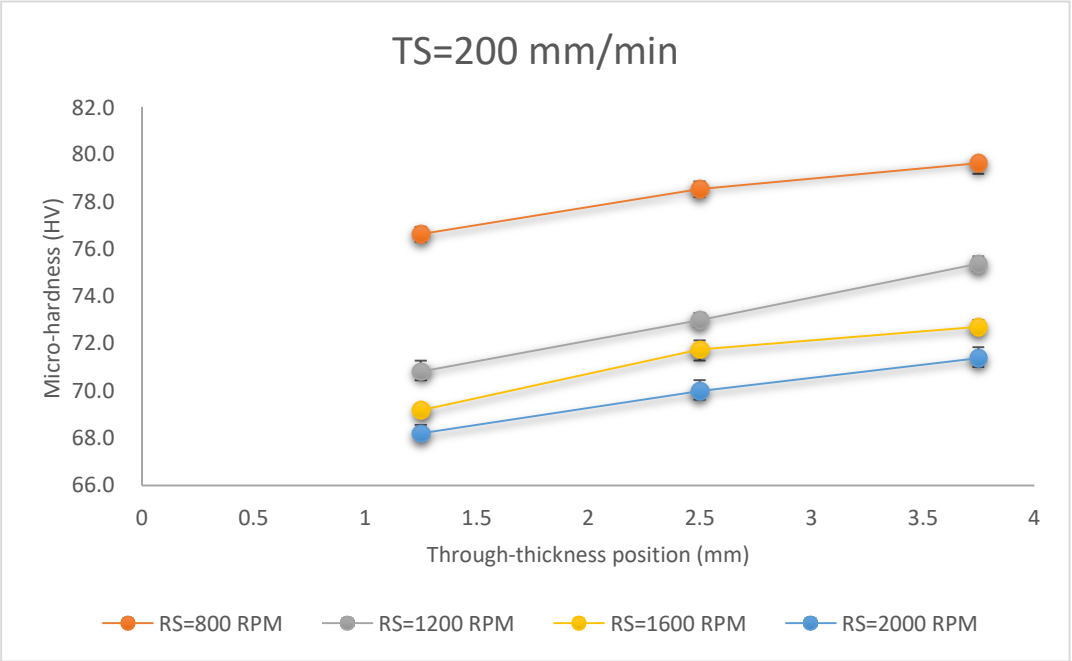

Figure 4.21: Effect of rotational speed @ TS=200 mm/min

Figures (4.22-4.25) represent the effect of rotational speed on micro-hardness for FSP with SiC. It can be observed that as the rotational speed increased, the micro-hardness values increased. These two observations are applicable inside the region with no SiC addition and are in agreement with the previous section. Furthermore, micro-hardness values below the 0.5 mm SiC groove by 0.3 mm were taken. The results suggest that the micro-hardness value for this through-thickness position is always higher than the micro-hardness value without addition of SiC. For example, in the case of a tool rotational speed of 800 rpm and a translational speed of 25 mm/min, the average micro-hardness reading within 0.8 mm from the upper edge, that is 0.3 mm below the groove, was about 74.5 HV which is higher by 1.8% than the maximum hardness value (73.2 HV) inside the region of FSP only without SiC. This is applicable for other FSP conditions. This suggests that the SiC particles were able to reach a very small distance under the groove during the process. The micro-hardness values inside the SiC groove region were between 81 HV and 103 HV. The maximum value of micro-hardness was obtained when a tool rotational speed of 1200 rpm and a translational speed of 200 mm/min were used. On the other hand, the lowest micro-hardness value inside the SiC groove region was obtained using an FSP condition of 2000 rpm and 100 mm/min. The variation within the readings is almost negligible as can be seen from the error bars provided in the graphs.

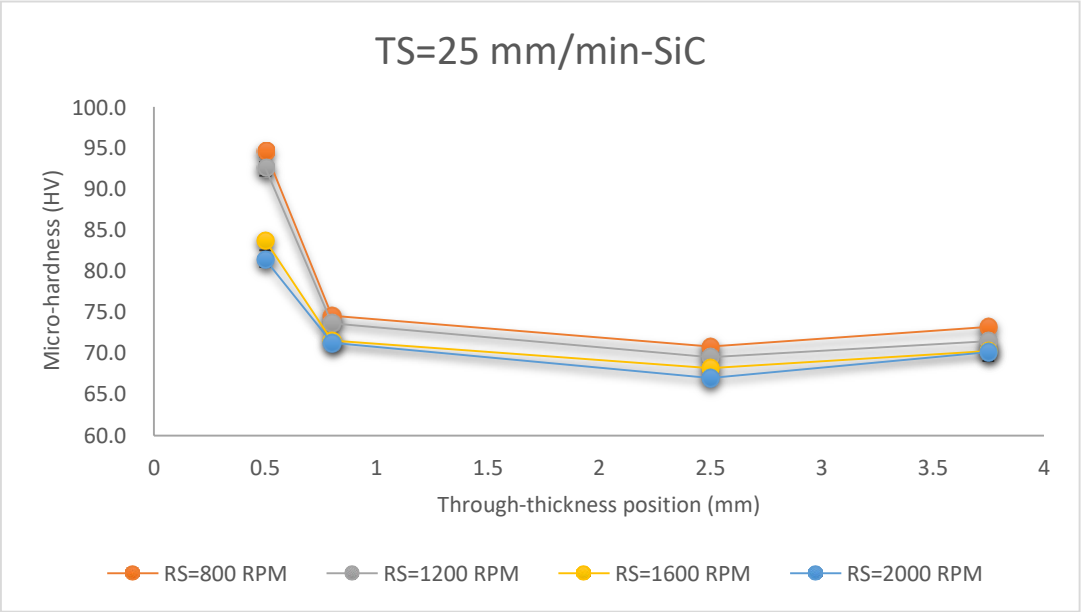

Figure 4.22: Effect of rotational speed @ TS=25 mm/min with SiC

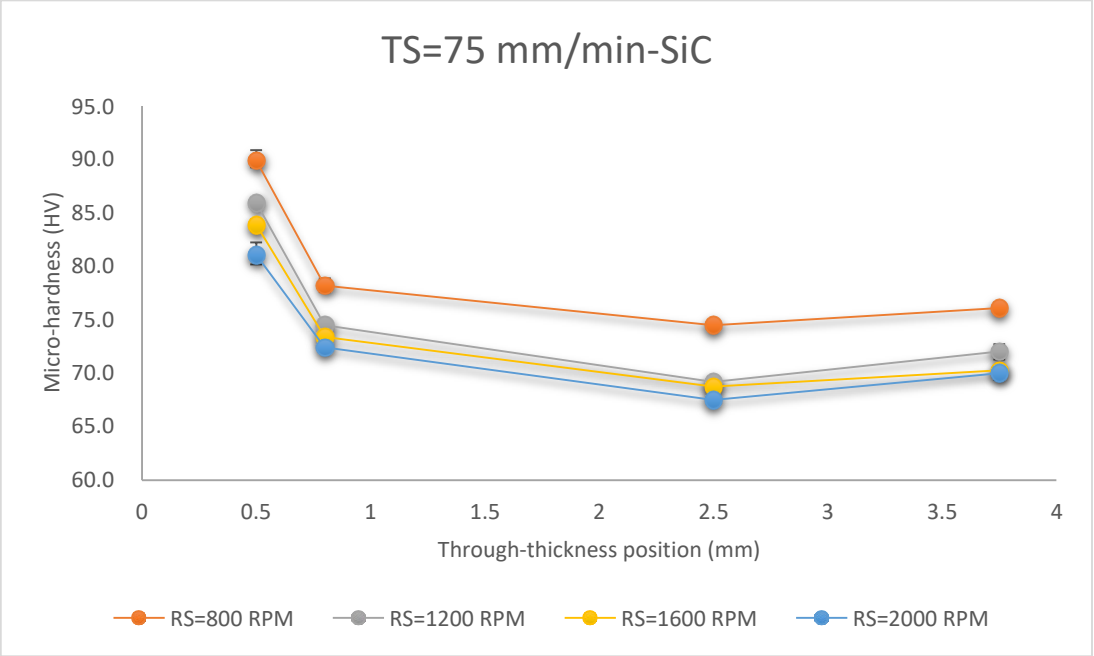

Figure 4.23: Effect of rotational speed @ TS=75 mm/min with SiC

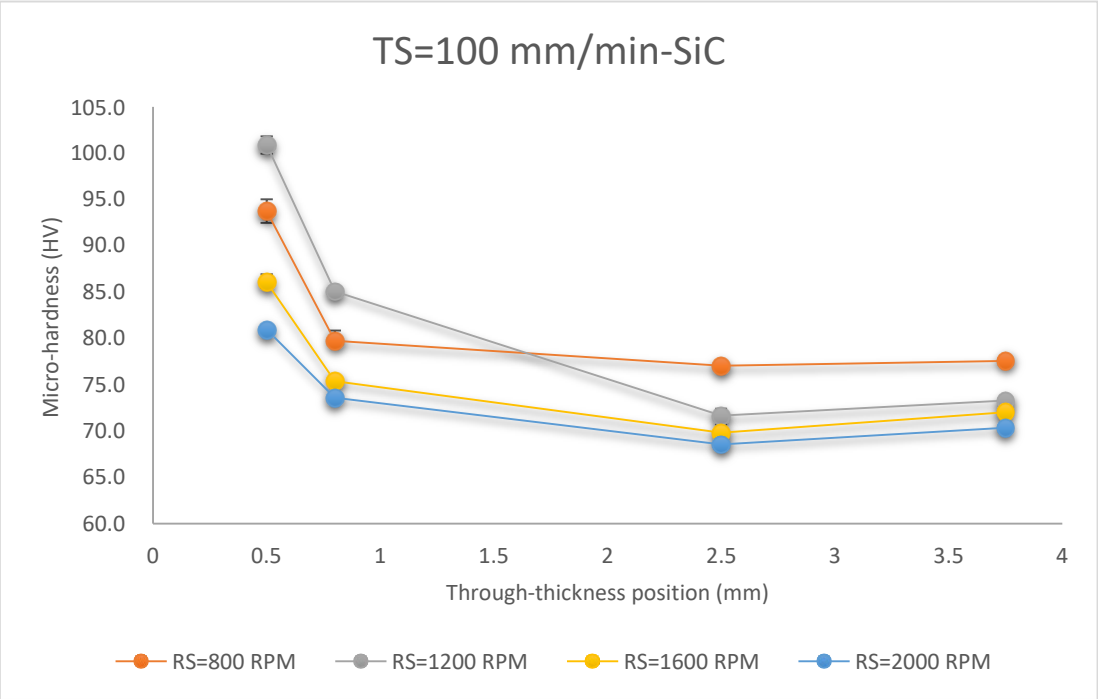

Figure 4.24: Effect of rotational speed @ TS=100 mm/min with SiC

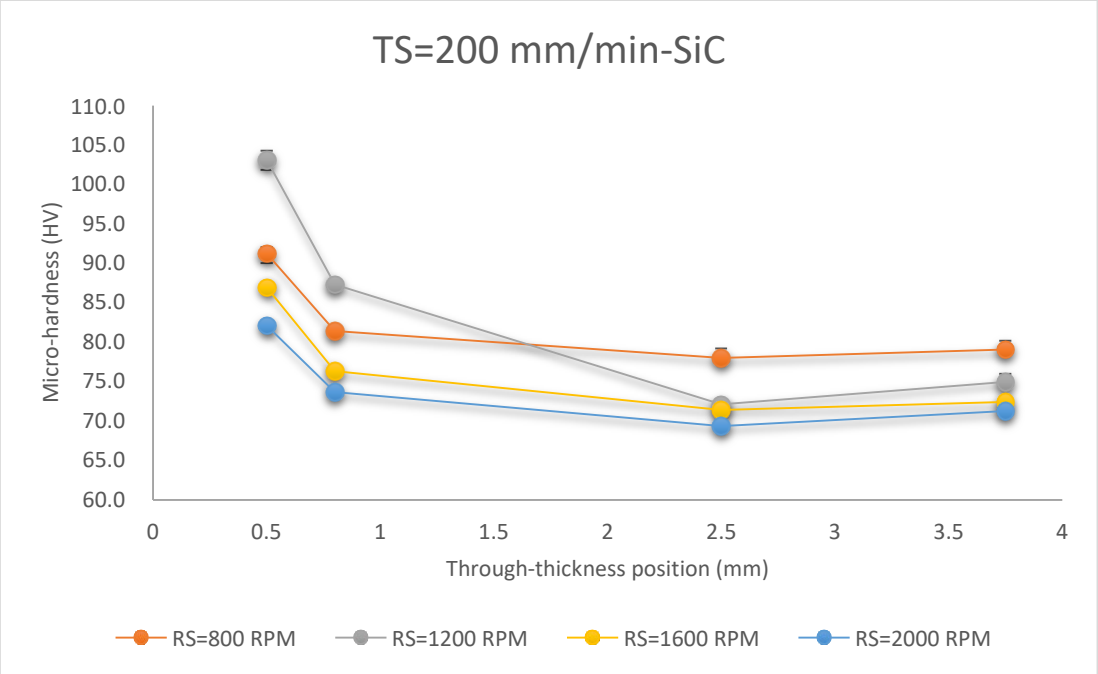

Figure 4.25: Effect of rotational speed @ TS=200 mm/min with SiC

Table 3 in Appendix D introduces a micro-hardness comparison between FSP with SiC and both FSP without SiC and as-processed. The maximum micro-hardness value inside the 0.5 mm SiC groove was compared with the maximum micro-hardness value for FSP without SiC for each FSP condition and with the micro-hardness value of the as-received specimen. The result suggests that the addition of SiC can guarantee

an increase of up to 37.7% in the micro-hardness when compared to the maximum value of FSP with no SiC addition. This percentage increase corresponds to the FSP condition of 1200 rpm and 100 mm/min. Furthermore, with the addition of SiC the micro-hardness value was increased to more than its half value that is 52.3% when compared to as-received value. This percentage increase was obtained in FSP condition of 1200 rpm and 200 mm/min. On the other hand, the minimum percentage increase of the micro-hardness value that the addition of SiC can guarantee were 14.4% and 19.6% when compared to FSP without SiC and as-received respectively. These two percentages were both obtained using FSP condition of 2000 rpm and 100 mm/min. Micro-hardness results are in excellent agreement with both the thermal and microstructural analysis.

Chapter 5: Response Surface Modeling & Optimization

5.1 Background & Review of Literature

One way to find out the optimum operating conditions for a process is to use a set of experimental methods called the Response-Surface Methodology (RSM). Generally, this includes performing different experiments, then using the results obtained to come up with a methodology about the next step. This technique is a collection of statistical and mathematical techniques used to analyze and model problems where an output or a response of interest is affected by other inputs or variables with an objective to optimize this response [69]. The response-surface methodology is considered important in developing, analyzing, designing, and formulating recent products and scientific studies. Furthermore, it can be engaged in improving current studies [70]. The factors in each set of experiments consist of various values or levels of the operating conditions. Some may be quantitative such as temperatures and rotational speeds, while others can be categorical. Usually, the categorical variables are analyzed separately via establishing a comparison between the best operating conditions and the quantitativevariables through the various combinations of the categoricalones. The major method followed for quantitative variables consists of fitting a second order (quadratic) or first order (linear) function in order to predict one or more outputs or response variables. After this, different analyses are used in order to find the optimum operating conditions or input variables. Although the response surface may seem like a simple regression problem, throughout the analysis there are different intricacies used which are enough to consider the RSM different from routine regression problems. Some of these intricacies are the assessment of the fit, the various follow-up analyses that are used depending on the type of model used in the fitting, the use of coded predictor variables, and the significance of visualizing the response surface. Moreover, the method includes unique experimental-design issues, as a result of the emphasis on iterative experimentation as well as the need for sparse designs which can be built-up according to the requirements of the experimenter [71]. In this study, a quadratic model was developed for micro-hardness. Three different input variables were used which are the tool rotational speed, the translational speed, and the through-thickness position. An optimization of the response was then conducted in order to decide the optimum input variables that can give maximum hardness. Finally,

sensitivity analysis was carried out for the sake of finding the variables that highly affect the response. In general, the mathematical models are used to predict one or more output responses. In addition, they can be used to establish a relationship between input variables and outputs via optimization. Several research studies proved that the development of an empirical methodology can be achieved by an appropriate use of statistical design of experimental techniques. Elangovan et al. [69] predicted the tensile strength of friction stir welded AA2219 aluminum alloy joints that had a thickness of 6 mm by developing an empirical relationship. This was successfully done by an appropriate incorporation of tool profiles and welding parameters. The mathematical model was able to predict that at a tool rotational speed of 1600 rpm, translational speed of 75 mm/sec, and at an axial force of 12 kN, the joint fabricated using square pin profile tool showed excellent tensile properties. Palanivel et al. [72] developed a mathematical model to predict the mechanical properties of friction stir welded AA6351 aluminum alloy with a thickness of 6 mm. The results showed that by increasing the tool rotational speed, translational speed, and the axial force, the yield strength and the ultimate tensile strength reached a maximum value; then they decreased. Both Laxminarayan and Balasubramanian [73,74] were able to develop a mathematical model of 6 mm thickness friction stir welded AA7039 aluminum and RDE 40 Al alloy. In both studies, three input variables were used: the tool rotational speed, the translational speed, and the axial force. Results from both studies showed that the greatest influence on tensile strength was from rotational speed. After optimization, a maximum tensile strength of 319 MPa was obtained at optimized tool rotational speed of 1460 rpm, translational speed of 40 mm/min, and axial force of 6.5 kN. Using the same input variables, Palanivel et al. [75] studied the tool pin profile in FSW of aluminum alloy dissimilar AA6351-T6 and AA5083-T6 6mm butt joint. At a tool rotational speed of 950 rpm, translational speed of 63 mm/min, and an axial force of 14.72 kN, the joints fabricated straight square pin profiled tool revealed the best tensile properties. In another study, Al-Jarah et al. [70] successfully developed an empirical relationship to predict the micro-hardness and the yield strength of FS welded aluminum alloy. Four different input variables were considered in the study: tool rotational speed, translational speed, tool shoulder diameter, and welding plate thickness. Optimization results showed that the maximum micro-hardness can be obtained at a tool rotational speed of 1000 rpm, translational speed of 0.5 mm/sec, shoulder diameter of 24 mm, and welding plate thickness of 6 mm. However, the best

combination of the input variables that resulted in a maximum yield strength were at a tool rotational speed of 1000 rpm, translational speed of 1.5 mm/sec, shoulder diameter of 24 mm, and welding plate thickness of 6 mm. Both the experimental and the modeled results showed excellent agreement. Dinaharan and Murugan [76] were able to identify a set of input variables that will guarantee higher ductility, wear resistance, and tensile strength while using FSW in joining aluminum matrix composite. A mathematical model was successfully developed with four different parameters: the tool rotational speed, translational speed, the axial force, and the weight percentage of ZrB_2. The optimized results showed that, at a tool rotational speed of 1132 rpm, translational speed of 51 mm/min, axial force of 5.8 kN and with 10% weight of ZrB_2, maximum ultimate tensile strength of 226 MPa, percentage elongation of 0.76%, whereas a minimum wear resistance of 286.15×10^{-5}mm³/m were obtained. These optimized input variables can be used to automate the friction stir welding process in order to obtain desirable joint properties.

5.2 Working Limits of Parameters

As mentioned earlier, different trials were FSPed using different combinations of tool rotational and translational speeds. This was done so as to discover the feasible working limits of FSP parameters. Three factors -- the tool rotational speed (S), the translational speed (T), and the through-thickness position (P) were used to find out the micro-hardness model. Before starting, it was required to define the working range of tool rotational speed and translational speed. Since the purpose of the optimization is to maximize the response, the working range was decided upon after careful analysis of micro-hardness results. Furthermore, this was followed by an inspection of the microstructure for all the trials. The results obtained were then compared to the base metal mechanical properties and microstructure. At a value of rotational speed of 2000 rpm, the results for the micro-hardness and tensile properties were lower than those obtained at the other rotational speeds and base metal properties. This was also the case for a translational speed of 25 mm/min. However, for rotational speeds of 800 rpm, 1200 rpm, and 1600 rpm and for translational speeds of 75 mm/min, 100 mm/min, and 200 mm/min, the results were better and higher than both the results obtained using a rotational speed of 2000 rpm, and those obtained at translational speed of 25 mm/min. Furthermore, they were higher than those of the base sample. Hence, the working limit was defined accordingly. Previous discussion of the microstructure showed that the

structure of the trials selected within the working limit were homogenous and equiaxed. The chosen levels of the selected process parameters with their units and notations are presented in Table 5-1.

Table 5-1: Micro-hardness model parameters and their levels

Variable	Level		
	(−1)	(0)	(+1)
Rotational speed (rpm)	800	1200	1600
Translational speed (mm/min)	75	100	200
Through thickness (mm)	1.25	2.5	3.75

5.3 Development of Mathematical Model

Response surface methodology (RSM) is a collection of statistical and mathematical techniques used to analyze and model problems where an output or a response of interest is affected by other inputs or variables with an objective to optimize this response [77]. The representation of independent factors in a quantitative form is possible in several experimental conditions. Eq. (1) can be thought of as a functional relationship of these factors. In such equation the function Φ is usually called the response function.

$$Y=\Phi(x1, x2\ldots xk) \pm er \quad (1)$$

The term e_r is called the residual and is used to measure the variation or experimental errors. A characteristic surface is responded for a certain set of independent variables. Generally, the mathematical form of the response function is unknown; however, it can be approximated inside the working limit region through a polynomial. Throughout this study, RSM was used to come up with a mathematical model in the form of multiple regression equations for the micro-hardness (Hv) of FSPed Mg/SiC magnesium alloy composite. The independent variable considered in this investigation was viewed as a surface to which the model was fitted. Eq. (2) is the general second order regression equation that is used to represent the response surface [74]. However, when only three factors are considered in the analysis, Eq. (2) can be displayed as shown in Eq. (3) [73].

$$Y = b_0 + \sum b_i x_i + \sum b_{ii} x_{i+} \sum b_{ij} x_i x_j + e_r \quad (2)$$

$$Hv = b0 + b1(R) + b2(T) + b3(D) + b11(R^2) + b22(T^2) + b33(D^2) + b12(RT) + b13(RD) + b23(TD) \quad (3)$$

In this study, central composite face centered (CCF) design shown in Table 5-2 was implemented to estimate the regression coefficients. The star points were located at the center of each face of every factorial space that was used, hence, $\alpha = \pm 1$. This diversity requires three levels of each of the three factors. The central composite face centered technique delivers high quality predictions inside the entire design working limit and, therefore, there is no need for points outside the original factor limit/range. The required number of experimental points is $N = 2^3 + 6 + 6 = 20$. There are eight factorial experiments (3 factors on two levels, 2^3) with added 6 star points and center point (average level) repeated 6 times to calculate the pure error. The analysis was carried out using the Design Expert statistical software package where the upper limit of a factor and the lower limit were coded as +1 and -1 respectively. Before determining the mathematical model, it was required to define the significant coefficients at 95% confidence level. Considering only these coefficients, the final mathematical model to estimate the micro-hardness is given:

$$\text{Micro-hardness } (Hv) = 71.73 - 3.32\,(S) + 1.70\,(T) + 2.03\,(P) + 2.07S^2 - 0.53T^2 - 0.48P^2 - 0.24\,(ST) + 0.26\,(SP) - 0.44\,(TP) \quad (4)$$

Table 5-2: Experimental design matrix and results

Coded Value			Real Values			Micro-hardness
S	*T*	*P*	Rotational speed (rpm)	Translational speed (mm/min)	Through thickness (mm)	(Hv)
−1	−1	−1	800	75	1.25	72.00
+1	−1	−1	1600	75	1.25	65.00
−1	+1	−1	800	200	1.25	76.60
+1	+1	−1	1600	200	1.25	69.10
−1	−1	+1	800	75	3.75	76.30
+1	−1	+1	1600	75	3.75	70.80
−1	+1	+1	800	200	3.75	79.60
+1	+1	+1	1600	200	3.75	72.70
−1	0	0	800	100	2.5	77.10
+1	0	0	1600	100	2.5	70.80
0	−1	0	1200	75	2.5	69.80
0	+1	0	1200	200	2.5	72.90
0	0	−1	1200	100	1.25	69.60
0	0	+1	1200	100	3.75	73.20
0	0	0	1200	100	2.5	71.70
0	0	0	1200	100	2.5	71.80
0	0	0	1200	100	2.5	71.60
0	0	0	1200	100	2.5	71.80
0	0	0	1200	100	2.5	71.60
0	0	0	1200	100	2.5	71.30

5.4 Checking Adequacy of Model

The analysis of variance (ANOVA) technique was used to test the adequacy of the suggested model. The complete ANOVA analysis is shown in Table 5-3. The determination coefficient (R^2) shows how good the fit for the developed model is. Results of the analysis show that the determination coefficient is R^2=0.9963. Hence, less than 1% of the total variations cannot be explained by the model. Results also show a high significance of the model since the adjusted R^2=0.9929 which is considered high. Both adjusted and predicted R^2 show a good match. A comparison of the predicted values at the design points to the average prediction error is given by the adequate precision. Furthermore, the value of the coefficient of variation (CV=0.37) is considered a low value and this shows improved reliability and precision of the conducted experiments. Looking at the probability value higher than F of the model, it can be seen that it is less than 5%. This also insures that the model is significant. The

lack of fit is also not significant which is always desirable. Tool rotational speed (S), translational speed (T) and through-thickness position (P), in addition to the interaction effect of rotational speed with through- thickness position (SP), interaction effect of rotational and translational speeds (ST), interaction effect of translational speed with through-thickness position (TP) and second order term of tool rotational speed (S), translational speed (T) and through-thickness position (P) all have significant effect.

Different combinations of process parameters and through-thickness positions that are not included in the experimental design matrix but inside the working range were used to verify the model. When tool rotational speed of 1600 rpm, translational speed of 75 mm/min and at 3.75 mm through-thickness position the model was able to predict a micro-hardness value of 70.7466 Hv. Average of three micro-hardness readings were taken using same process parameters, and the experimental micro-hardness value was obtained to be 70.8 Hv. The same thing was repeated at 800 rpm, 100 mm/min, and at 3.75 mm/min through-thickness position. Predicted micro-hardness value was 78.4017 Hv compared to an average experimental micro-hardness value of 78.4 Hv. Finally, when tool rotational speed of 1200 rpm, translational speed of 200 mm/min and at 1.25 mm through-thickness position the model was able to predict a micro-hardness value of 70.830 Hv while the average experimental value obtained to be 70.8 Hv. Hence, the developed model shows excellent capability of predicting micro-hardness values inside the working range.

Normal distribution of the residuals was insured through the normal probability plot of the micro-hardness shown in Figure 5.1 that shows how the residuals are falling on the straight line. From all the above, excellent adequacy of the regression model can be concluded. Figure 5.2 shows a comparison plot of the actual and the prediction for each observed value. It can be seen from the F value and percentage contribution that the tool rotational speed is most sensitive to micro-hardness followed by through-thickness position and translational speed. Hence, a careful control of tool rotational speed is desirable to reach effective improvement in micro-hardness.

Table 5-3: ANOVA results for micro-hardness

Source	Sum of squares	df	Mean square	F value	p- value probability > F	Contribution (%)
Model	195.89	9	21.77	297.47	< 0.0001	-
Tool rotational speed, S	110.22	1	110.22	1506.40	< 0.0001	56.03
Translational speed, T	28.90	1	28.90	394.97	< 0.0001	14.60
Through thickness, P	41.21	1	41.21	563.19	< 0.0001	20.95
$\mathbf{S^2}$	11.81	1	11.81	161.47	< 0.0001	6.00
$\mathbf{T^2}$	0.76	1	0.76	10.45	0.0090	0.39
$\mathbf{P^2}$	0.63	1	0.63	8.56	0.0151	0.32
ST	0.45	1	0.45	6.17	0.0324	0.23
SP	0.55	1	0.55	7.53	0.0207	0.28
TP	1.53	1	1.53	20.93	0.0010	0.78
Residual	0.73	10	0.073	-	-	0.37
Lack of fit	0.56	5	0.11	3.22	0.1125	0.28
Pure error	0.17	5	0.035	-	-	0.08
Corrected total	196.63	19	-	-	-	-

Standard deviation = 0.27
Mean = 77.26
Coefficient of variation = 0.37
Press = 5.43

R^2= 0.9963
Adjusted R^2= 0.9929
Predicted R^2= 0.9724
Adequate R^2= 73.717

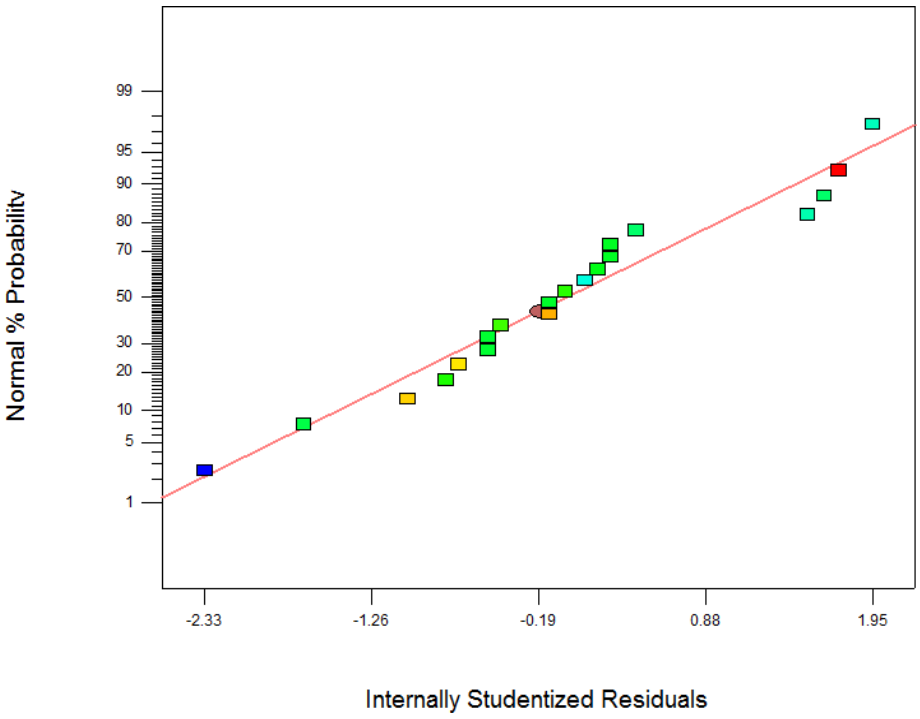

Figure 5.1: Normal probability plot for residuals

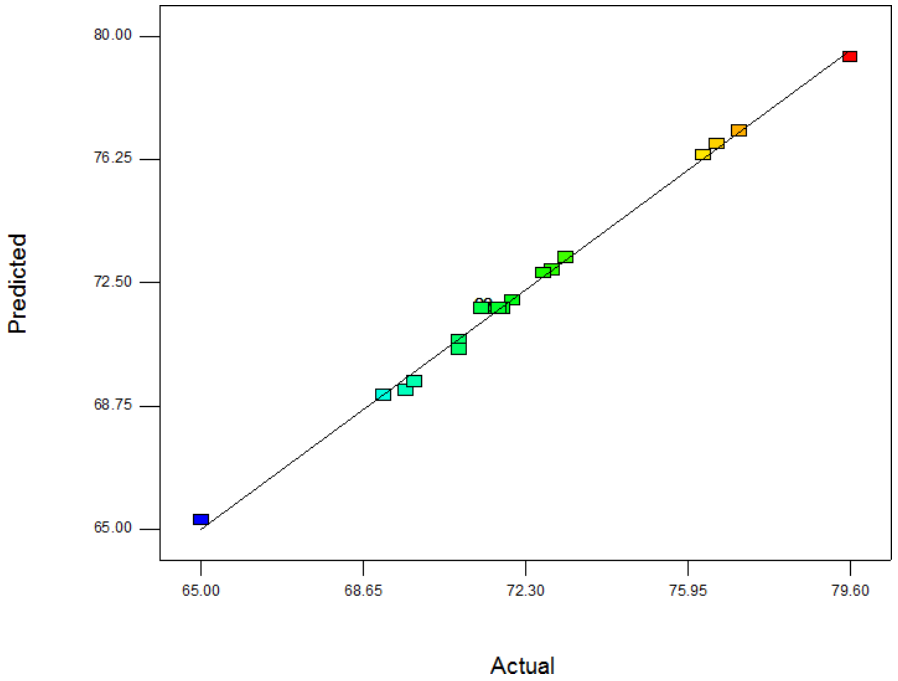

Figure 5.2: The actual vs. predicted response for micro-hardness

5.5 Optimizing Parameters

Generally, a contour plot is used as a visual aid to display the region of optimal factor settings. For first order models, such plot can be represented as a simple series of parallel lines; nevertheless, contour plot can show more complexity for second order response surfaces. A stationary point can present either a saddle point, maximum response, or minimum response point. Hence, when the stationary point is obtained, a characterization of the response surface is necessary. This can be done by identifying the type of stationary point found through an examination of the contour plot. After that, the optimum is located with an acceptable accuracy by characterizing the shape of the surface [78]. Response surfaces were developed for the model. The objective function was to maximize the response. Constraints on the three parameters with a goal to stay within the working range were set. The optimal response point was clearly identified through the response surfaces. According to Hou et al. [79] the response surface methodology is used to find the optimal process parameters which can guarantee a maximum or minimum value of the response. Since the objective function in this study is to maximize the response which is the micro-hardness, the optimum process parameters are considered to be those that correspond to the highest value of the micro-hardness. Maximum micro-hardness estimated from the response surface and contour plots is 79.39 HV which is given by the following optimized FSP parameters: rotational speed of 800 rpm and translational speed of 200 mm/min. This optimized value was recorded at through-thickness position of 3.75 mm. This shows excellent agreement with the experimental work. Figure 5.3 represents the contour plots of the process parameters of FSP in addition to the through-thickness position. From Fig 5.3 (a) it can be noticed that maximum micro-hardness can be obtained at lowest rotational speed and highest translational speed. This contour plot is at a through-thickness position of 3.75 mm. As the rotational speed decreases more temperature will be included in the process which will result in grain growth and accordingly lower micro-hardness. However, decreasing the translational speed will save processing time and will subject the work piece under process to less temperature and thus lower grain growth. This will result in higher micro-hardness. Figure 5.3 (b) suggests that micro-hardness increases as through-thickness position increases. This is true because the top surface is closer to the heat source, and this means higher temperature. Hence, lower

micro-hardness values near the top edge can be observed. The contour plot is at the highest translational speed that is at 200 mm/min. Figure 5.3 (c) shows the effect of translational speed and through-thickness position on micro-hardness values. The optimum point of micro-hardness can be seen at the top right at maximum translational speed and through-thickness position. The contour plot is at a rotational speed of 800 rpm. The 3D response surface plots for micro-hardness are shown in Figure 5.4. It can be seen that the optimum value (highest value) of micro-hardness is shown on the apex of the response surface. By examining the plots, it is clear that variation in micro-hardness is more sensitive to variation in rotational speed more than variations in through-thickness position and translational speed. The plots also show an interaction between the factors.

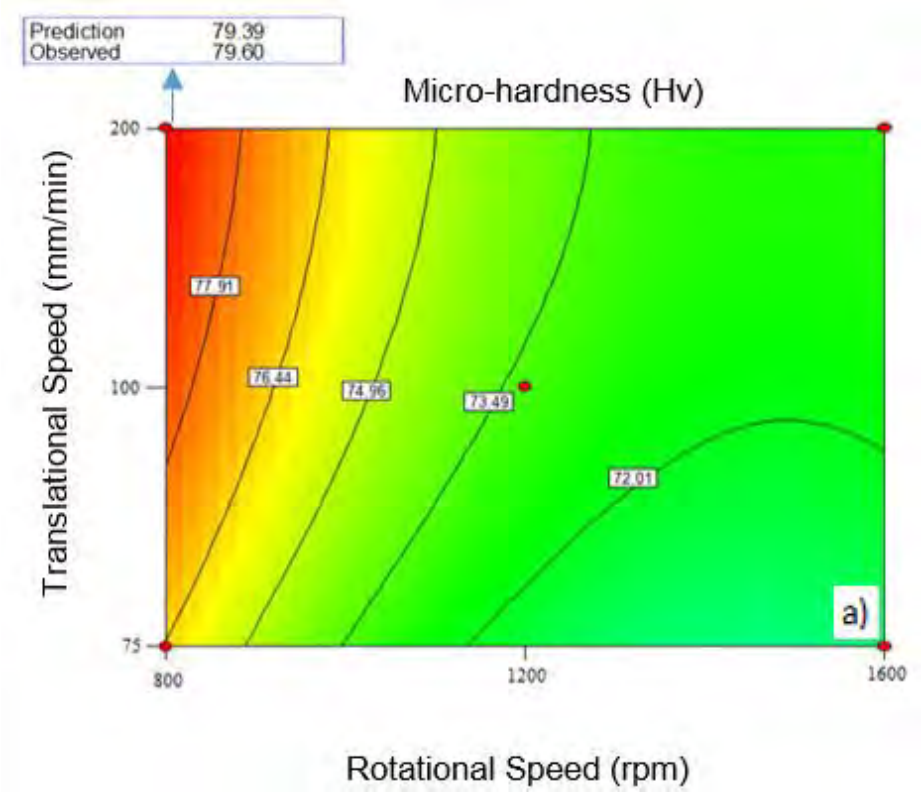

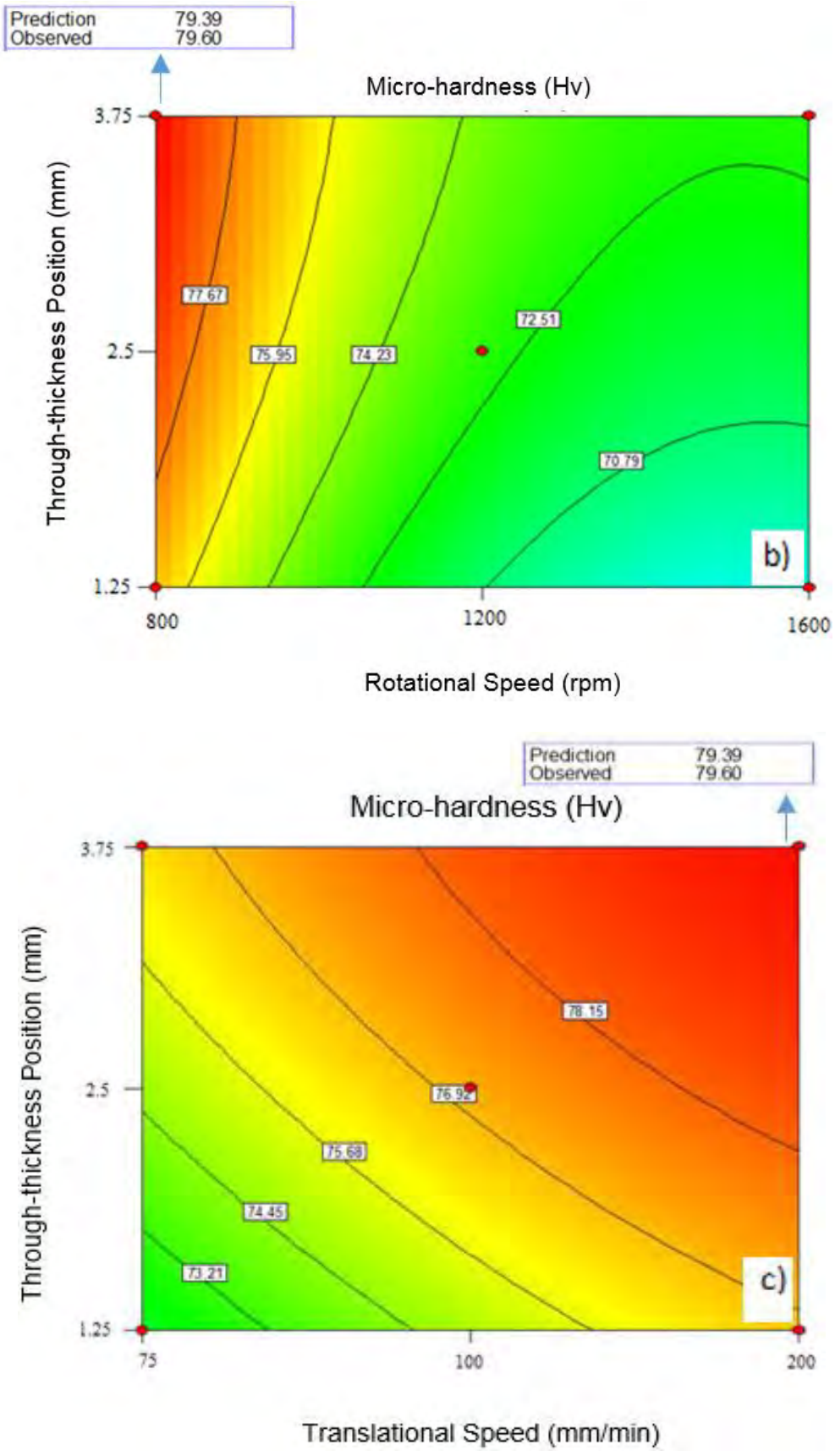

Figure 5.3: Contour plots for micro-hardness

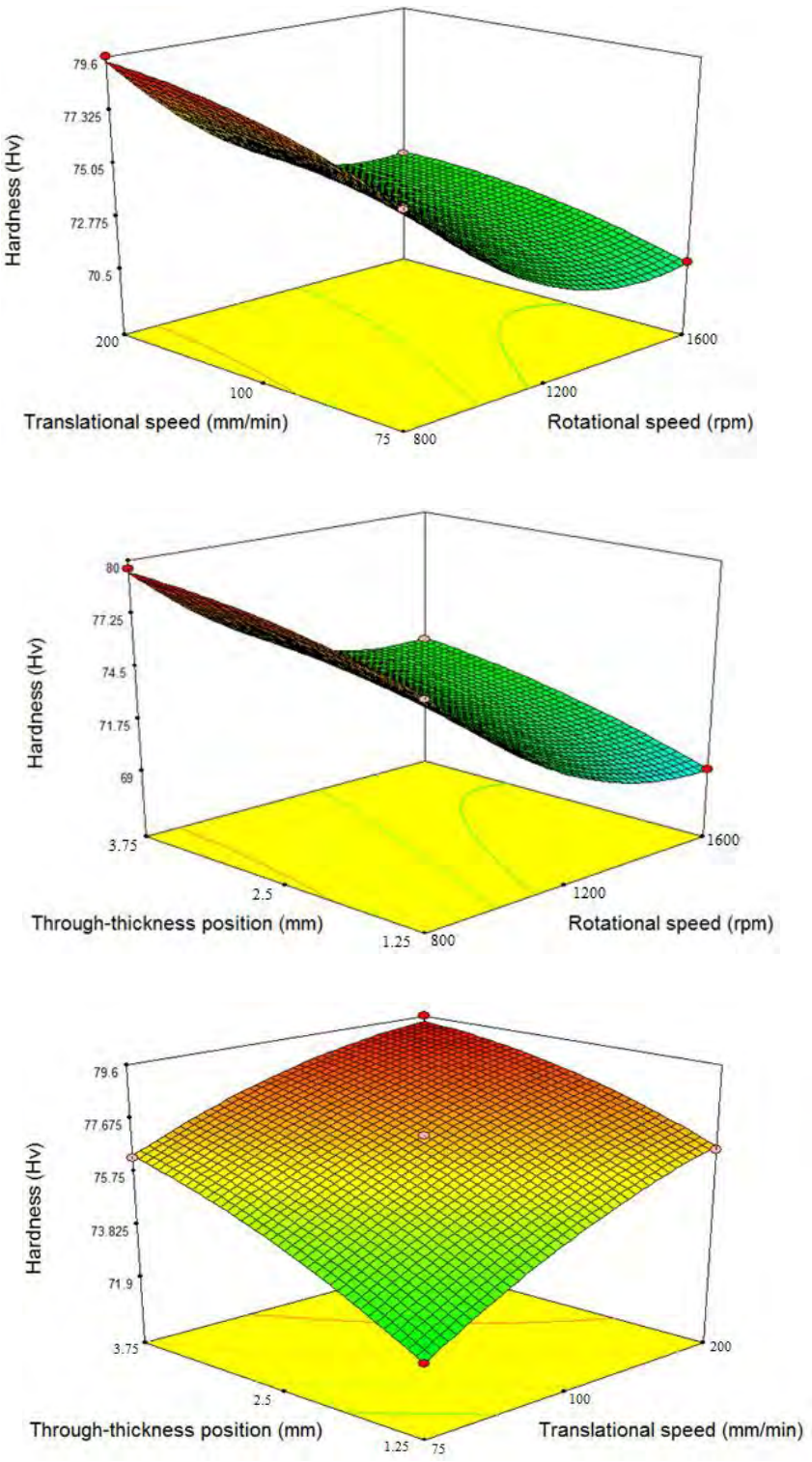

Figure 5.4: Response plots for the three factors

Chapter 6: Conclusion & Future work

6.1 Conclusion

Friction stir processing is a relatively new fabrication technique which can be easily used to achieve better mechanical properties in magnesium alloys compared to other fabrication processes. The process is controlled by various parameters like tool rotational speed, and translational speed. Using FSP with SiC particles to get the Mg/SiC composite proved to be very effective in obtaining superb mechanical and microstructural properties of the processed material. The conclusions of this research are as follows:

(1) Friction stir processing of Mg AZ 31 magnesium alloy was successfully conducted using different combinations of tool rotational speed and translational speed.
(2) Mg/SiC composite was successfully fabricated using FSP at different combinations of tool rotational speed and translational speed.
(3) In both cases, defect free processed samples were obtained. micro-hardness and microstructural tests were carried out
(4) Three level comparison between the micro-hardness and grain size of the base material, FSPed samples, and FSPed samples of Mg/SiC composite was introduced.
(5) The data from thermal profile suggests that more grain growth is obtained at higher rotational speeds, while grain refinement is obtained at higher translational speeds.
(6) Results suggested that controlling the process parameters can have a high effect on the resulting micro-hardness and microstructure.
(7) Finer and more homogenous grain structure can be achieved by FSP. This helps in improving ductility and formability of the material at elevated temperatures, and improves its superplastic behavior. Microstructural results were in excellent agreement with the thermal analysis.
(8) Maximum micro-hardness and finer grain size were obtained at lowest rotational speed and highest translational speed. As the rotational speed decreases more temperature will be included in the process which will result in grain growth and accordingly lower micro-hardness. However, decreasing the translational speed

will save processing time and will subject the work piece under process to less temperature and thus lower grain growth. This will result in higher micro-hardness.

(9) Micro-hardness results suggest an increase as through-thickness position increased. This is because the top surface is closer to the heat source which means higher temperature. Hence, lower micro-hardness values near the top edge were observed.

(10) Micro-hardness results showed that a significant amount of increase in the micro-hardness can be obtained by using the Mg/SiC composite

(11) Micro-hardness results were in excellent agreement with both the thermal and microstructural analysis.

(12) The model developed using the Response Surface Methodology showed an excellent adequacy and fit with a determination coefficient (R^2) of 0.9963 and a negligible amount of lack of fit. The model showed that all tool rotational speed (S), translational speed (T) and through-thickness position (P), in addition to the interaction effect of rotational speed with through-thickness position (SP), interaction effect of rotational and translational speeds (ST), interaction effect of translational speed with through-thickness position (TP) and second order term of tool rotational speed (S), translational speed (T) and through- thickness position (P) all have significant effect.

(13) Model showed that the tool rotational speed was the most sensitive parameter to micro-hardness. Hence, micro-hardness can be improved by a careful control of the tool rotational speed.

6.2 Future work & Recommendations

Some of the future works can include an investigation of the effect of FSP of Mg/ SiC composite on specimens with larger and deeper groove size. Another future work is to study the effect of increasing the number of FSP passes on the uniform distribution of the SiC particles within the Mg/SiC composite. The effect of other reinforcement such as multi-walled carbon nanotubes on the different mechanical properties can be also studied. Some of the recommendations can include enhancing the Response Surface Model by adding other inputs such as shoulder diameter and axial force. Other outputs/ responses such as grain size can be obtained using the same approach used to come up with the micro-hardness model. Finally, it is also recommended to explore different techniques to control the heat gain and the grain growth during the process such as the coolant type.

References

[1] Zweben C. (2002) *Metal matrix composites, ceramic matrix composites, carbon matrix composites and thermally conductive polymers matrix composites*. In: Harper CA (ed) Handbook of plastics, elastomers, and composites, 4th edn. McGraw Hill, New York, p. 321.

[2] Mangalgiri D. (1999) "Composite materials for aerospace applications". *J Bull Mater Sci.,* 22(3):657–664.

[3] Lloyd, D.J. (1994) "Particle reinforced aluminium and magnesium matrix composites".
Int. Mater. Rev., 39, 1-23.

[4] Tjong C., Ma Y. (2000) "Microstructural and mechanical characteristics of in-situ metal matrix composites". *Mater Sci Eng R.,* 29, 49–113.

[5] Thomas M., Nicholas D., Needham C., Church G., Templesmith P., Dawes J. (1991) The Welding Institute,TWI, International Patent Application No. PCT/GB92/02203 and GB Patent Application No. 9125978.8.

[6] Mishra S., Mahoney W., McFadden X., Mara A., Mukherjee K. (2000) "High strain rate superplasticity in a friction stir processed 7075 Al alloy". *Scripta Materialia,* 42(2), 163-168.

[7] Ma, Z.Y., Mishra, R.S., Mahoney, M.W. (2002) "Superplastic deformation behavior of friction stir processed 7075Al alloy". *Acta Mater.,* 50, 4419–4430.

[8] Kwon, Y.J., Shigematsu, I., Satio, N. (2003) "Mechanical properties of fine-grained aluminium alloy produced by friction stir process". *Scripta Materialia*, 49,785-789.

[9] Rhodes, C. G., Mahoney, M. W., Bingel, W. H., Spurling, R. A., Bampton, C. (1997) "Effects of Friction Stir Welding on Microstructure of 7075 Aluminium". *Scripta*
Materialia, 36(1), 69-75.

[10] Chang, C.I., Lee, C.J., Huang, J.C. (2004) "Relationship between grain size and Zener-Holloman parameter during friction stir processing in AZ31 Mg alloys". *Scr. Mater.,* 51, 509–514.

[11] Su, J.Q., Nelson, T.W., Sterling, C.J. (2003) "A new route to bulk nanocrystalline materials". *J. Mater. Res.,* 18(8), 1757–1760.

[12] Sun, N., Apelian, D. (2011) “Friction stir processing of aluminum cast alloys for high performance applications”. *The Journal of the Minerals, Metals & Materials Society,* 63(11), 44.

[13] Darras B., Khraisheh M., Abu-Farha F., Omar M. (2007) “Friction Stir Processing of Commercial AZ31 Magnesium Alloy”. *Journal of Materials Processing Technology,* 191, 77-81.

[14] Peel M., Steuwer A., Preuss M., Withers J. (2003) “Microstructure, mechanical properties and residual stresses as a function of welding speed in aluminum AA5083 friction stir welds”. *Acta Materialia,* 51, 4791–4801.

[15] Mirsha S., Ma Y. (2005) “Friction stir welding and processing”. *Materials Science and Engineering,* 50(2), 1-78.

[16] Khraisheh K., Darras B., Kalu P., M. Adams-Hughes, Namas C. (2005) “Correlation between the Microstructure and Forces Generated During Friction Stir Processing of AA5052”. *Materials Science Forum*, 475, 3043-3046.

[17] London B., Mahoney M., Bingel B., Ca-labrese M., Waldron D., “High Strain Rate Superplasticity in Thick Section 7050 Aluminum Created by Friction Stir Processing,” Proceedings of the Third International Symposium on Friction Stir Welding, Kobe, Japan, 27-28 September, 2001.

[18] Rhodes G., Mahoney W., Bingel H., Spurling A., Bampton C. (1997) “Effect of Friction Stir Welding on Microstructure of 7075 Aluminum”. *Scr. Mater.*, 36, 69–75.

[19] Liu G., Murr E., Niou S., McClure C., Vega R. (1997) “Micro-structural aspects of the friction-stir welding of 6061-T6 aluminum”. *Scr. Mater.*, 37(3), 355–361.

[20] Jata, K., Semiatin, L. (2000) “Continuous dynamic recrystallization during friction stir welding of high strength aluminium alloys”. *Scr. Mater.,* 43 (8), 743-749.

[21] Benavides S., Li Y., Murr E., Brown D., McClure C. (1991) “Low temperature friction-stir welding of 2024 aluminum”. *Scr. Mater.*, 41, 809.

[22] Threadgill, P.L., Leonard, A.J., Shercliff, H.R, Withers, P.J. (2007) “Effect of Low Translational speed FSP on Microstructure and Mechanical Properties of Extruded Cast 2285 Aluminum Alloy”. *J. Mater. Sci. Technol.,* 23(05), 614-618.

[23] Thompson, B. “FSW Introduction and Process Fundamental”. Internet: https://ewi.org/interested-in-friction-stir-welding-check-this-out, Oct. 29, 2012 [Dec. 28, 2014].

[24] Threadgill, P. “Friction stir welds in aluminium alloys-preliminary micro structural assessment”, Industrial Report 513/2/97 of The Welding Institute- TWI Bulletin, Abington, UK, 1997.

[25] Murr E., Li Y., Flores D. (1998) “Intercalation vortices and related microstructural features in the friction stir welding of dissimilar metals”. *Mater. Res. Innov.,* 2(3), 150–163.

[26] Li,Y., Trillo, E.A., Murr, L.E.(2000) “Friction stir welding welding of aluminium alloy 2024 to silver”. *J. Mater. Sci. Lett.,* 19(12), 1047-1051.

[27] Li Y., Murr E., McClure C. (1999) “Flow visualization and residual microstructures associated with the friction stir welding of 2024 and 6061 aluminum”. *Mater. Sci. Eng.,* A271 (1), 213–223.

[28] H.B. Cary. *Modern Welding Technology*. New Jersey: Prentice-Hall, 2002.

[29] Dawes J., Thomas M. (1996) “Friction stir process welds aluminum alloys”. *Weld. J.,*75, 41–45.

[30] Jennifer S. “Friction Stir Welding Brings Together Reliability and Affordability for Space Launch System”. Internet: http://ezproxy.aus.edu/login?url=http://search.proquest.com/docview/1017925635?accountid=16946, May 21, 2012 [Nov. 15, 2014].

[31] Hancock R. (2004) “Friction Welding of Aluminum Cuts Energy Costs by 99%”. *Weld J.,* 83 (2), 40.

[32] Lakshminarayanan K., Balasubramanian V., Elangovan K. (2009) “Effect of welding processes on tensile properties of AA6061 aluminium alloy joints”. *International Journal of Advanced Manufacturing Technology,* 40(3/4), 286-296.

[33] Liua J., Fujiia H., Maedaa M., Nogia K. (2003) “Tensile properties and fracture locations of friction-stir-welded joints of 2017-T351 aluminum alloy”. *Journal of Materials Processing Technology,* 142(3), 692–696.

[34] Taban E., Kaluc E. (2007) “Comparison between microstructure characteristics and joint performance of 5086-H32 aluminium alloy welded by MIG, TIG and friction stir welding processes”. *Kovove Mater.,* 45, 241–248.

[35] Wang W., Shi Q., Liu P., Li H., Li T. (2009) “A novel way to produce bulk SiCp reinforced aluminum metal matrix composites by friction stir processing”. *J Mater. Process. Technol.,* 209, 2099–2103.

[36] Lim K., Shibayanagi T., Gerlicha P. (2009) “Synthesis of multiwalled CNT reinforced aluminum alloy composite via friction stir processing”. *Mater. Sci. Eng.,* 507,194–199.

[37] Ke L., Huang C., Xing L., Huang K. (2010) “Al–Ni intermetallic composites produced in situ by friction stir processing”. *J. of Alloys and Compounds.* 503(2), 494–499.

[38] Dixit M., Newkirk J., Mishra S. (2007) “Properties of friction stir-processed Al 1100–NiTi composite”. *Scr. Mater.,* 56,541–544.

[39] Asadi P., Faraji G., Besharati K. (2010) “Producing of AZ91/SiC composite by friction stir processing”. *Int. J. Adv. Manuf. Technol.,* 51,247–260.

[40] Mahmoud I., Takahashi M., Shibayanagi T., Ikeuchi K.(2010) “Wear characteristics of surface-hybrid-MMCs layer fabricated on aluminum plate by friction stir processing”. *Materials Transactions,* 268, 1111–1121.

[41] Alidokht A., Abdollah-zadeh A., Soleymani S., Assadi H. (2011) “Microstructure and tribological performance of an aluminum alloy based hybrid composite produced by friction stir processing”. *Mater. Des.,* 32, 2727–2733.

[42] Morisada Y., Fujii H., Nagaoka T., Fukusumim M. (2006) “MWCNTs/AZ31 surface composites fabricated by friction stir processing”. *Mater. Sci. Eng.,* A419, 344–348.

[43] Zarghani A., Kashani-Bozorg F., Zarei-Hanzaki A. (2009) “Microstructures and mechanical properties of Al/Al2O3 surface nano-composite layer produced by friction stir processing”. *Mater. Sci. Eng.,* A500, 84–91.

[44] Jata, K.V., Sankaran, K.K., Ruschau, J.J. (2000) “Friction stir welding effects on microstructure and fatigue of aluminum alloy 7050-T451”. *Metall. Mater. Trans.,* A31 (9), 2,181-2,192.

[45] Sato, Y.S, Kokawa, H. (2001) “Distribution of tensile property and microstructure in friction stir weld of 6063 aluminum”. *Metall.Mater.Trans.,* A32, 3,023-3,031.

[46] Yang M., Xu C., Wu C., Lin K., Chao Y., An L. (2010) “Fabrication of AA6061/Al2O3 nano ceramic particle reinforced composite coating by using friction stir processing”. *J. Mater. Sci.,* 45(16), 4431–4438.

[47] Sharifitabar M., Sarani A., Khorshahian S., Shafiee Afarani M. (2011) “Fabrication of 5052Al/Al2O3 nanoceramic particle reinforced composite via friction stir processing route”. *Mater. Des.,* 32, 4164–4172.

[48] Mazaheri Y., Karimzadeh F., Enayati H. (2011) “A novel technique for development of A356/Al2O3 surface nanocomposite by friction stir processing”. *Journal of materials processing technology*, 211, 1614-1619.

[49] Hsu J., Chang Y., Kao W., Ho J., Chang P. (2006) “Al–Al3Ti nanocomposites produced in situ by friction stir processing”. *Acta Mater.*, 54, 5241–5249.

[50] Zhang Q., Xiao L., Wang Z., Ma Y. (2011) “In situ Al_3Ti and Al_2O_3 nanoparticles reinforced Al composites produced by friction stir processing in an Al–TiO_2 system”. *Mater. Lett.*, 65, 2070–2072.

[51] Bauri R., Yadav D., Suhas G. (2011) “Effect of friction stir processing (FSP) on microstructure and properties of Al–TiC in situ composite”. *Mater. Sci. Eng.*, A528, 4732–4739.

[52] Tewari A., Spowart E., Gokhale M., Mishra S., Miracle B. (2006) “Characterization of the effects of friction stir processing on microstructural changes in DRA composites”. *Mater. Sci. Eng.*, A428, 80–90.

[53] Asadi P., Faraji G., Masoumi A., Besharati K. (2011) “Experimental investigation of magnesium-base nanocomposite produced by friction stir processing: effects of particle types and number of friction stir processing passes”. *Metall. Mater. Trans.*, A42 (9), 2820-2832.

[54] Xiaofei L., Tianmo L., Jian C., Bin M., Wen Z. (2011) “Microstructure and Mechanical Properties of Magnesium Alloy AZ31 Processed by Compound Channel Extrusion”. *Materials Transactions*, 52(6), 1082-1087.

[55] Zhan Y., C.M. Li, Zhang W., Zhan Y. (2012) “Processing of AZ31 magnesium alloy by accumulative roll-bonding at gradient temperature”. *Acta Metall. Sin.*, 25 (1), 65-75.

[56] Zhang Y., Wu K., Liang M., Kamado S., Kojima Y. (2004) “The effect of thermal exposure on the interface and mechanical properties of Al18B4O33W/AZ91 magnesium matrix composite”. *Mater. Sci. Eng. A*, 372, 66–74.

[57] Cao P., Zhang L., Han W., Yan D., Chen J. (2012) “Preparation of ternary Mg-Li-Sn alloys from molten salt by electrolysis”. *Acta Metall. Sin.*, 25 (4), 265–271.

[58] Tzimas E., Zavaliangos A. (2000) “Evolution of near-equiaxed microstructure in the semisolid state”. *Mater. Sci. Eng. A.* 289 (1), 228–240.

[59] Kleiner S., Beffort O., Uggowitzer. J. (2004) “Microstructure evolution during reheating of an extruded Mg-Al-Zn alloy into the semisolid state”. *Scripta Mater.,* 51 (5), 405–407.

[60] Darras B., Omar M., Khraisheh M. (2007) “Experimental Thermal Analysis of Friction Stir Processing”. *Mater. Sci. Forum,* 539-543, 3801-3806.

[61] Cavaliere, P. (2005) “Mechanical properties of Friction Stir Processed 2618/Al_2O_3/20p metal matrix composite”. *Composites Part A,* 36, 1657–1665.

[62] Salekrostam R., Givi B., Asadi P., Bahemmat P. (2010) “Influence of Friction Stir Processing Parameters on the Fabrication of SiC/316L Surface Composite”. *Defect and Diffusion Forum,* 297-301, 221-226.

[63] Asadi P., Faraji G., Besharat K. (2010) “Producing of AZ91/SiC composite by friction stir processing (FSP)”. *The International Journal of Advanced Manufacturing Technology,* 51(1), 247-260.

[64] Darras B. (2012) “A Model to Predict the Resulting Grain Size of Friction-Stir-Processed AZ31 Magnesium Alloy”. *Journal of Materials Engineering and Performance,* 21 (7), 1243-1248.

[65] Darras B., Khraisheh M. (2008) “Analytical modeling of strain rate distribution during friction stir processing”. *Journal of Materials Engineering and Performance,* 4(1), 168-177.

[66] Darras B. (2008) Integrated Thermo-Mechanical Investigations of Friction Stir Processing of Light Weight Alloys. Ph.D. Thesis. University of Kentucky (Lexington): USA.

[67] Emad Eldin K. (2013) Investigation of Submerged Friction Stir Welding of Marine-Grade Aluminum Alloy. M.Sc. Thesis. American University of Sharjah*:* UAE.

[68] Darras B, Deiab I., Ahmed N. (2014) “Prediction of friction stir processed AZ31 magnesium alloy micro-hardness using artificial neural networks”. *Advanced Materials Research,* 1043, 91–95.

[69] Elangovan K., Balasubramanian V., Babu S. (2008) “Developing an empirical relationship to predict tensile strength of friction stir welded AA2219 aluminum Alloy”. *Journal of Materials Engineering and Performance,* 17(6), 820-830.

[70] Al-Jarrah J., Swalha S., Abu Mansour T., Ibrahim M., Al-Rashdan M. (2013) “Optimization of friction stir welding parameters for joining aluminum alloys using RSM”. *Adv. Theor. Appl. Mech.,* 6 (1), 13-26.

[71] Russell L. (2009) “Response-Surface Methods in R, using rsm”. *Journal of Statistical Software,* 32(7), 1-17.

[72] Palanivel R., Mathews K., Murugan N. (2011) “Development of mathematical model to predict the mechanical properties of friction stir welded AA6351 aluminum alloy”. *Journal of Engineering Science and Technology,* 4(1), 25-31.

[73] Lakshminarayanan K., Balasubramanian V. (2009) “Comparison of RSM with ANN in predicting tensile strength of friction stir welded AA7039 aluminum alloy joints”. *Transactions of Nonferrous Metals Society of China,* 19, 9-18.

[74] Balasubramanian V., Lakshminarayanan K. (2007) “Comparison of Response Surface Model with Neural Network in predicting the tensile strength of friction stir welded RDE- 40 aluminum alloy”. *Journal on Design and Manufacturing Technologies,* 1 (1), 41-46.

[75] Palanivel R., Mathews P., Murugan N. (2012) “Development of mathematical model to predict the ultimate tensile strength of friction stir welded dissimilar aluminum alloy”. *Mechanics,* 18(5), 517-523.

[76] Dinaharan I., Murugan N. (2012) “Automation of friction stir welding process to join aluminum matrix composite by optimization”. *Procedia Engineering,* 38 (1),105-110.

[77] Cochran, Cox M. *Experimental Design*. New Delhi: Asia Publishing House, 1962.

[78] Montgomery C. Design and Analysis of Experiments. New York: John Wiley, 2001.

[79] Tung-Hsu H., Chi-Hung S., Wang-Lin L. (2007) “Parameters optimization of a nano-particle wet milling process using the Taguchi Method, Response Surface Method and Genetic Algorithm”. *Powder Technology,* 173(1), 153−162.

Appendix A: FSPed Workpieces

Figure 1: FSP sample @800 rpm, and 25 mm/min

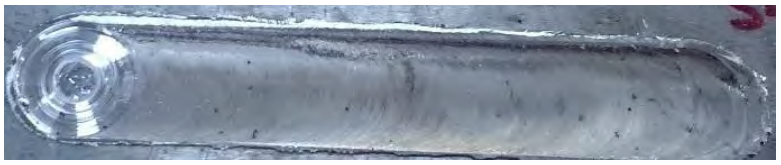

Figure 2: FSP (with SiC) sample @800 rpm, and 25 mm/min

Figure 3: FSP sample @800 rpm, and 75 mm/min

Figure 4: FSP (with SiC) sample @800 rpm, and 75 mm/min

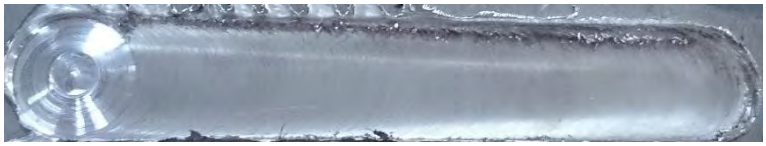

Figure 5: FSP sample @800 rpm, and 100 mm/min

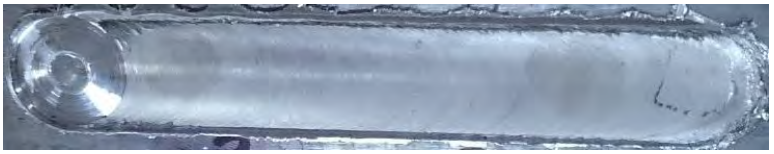

Figure 6: FSP (with SiC) sample @800 rpm, and 100 mm/min

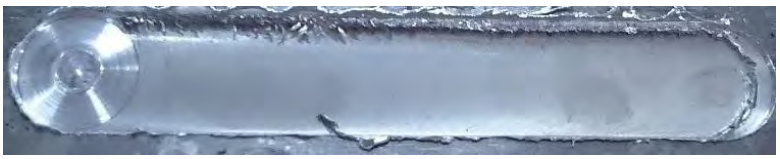

Figure 7: FSP sample @800 rpm, and 200 mm/min

Figure 8: FSP (with SiC) sample @800 rpm, and 200 mm/min

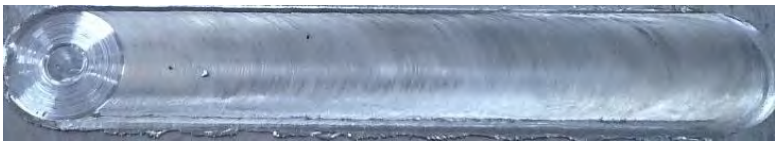

Figure 9: FSP sample @1200 rpm, and 25 mm/min

Figure 10: FSP (with SiC) sample @1200 rpm, and 25 mm/min

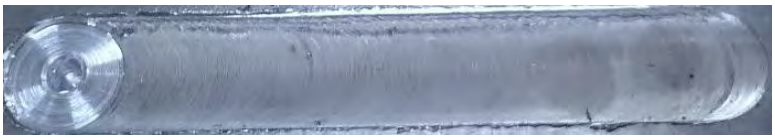

Figure 11: FSP sample @1200 rpm, and 75 mm/min

Figure 12: FSP (with SiC) sample @1200 rpm, and 75 mm/min

Figure 13: FSP sample @1200 rpm, and 100 mm/min

Figure 14: FSP (with SiC) sample @1200 rpm, and 100 mm/min

Figure 15: FSP sample @1200 rpm, and 200 mm/min

Figure 16: FSP (with SiC) sample @1200 rpm, and 200 mm/min

Figure 17: FSP sample @1600 rpm, and 25 mm/min

Figure 18: FSP (with SiC) sample @1600 rpm, and 25 mm/min

Figure19: FSP sample @1600 rpm, and 75 mm/min

Figure 20: FSP (with SiC) sample @1600 rpm, and 75 mm/min

Figure21: FSP sample @1600 rpm, and 100 mm/min

Figure 22: FSP (with SiC) sample @1600 rpm, and 100 mm/min

Figure 23: FSP sample @1600 rpm, and 200 mm/min

Figure 24: FSP (with SiC) sample @1600 rpm, and 200 mm/min

Figure25: FSP sample @2000 rpm, and 25 mm/min

Figure 26: FSP (with SiC) sample @2000 rpm, and 25 mm/min

Figure 27: FSP sample @2000 rpm, and 75 mm/min

Figure 28: FSP (with SiC) sample @2000 rpm, and 75 mm/min

Figure 29: FSP sample @2000 rpm, and 100 mm/min

Figure 3.30: FSP (with SiC) sample @2000 rpm, and 100 mm/min

Figure 31: FSP sample @2000 rpm, and 200 mm/min

Figure 32: FSP (with SiC) sample @2000 rpm, and 200 mm/min

Appendix B: Temperature Profiles

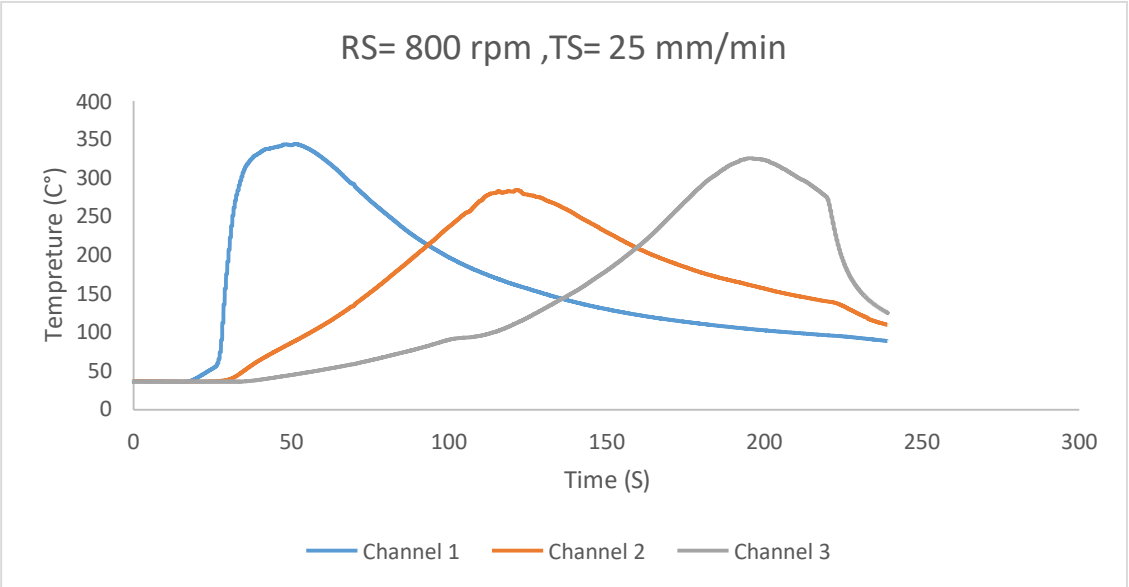

Figure 1: Recorded temperature @ RS=800 rpm, TS=25 mm/min

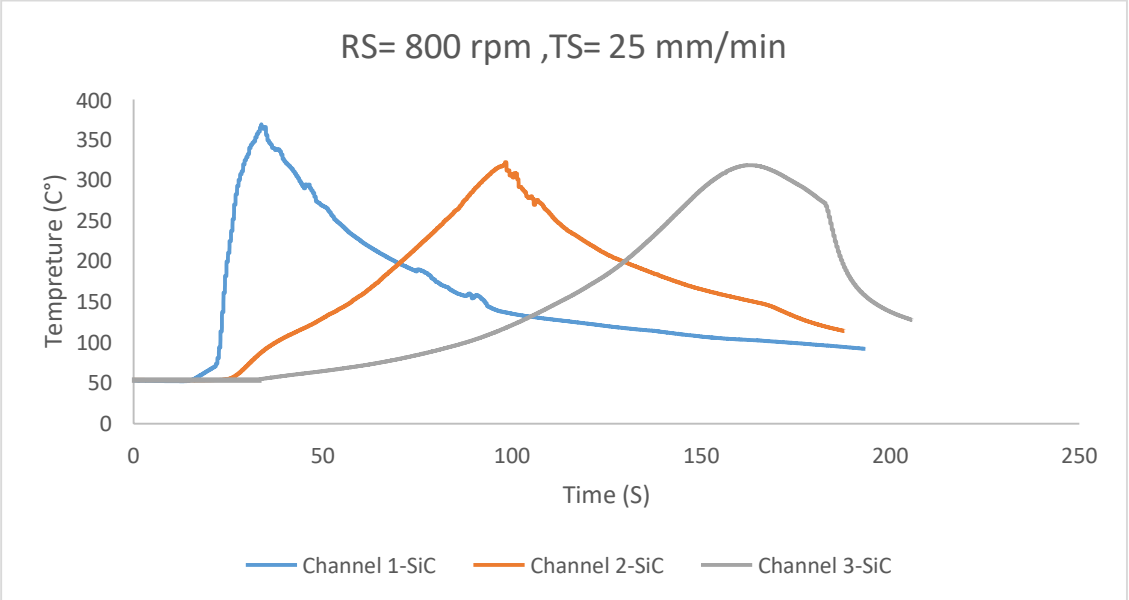

Figure 2: Recorded temperature @ RS=800 rpm, TS=25 mm/min (SiC)

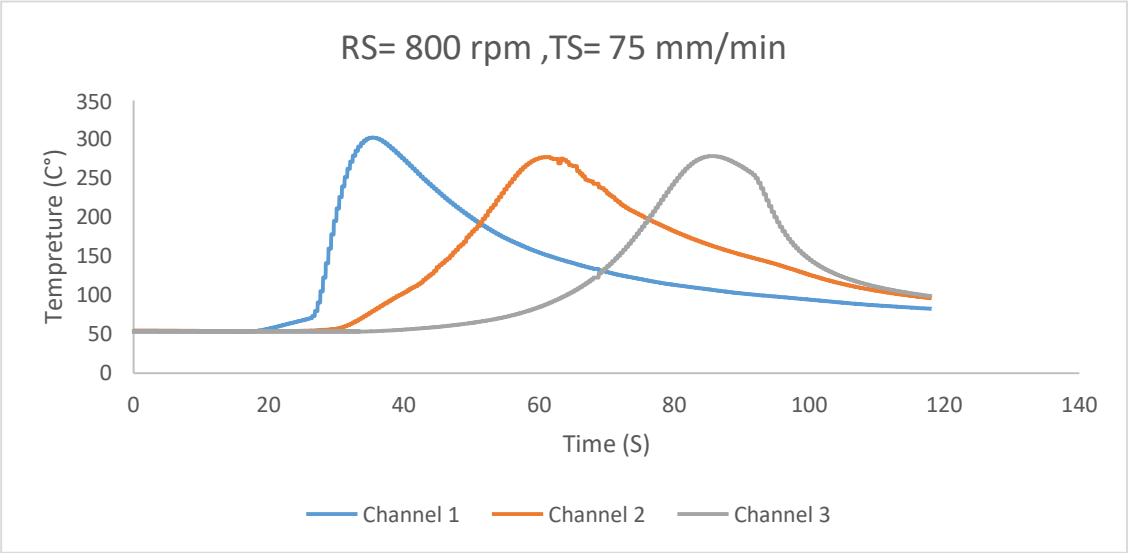

Figure 3: The recorded temperature @ RS=800 rpm, TS=75 mm/min

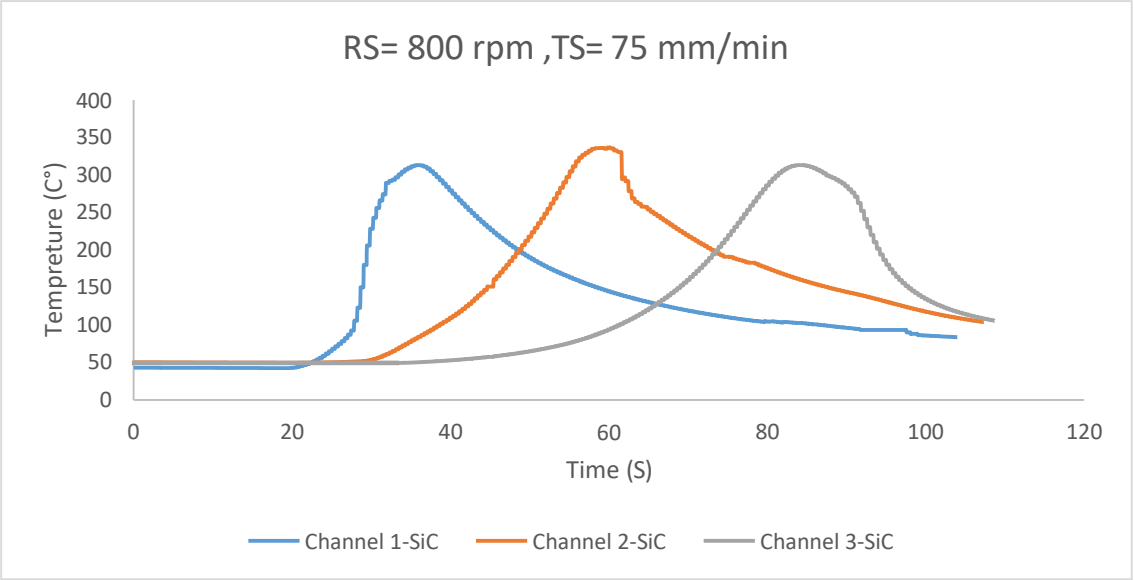

Figure 4: Recorded temperature @ RS=800 rpm, TS=25 mm/min (SiC)

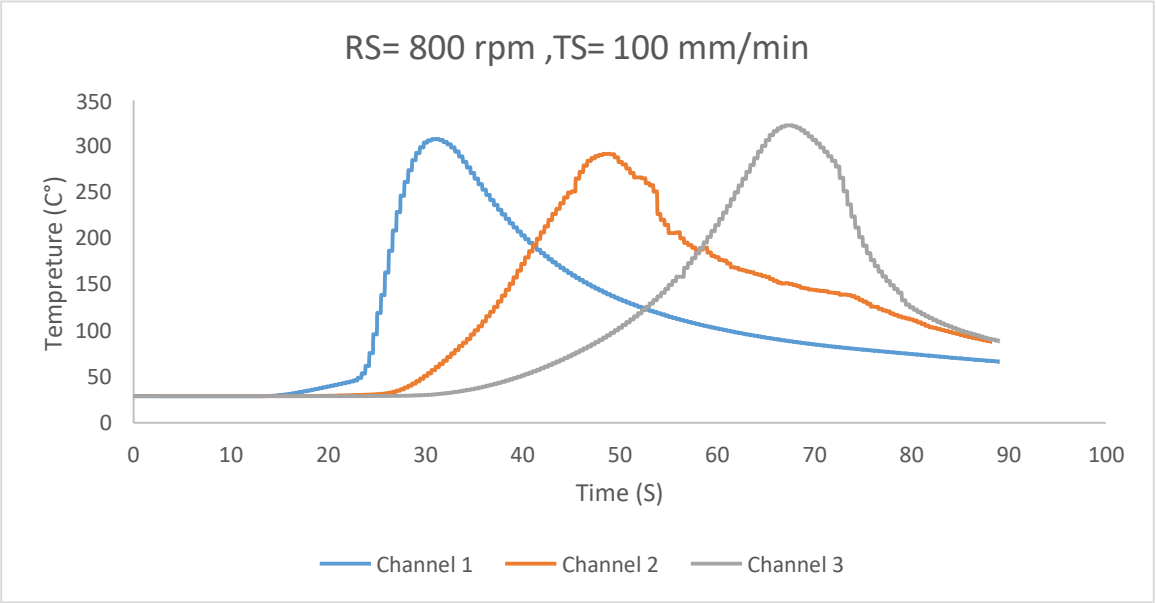

Figure 5: The recorded temperature @ RS=800 rpm, TS=100 mm/min

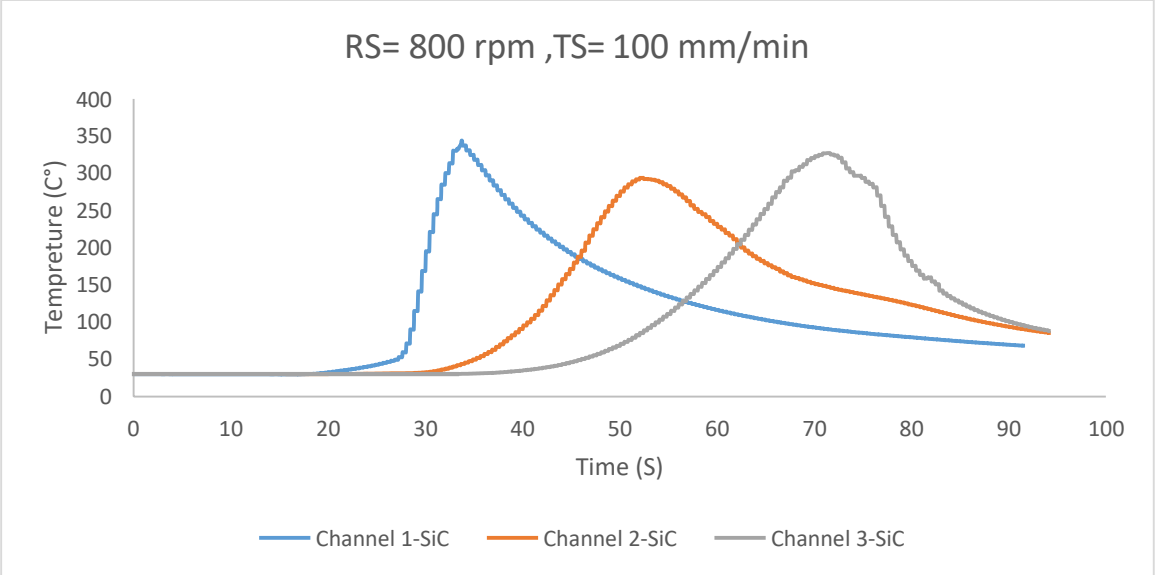

Figure 6: The recorded temperature @ RS=800 rpm, TS=100 mm/min (SiC)

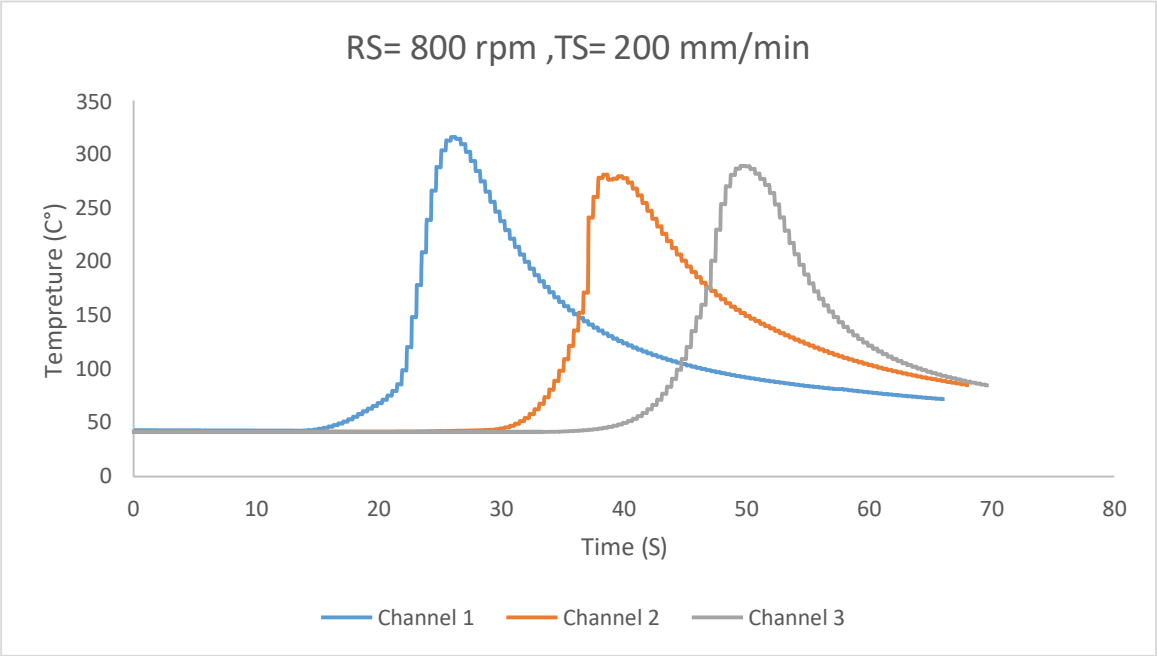

Figure 7: The recorded temperature @ RS=800 rpm, TS=200 mm/min

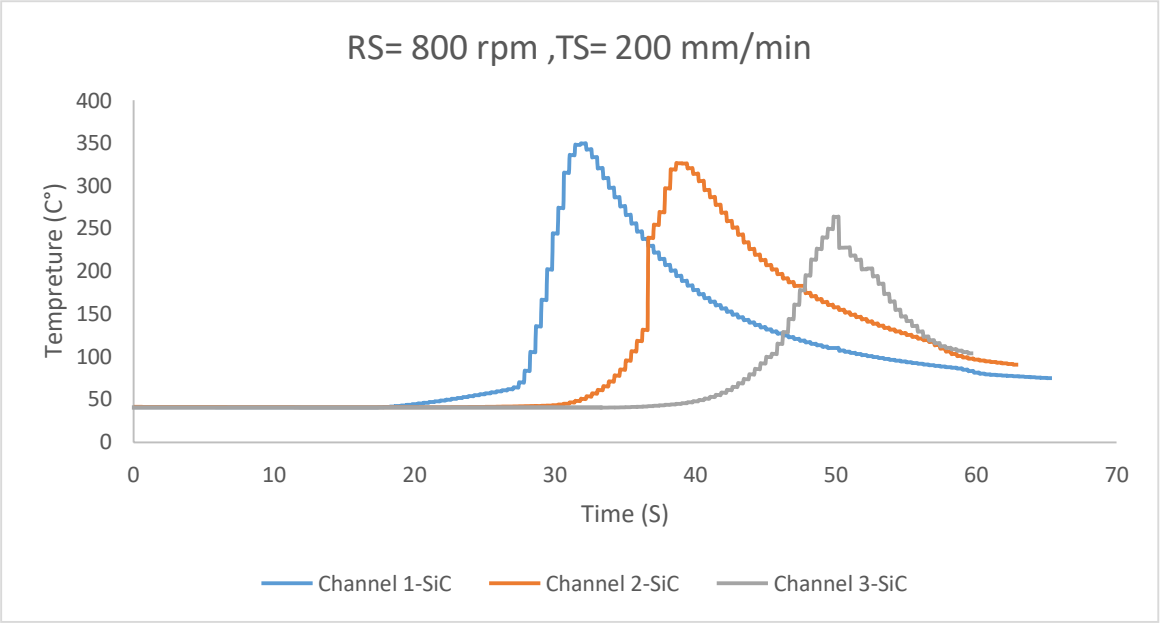

Figure 8: The recorded temperature @ RS=800 rpm, TS=200 mm/min (SiC)

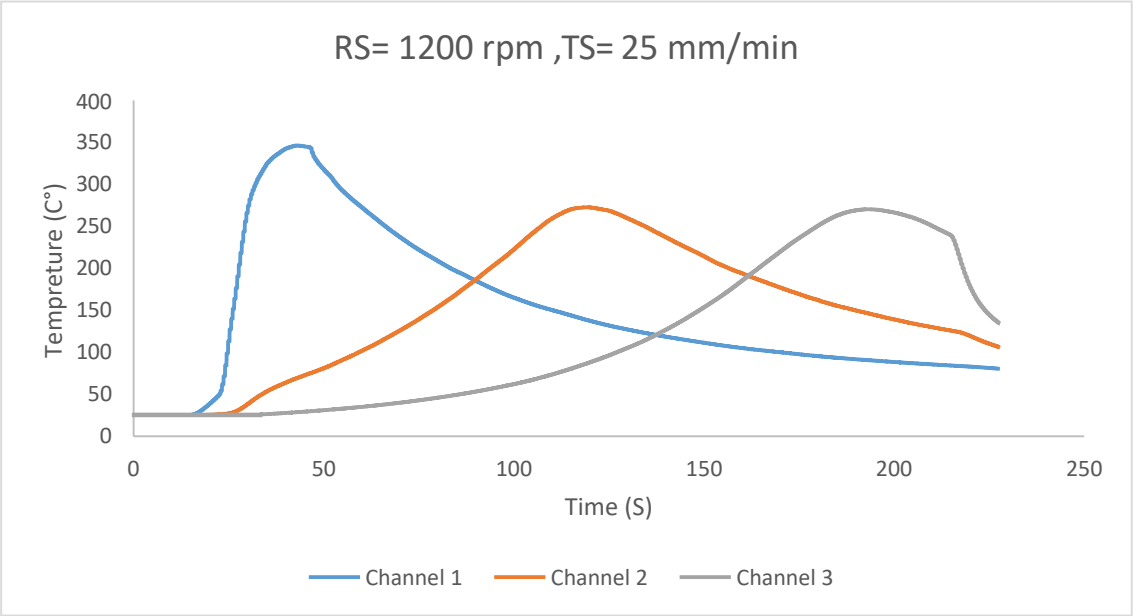

Figure 9: The recorded temperature @ RS=1200 rpm, TS=25 mm/min

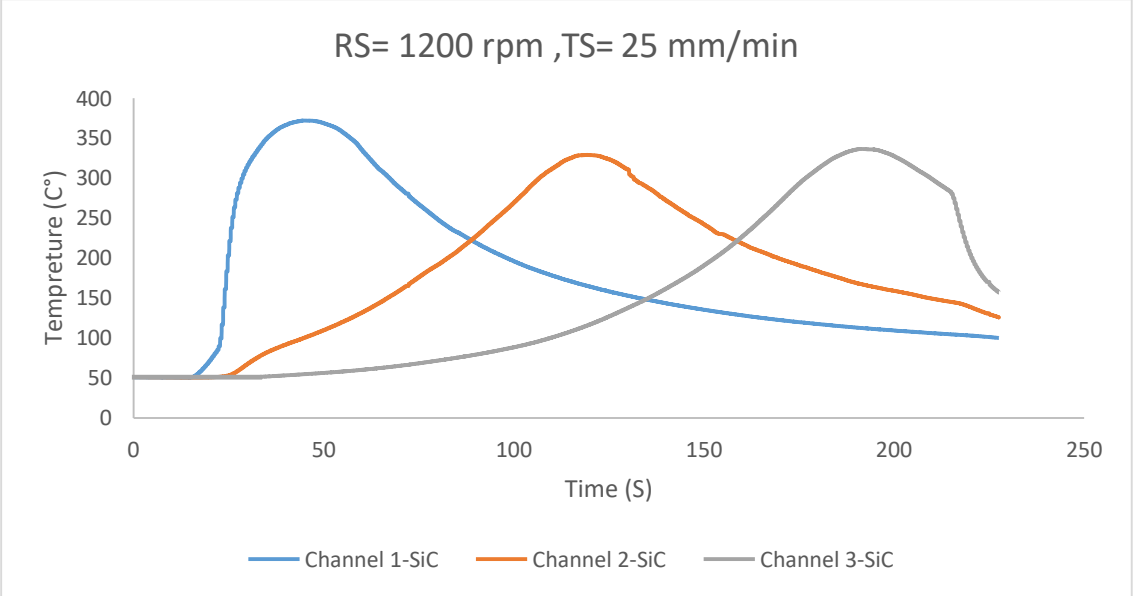

Figure 10: The recorded temperature @ RS=1200 rpm, TS=25 mm/min (SiC)

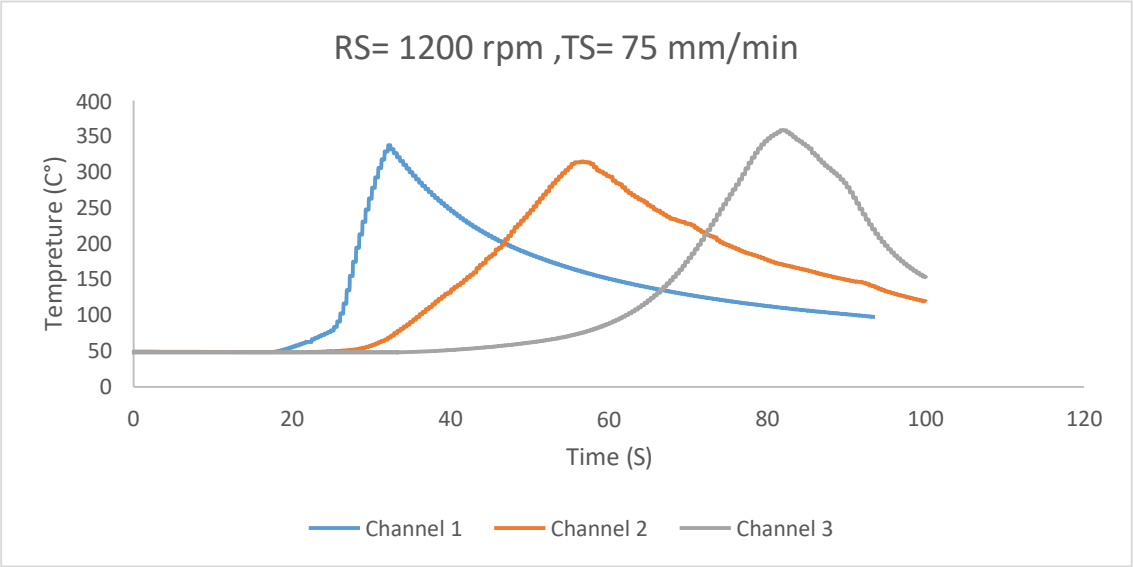

Figure 11: The recorded temperature @ RS=1200 rpm, TS=75 mm/min

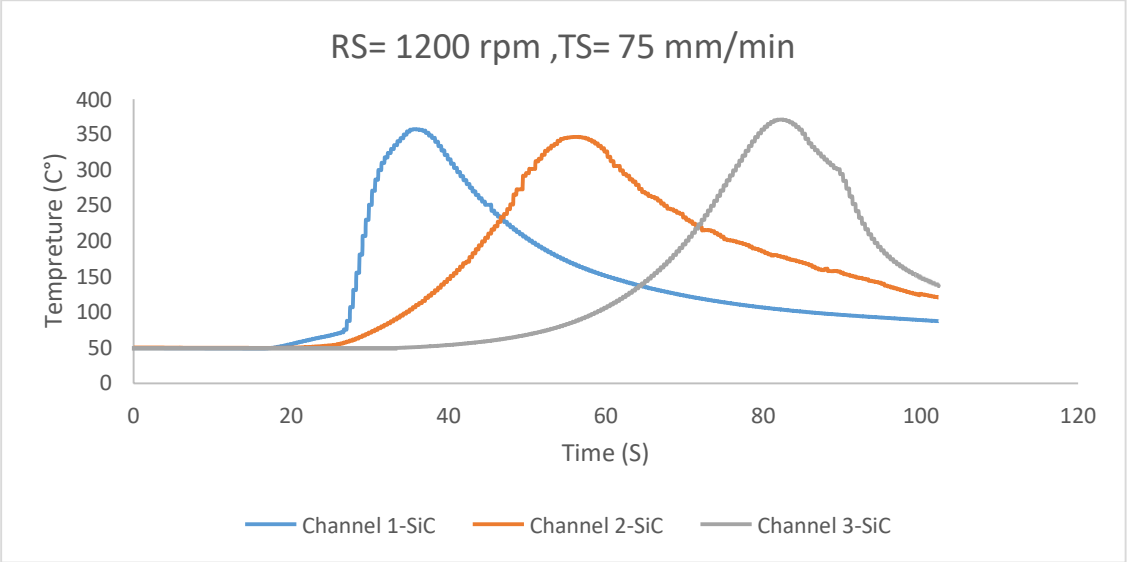

Figure 12: The recorded temperature @ RS=1200 rpm, TS=75 mm/min (SiC)

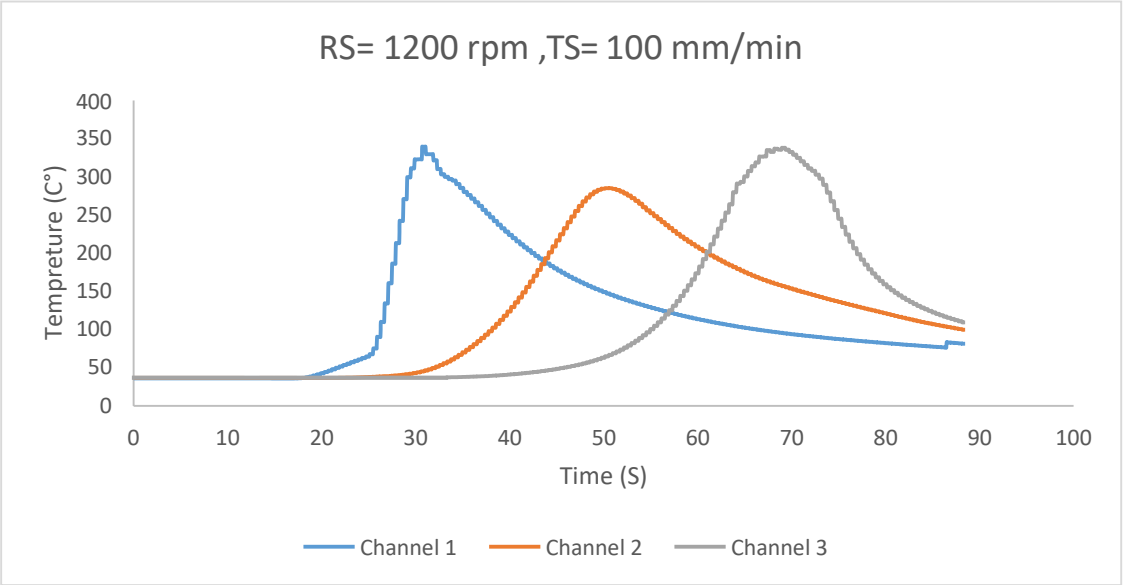

Figure 13: The recorded temperature @ RS=1200 rpm, TS=100 mm/min

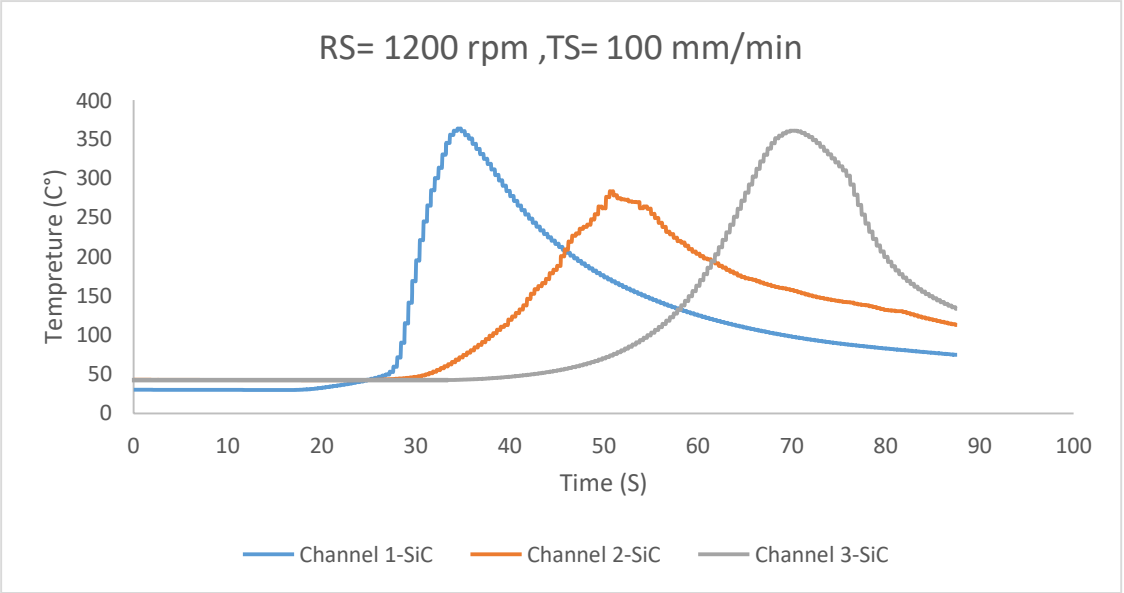

Figure 14: The recorded temperature @ RS=1200 rpm, TS=100 mm/min (SiC)

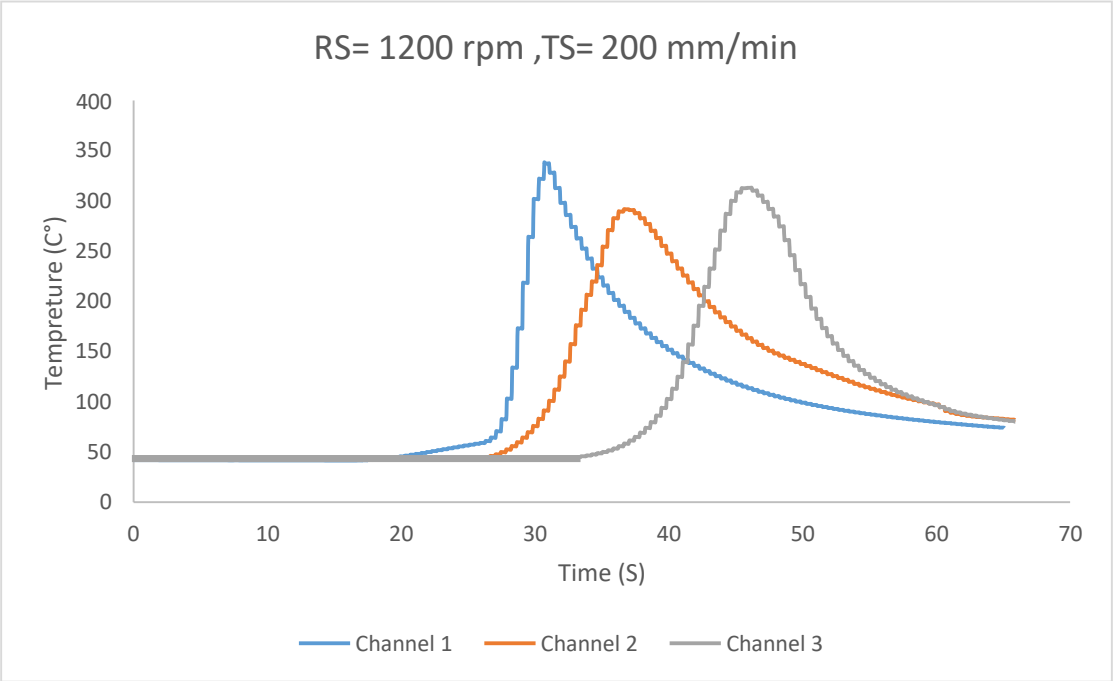

Figure 15: The recorded temperature @ RS=1200 rpm, TS=200 mm/min

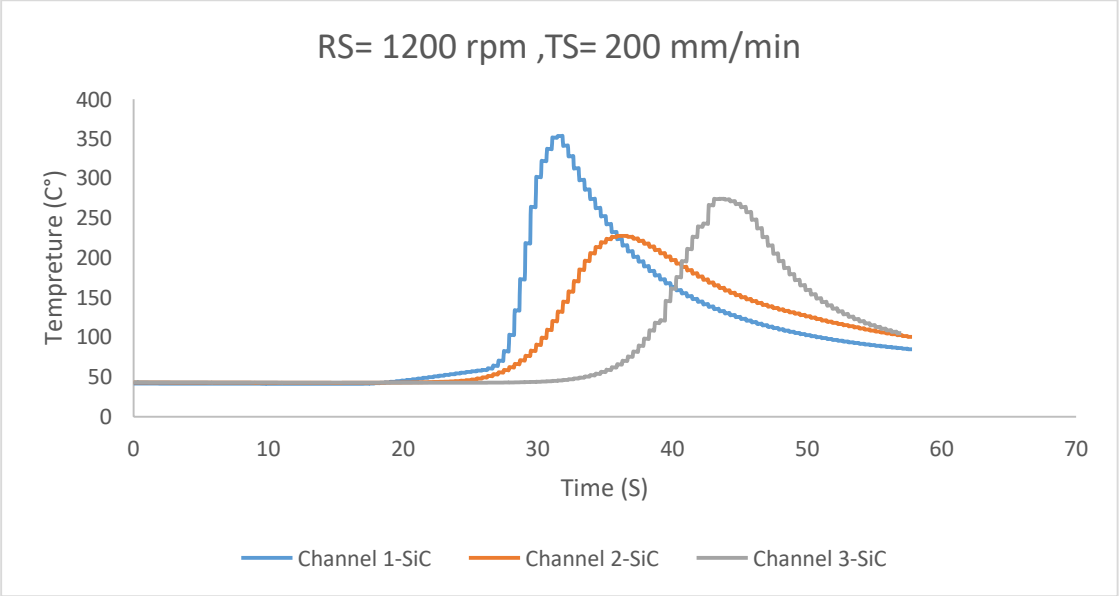

Figure 16: The recorded temperature @ RS=1200 rpm, TS=25 mm/min (SiC)

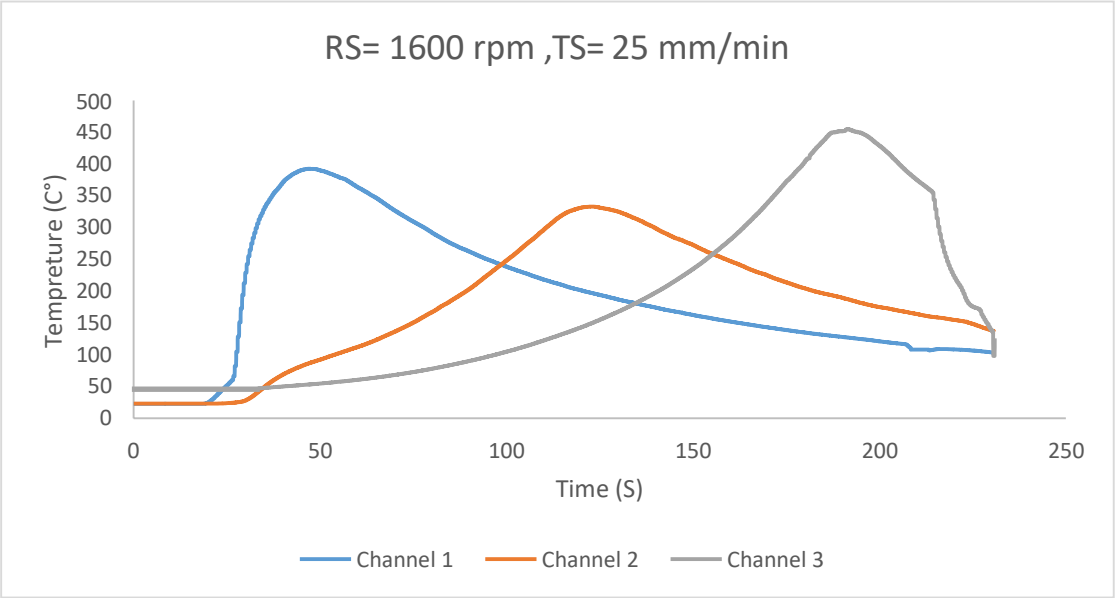

Figure 17: The recorded temperature @ RS=1600 rpm, TS=25 mm/min

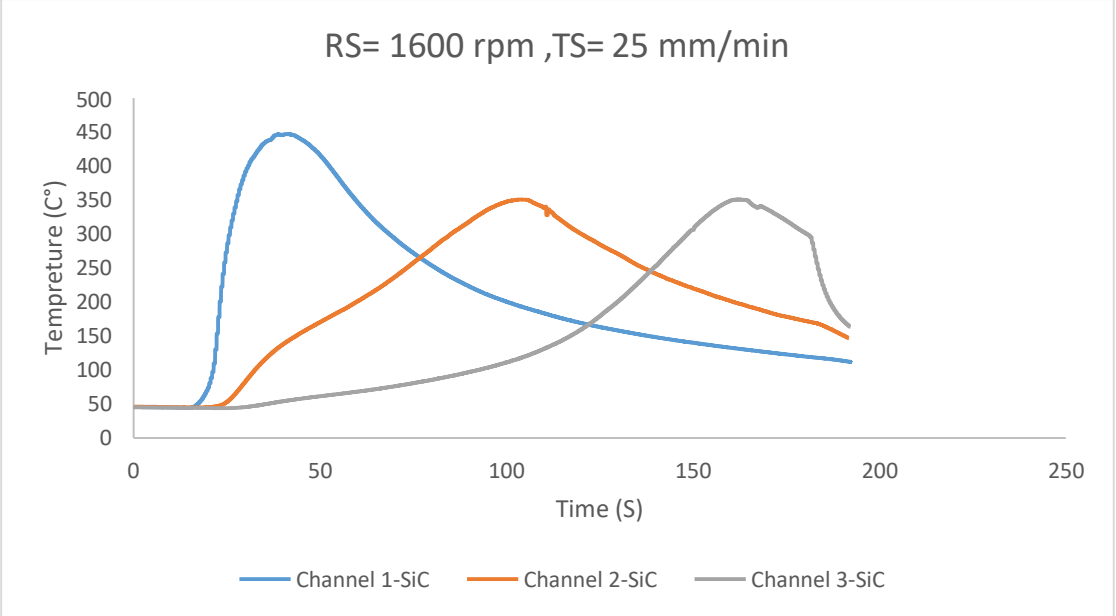

Figure 18: The recorded temperature @ RS=1600 rpm, TS=25 mm/min (SiC)

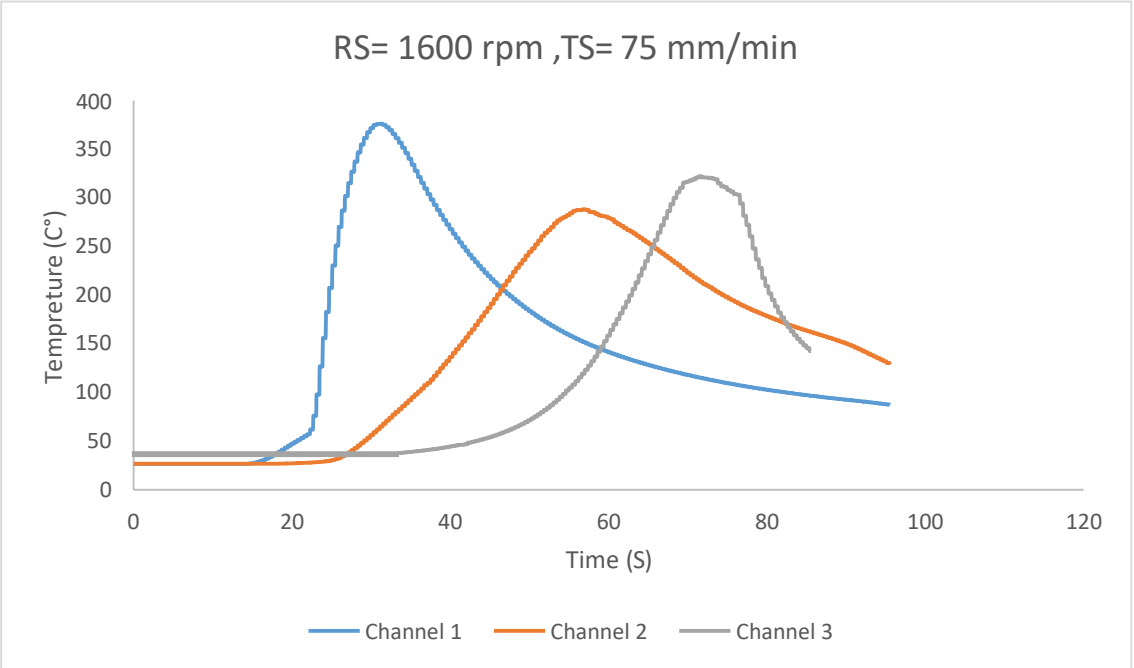

Figure 19: The recorded temperature @ RS=1600 rpm, TS=75 mm/min

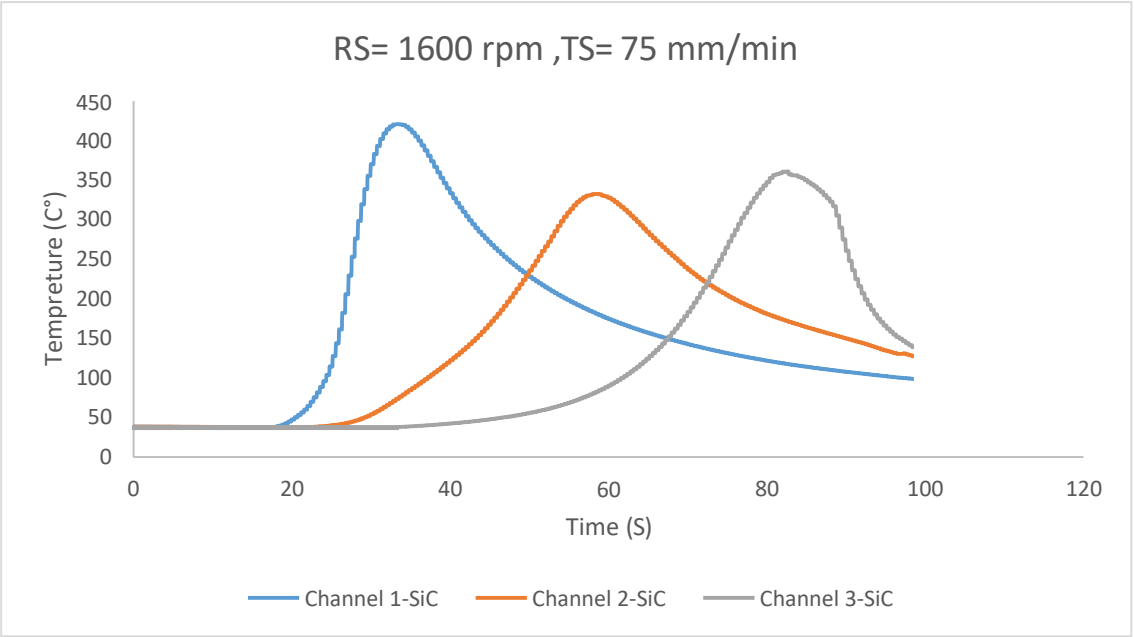

Figure 20: The recorded temperature @ RS=1600 rpm, TS=75 mm/min (SiC)

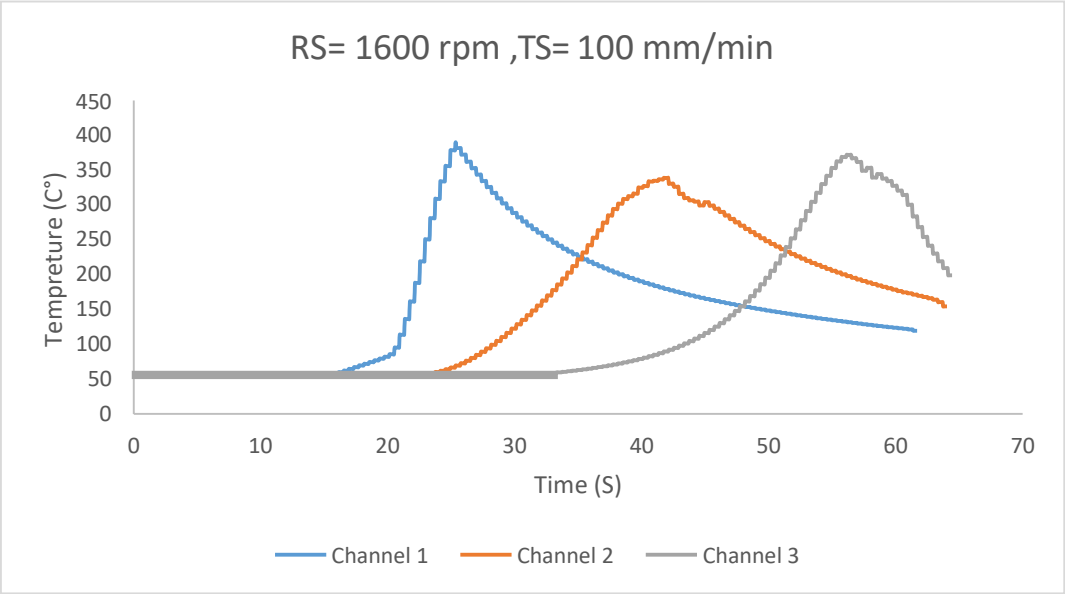

Figure 21: The recorded temperature @ RS=1600 rpm, TS=100 mm/min

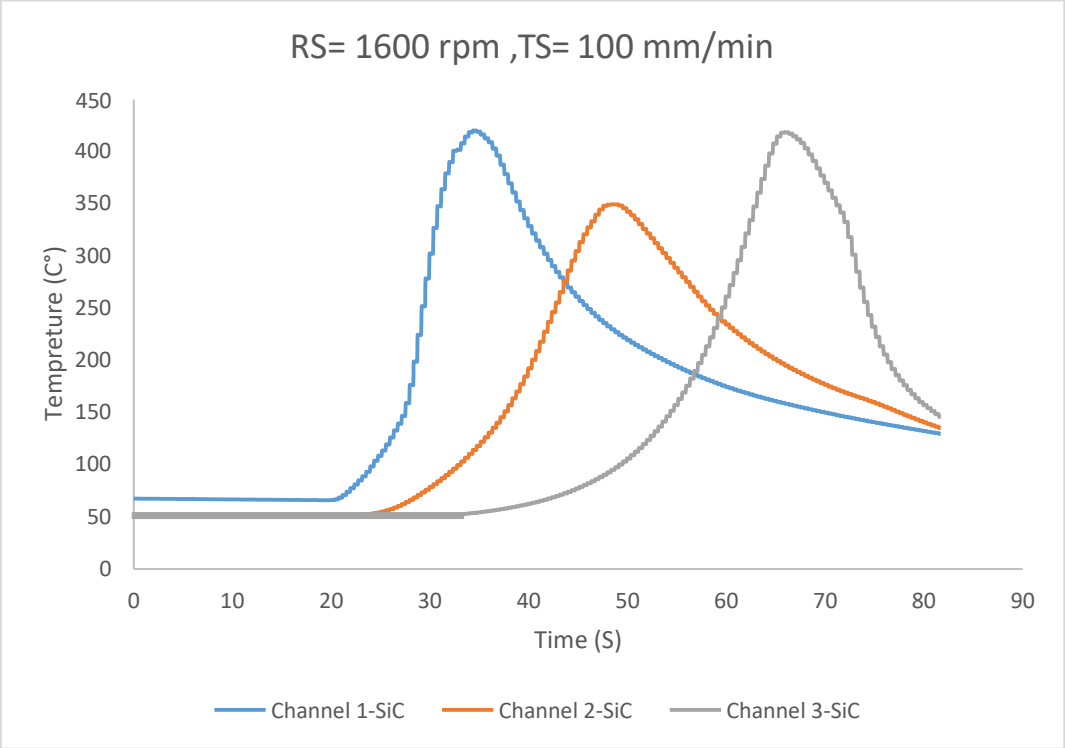

Figure 22: The recorded temperature @ RS=1600 rpm, TS=100 mm/min (SiC)

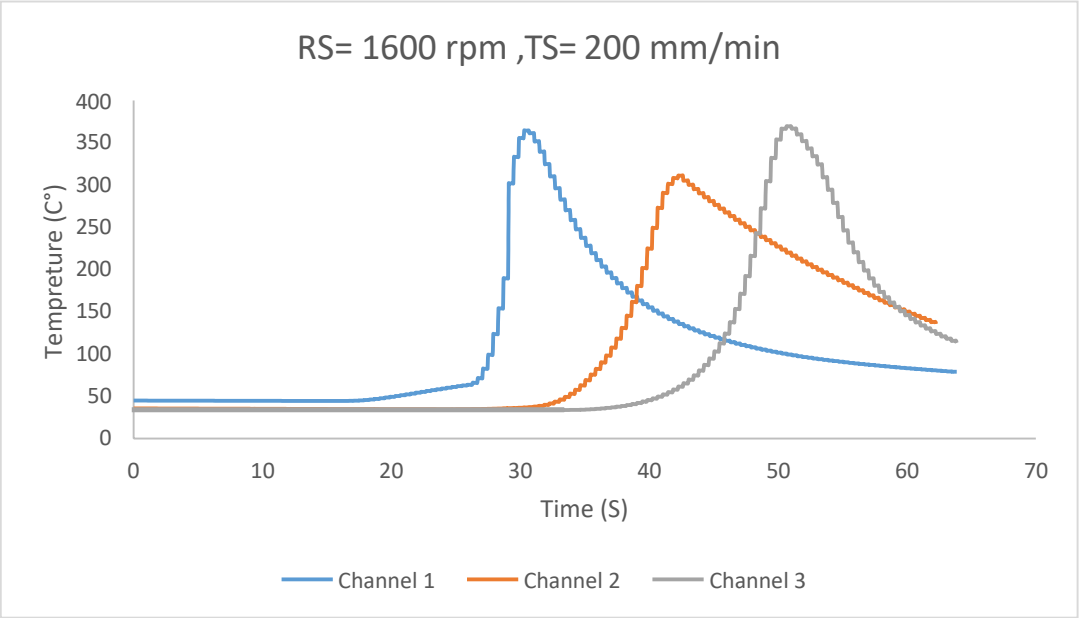

Figure 23: The recorded temperature @ RS=1600 rpm, TS=200 mm/min

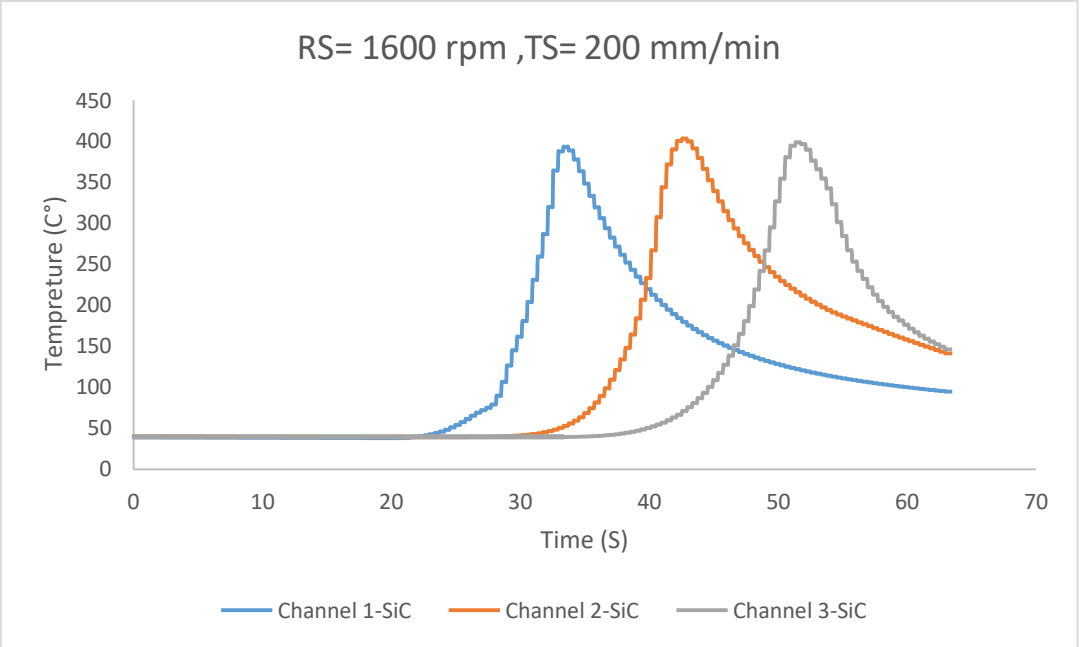

Figure 24: The recorded temperature @ RS=1600 rpm, TS=200 mm/min (SiC)

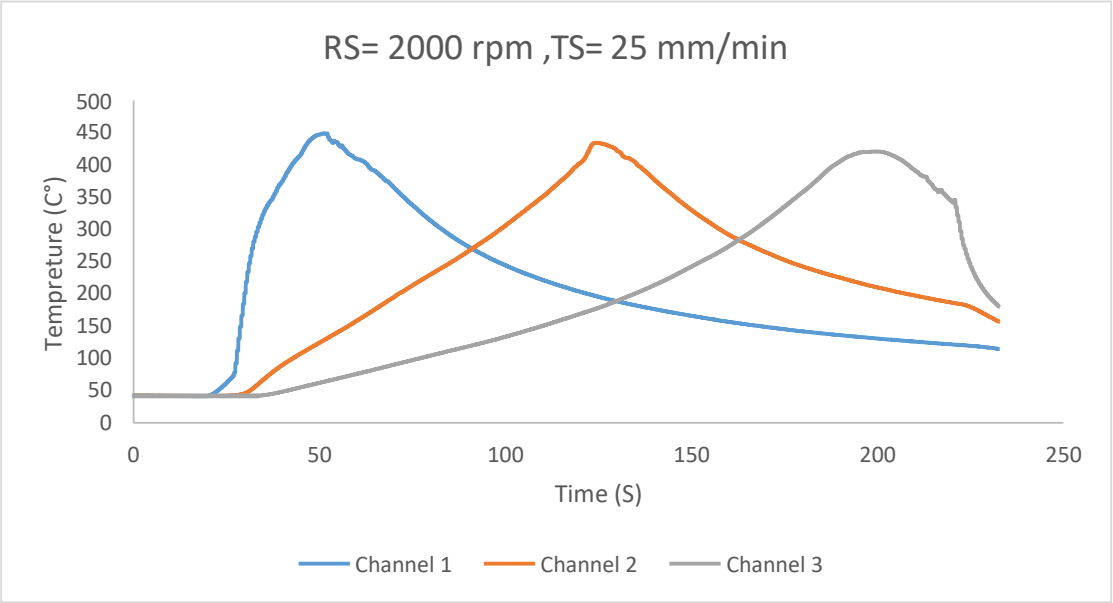

Figure 25: The recorded temperature @ RS=2000 rpm, TS=25 mm/min

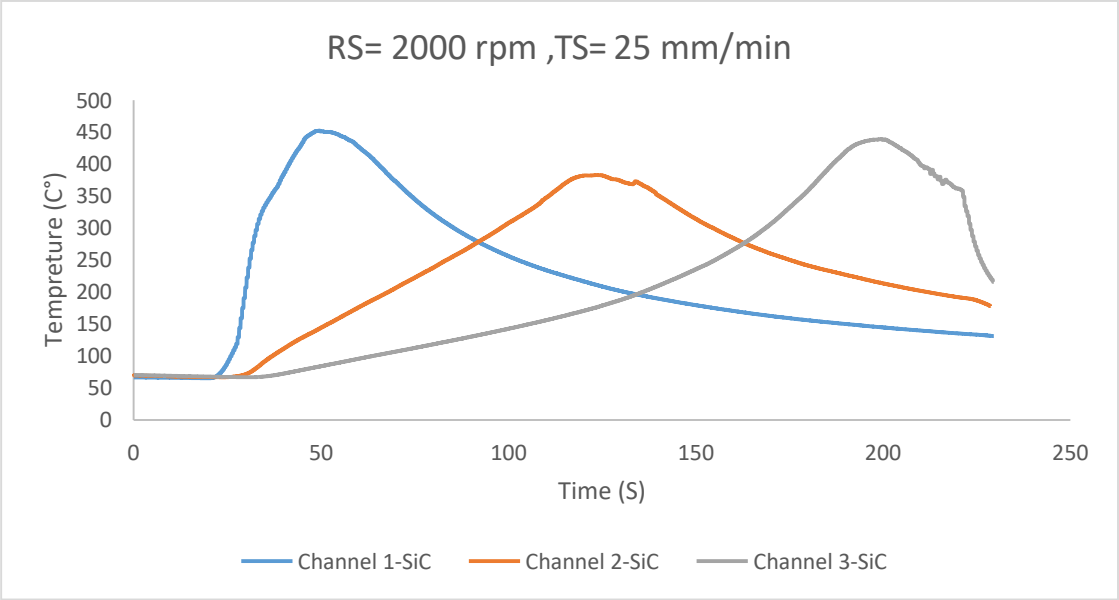

Figure 26: The recorded temperature @ RS=2000 rpm, TS=25 mm/min (SiC)

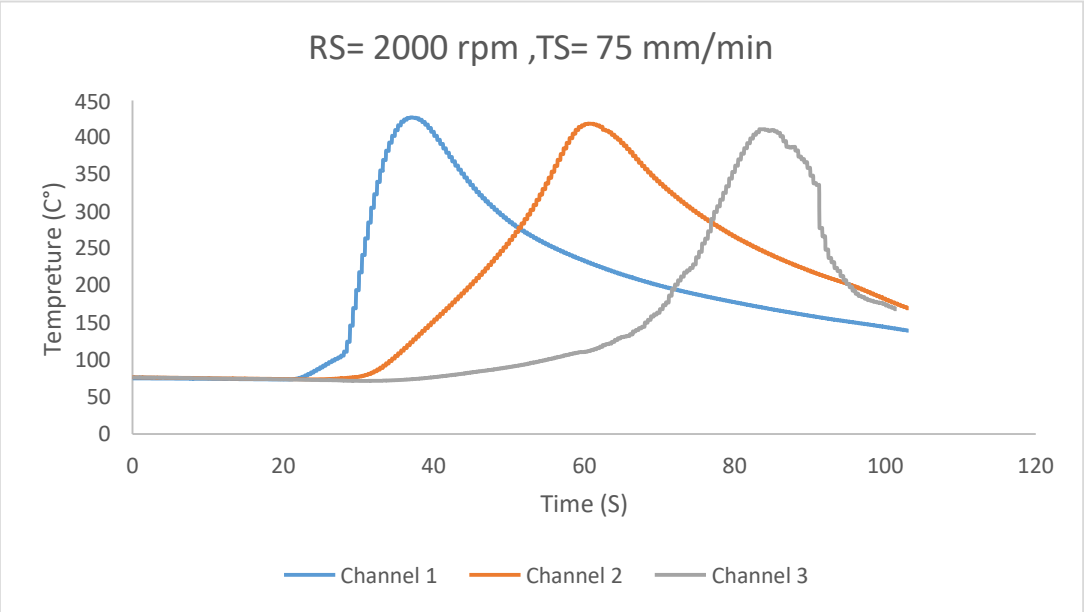

Figure 27: The recorded temperature @ RS=2000 rpm, TS=75 mm/min

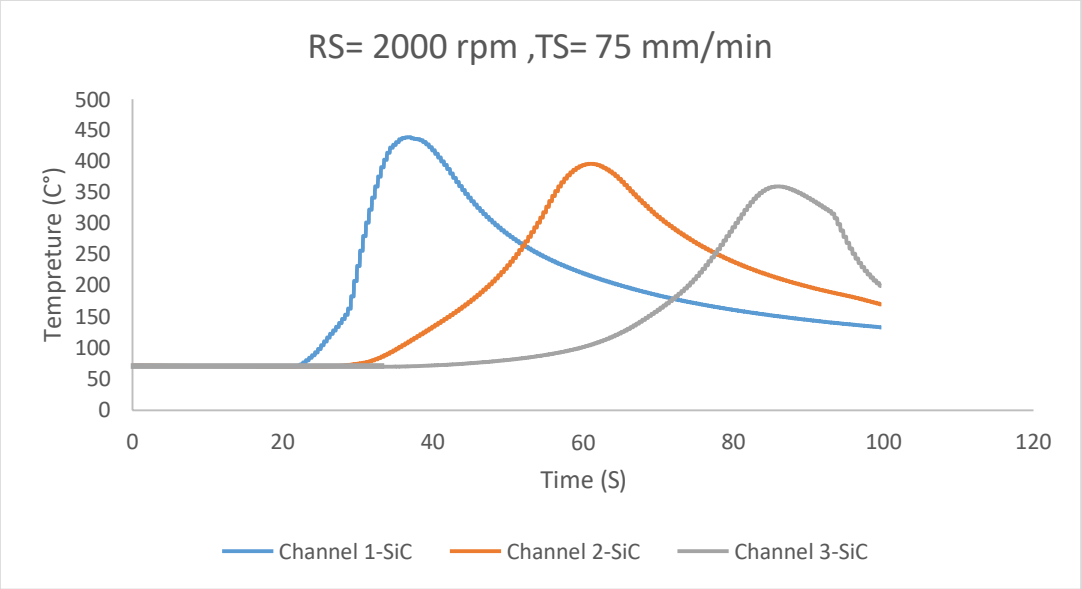

Figure 28: The recorded temperature @ RS=2000 rpm, TS=75 mm/min (SiC)

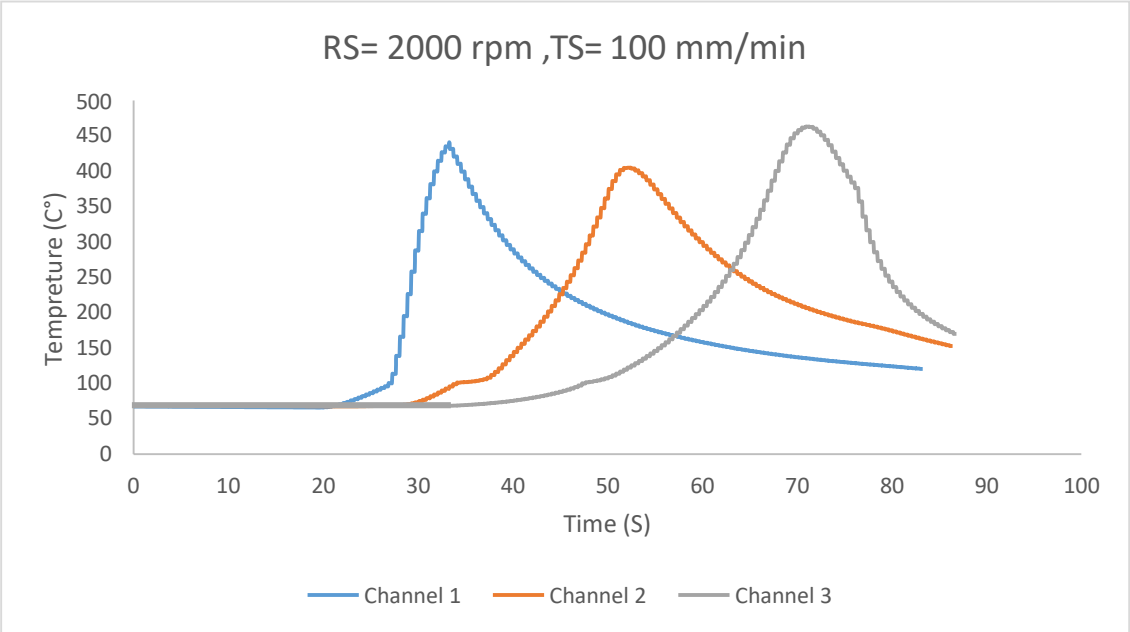

Figure 29: The recorded temperature @ RS=2000 rpm, TS=100 mm/min

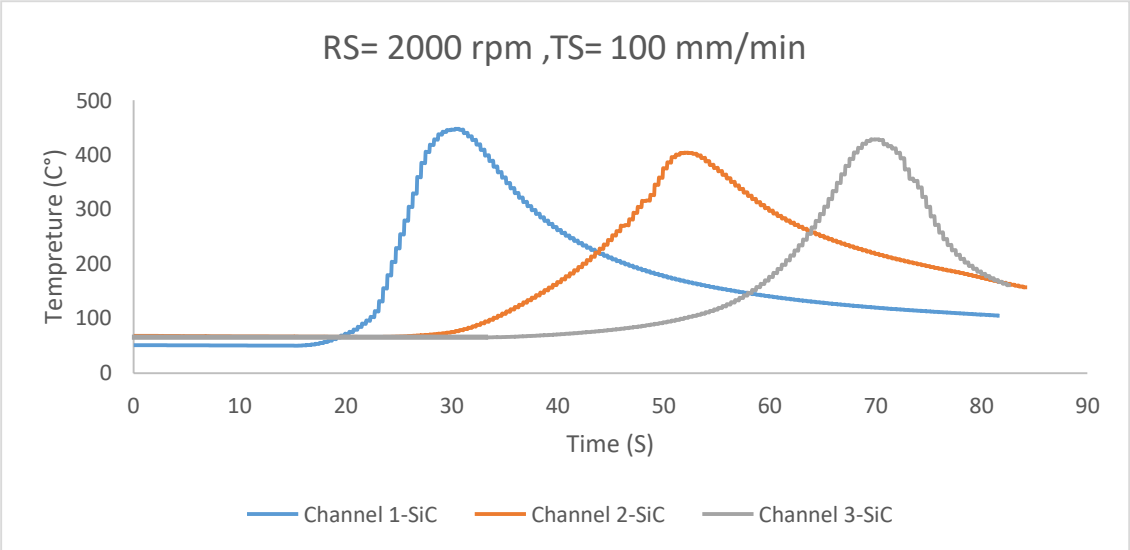

Figure 30: The recorded temperature @ RS=2000 rpm, TS=100 mm/min (SiC)

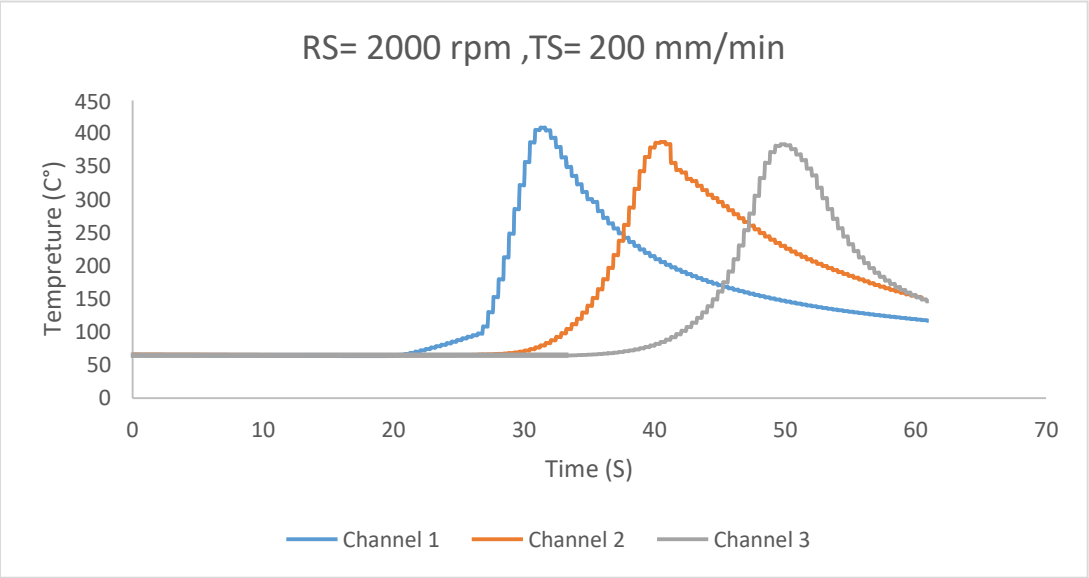

Figure 31: The recorded temperature @ RS=2000 rpm, TS=200 mm/min

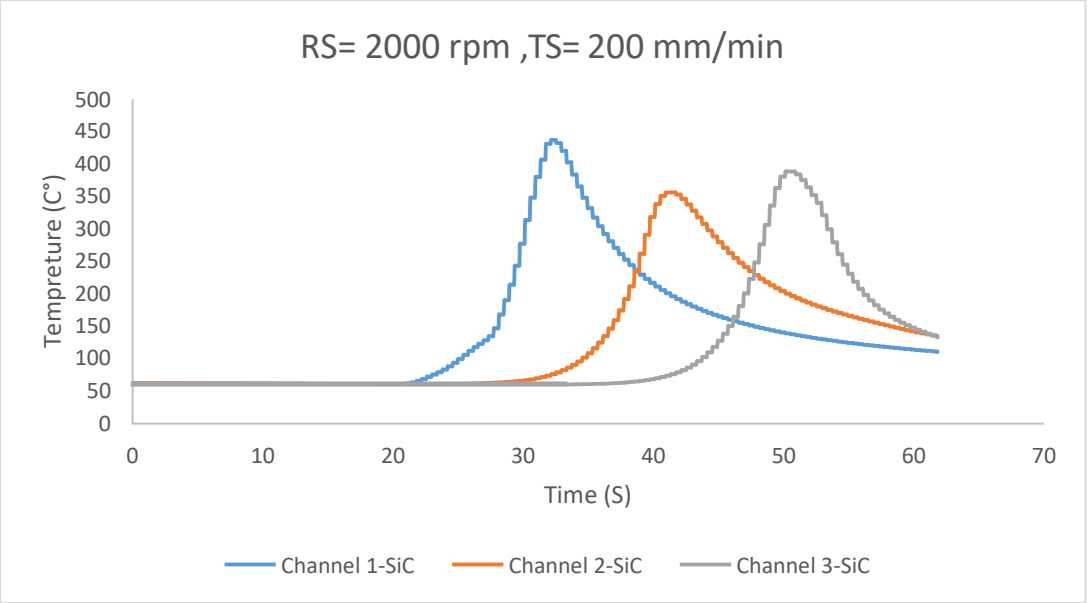

Figure 32: The recorded temperature @ RS=2000 rpm, TS=200 mm/min (SiC)

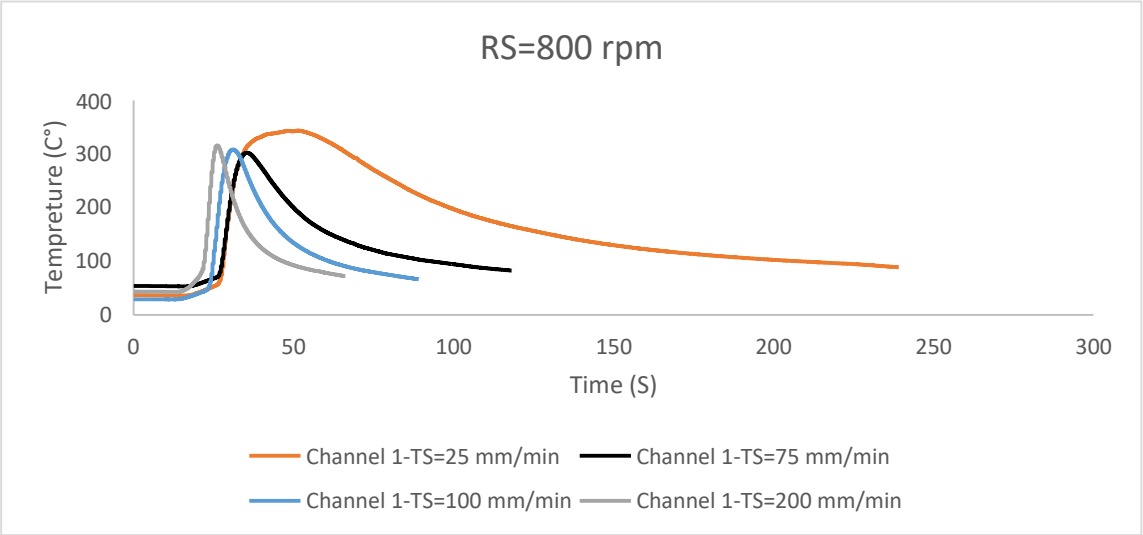

Figure 4.33: Effect of translational speed @ RS=800 rpm

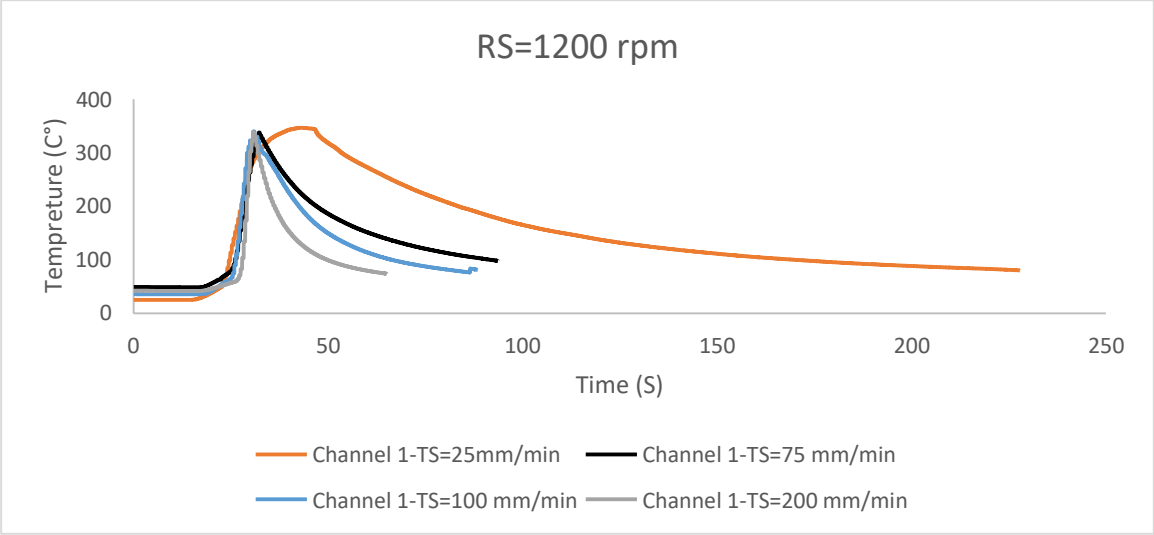

Figure 4.34: Effect of translational speed @ RS=1200 rpm

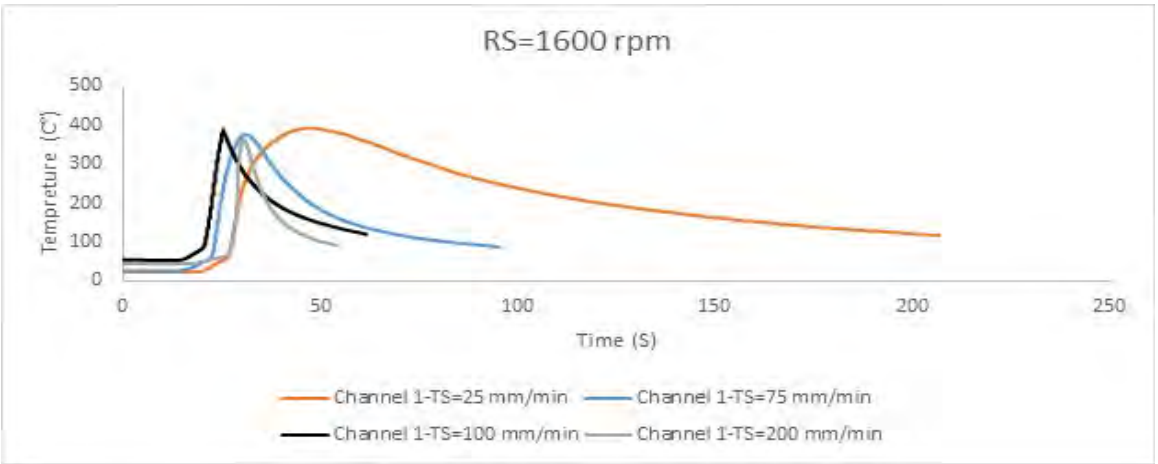

Figure 4.35: Effect of translational speed @ RS=1600 rpm

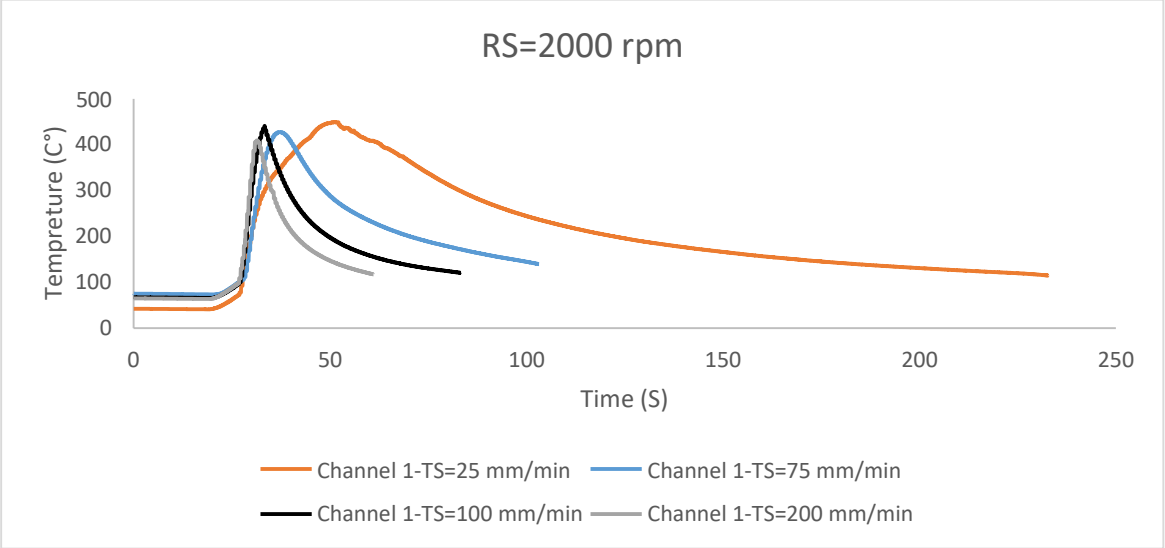

Figure 4.36: Effect of translational speed @ RS=2000 rpm

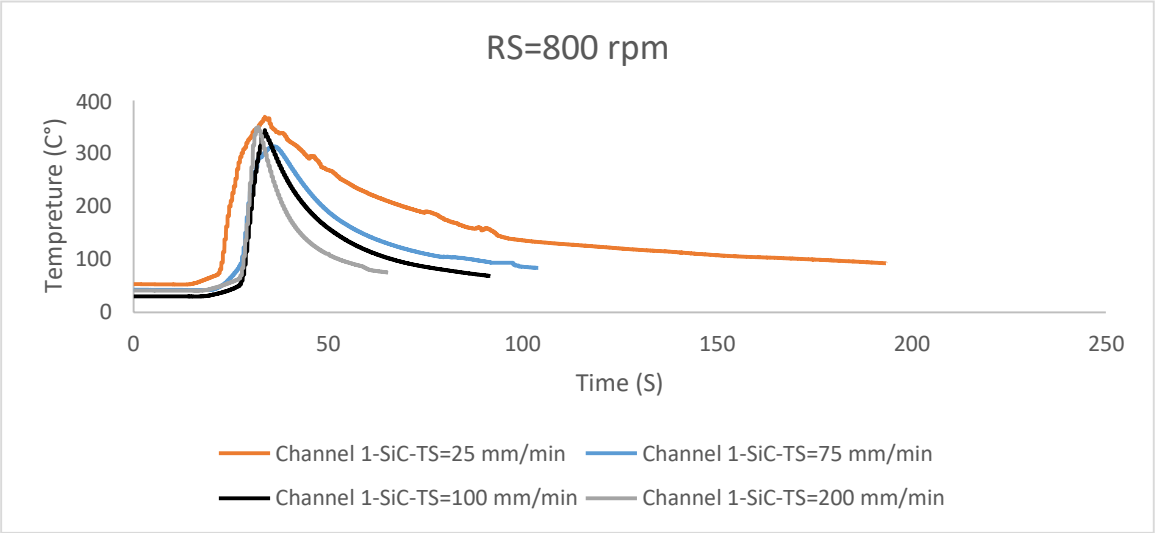

Figure 4.37: Effect of translational speed @ RS=800 rpm with SiC

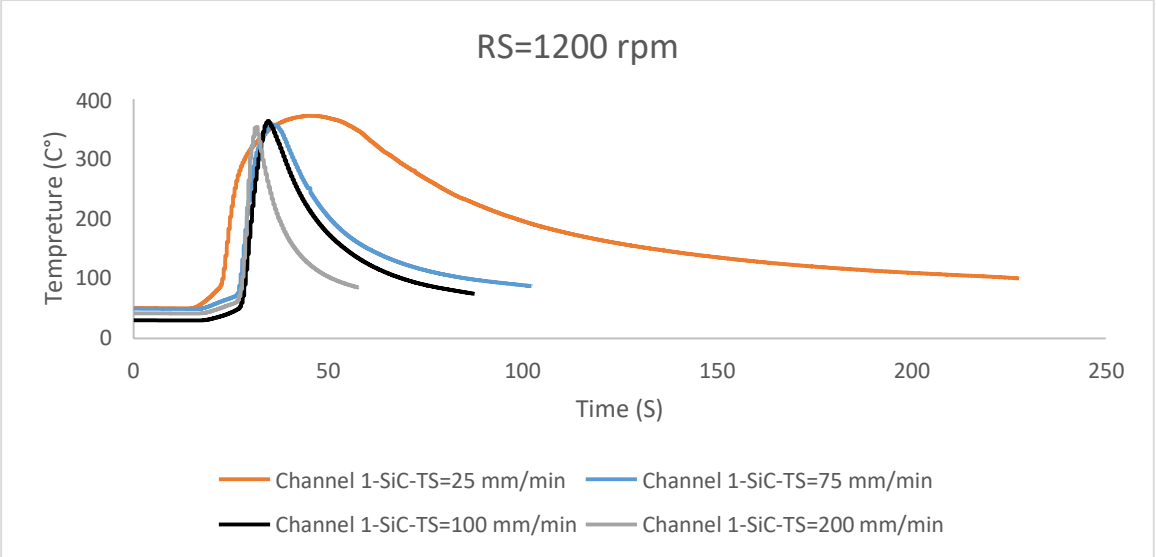

Figure 4.38: Effect of translational speed @ RS=1200 rpm with SiC

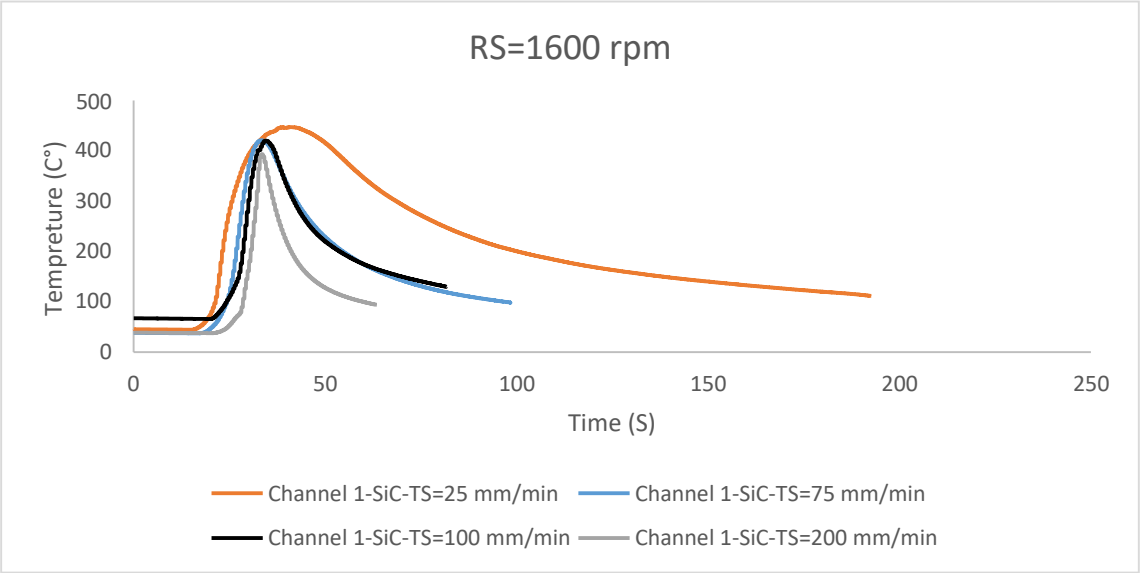

Figure 4.39: Effect of translational speed @ RS=1600 rpm with SiC

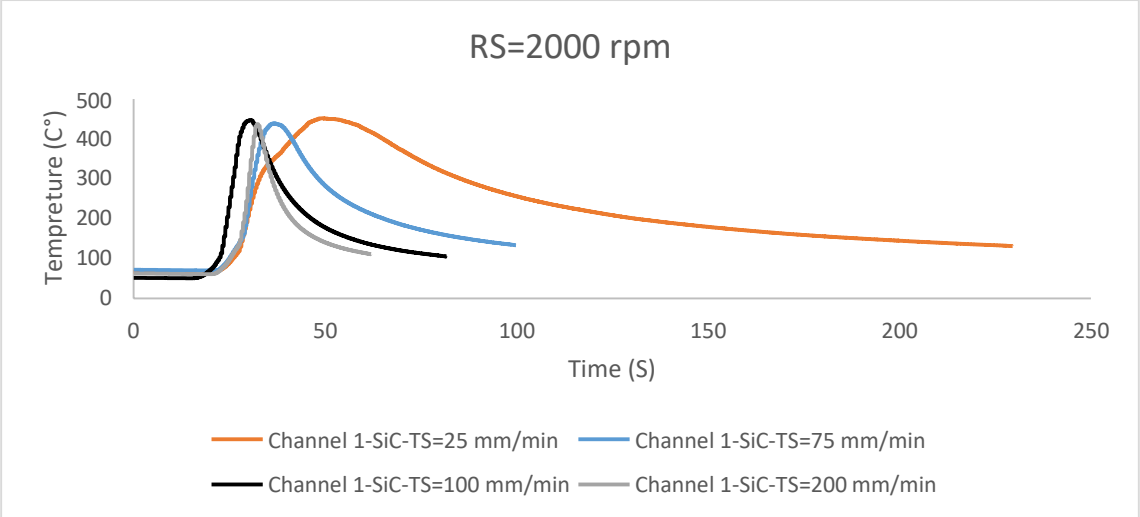

Figure 4.40: Effect of translational speed @ RS=2000 rpm with SiC

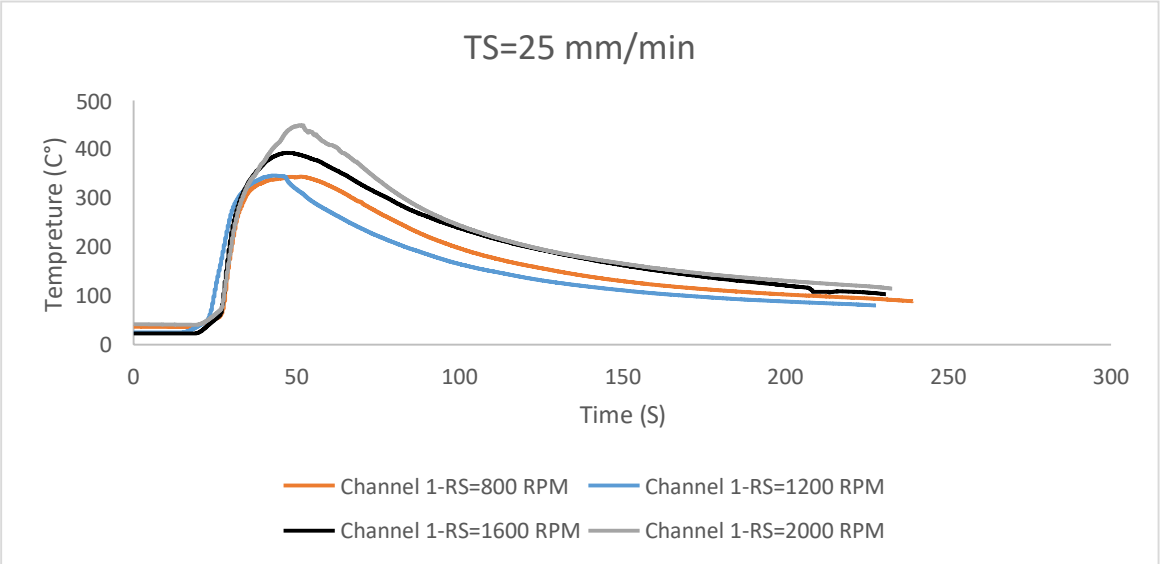

Figure 4.41: Effect of rotational speed @ TS=25 mm/min

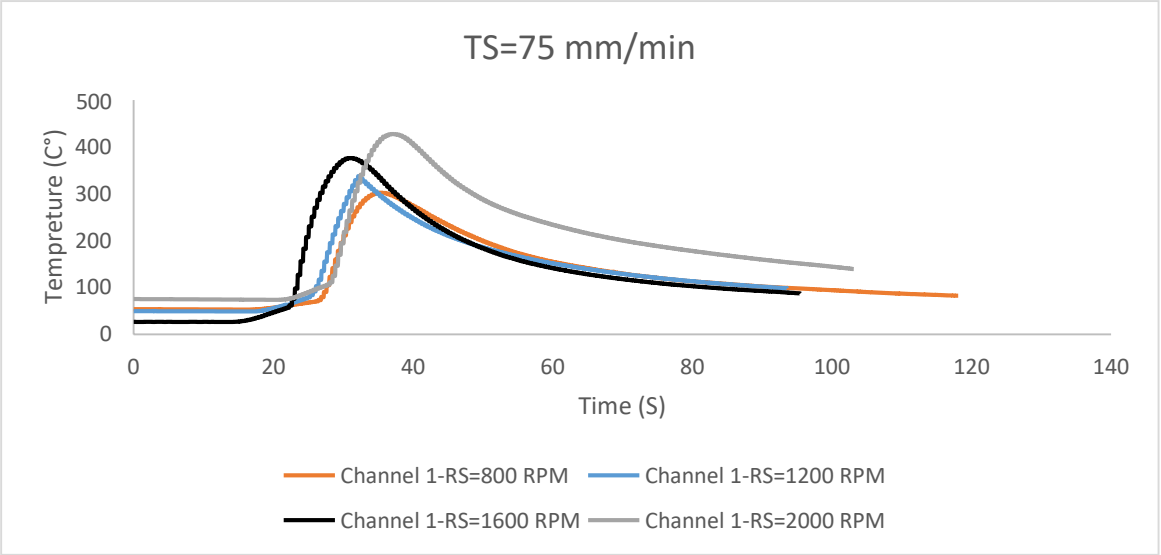

Figure 4.42: Effect of rotational speed @ TS=75 mm/min

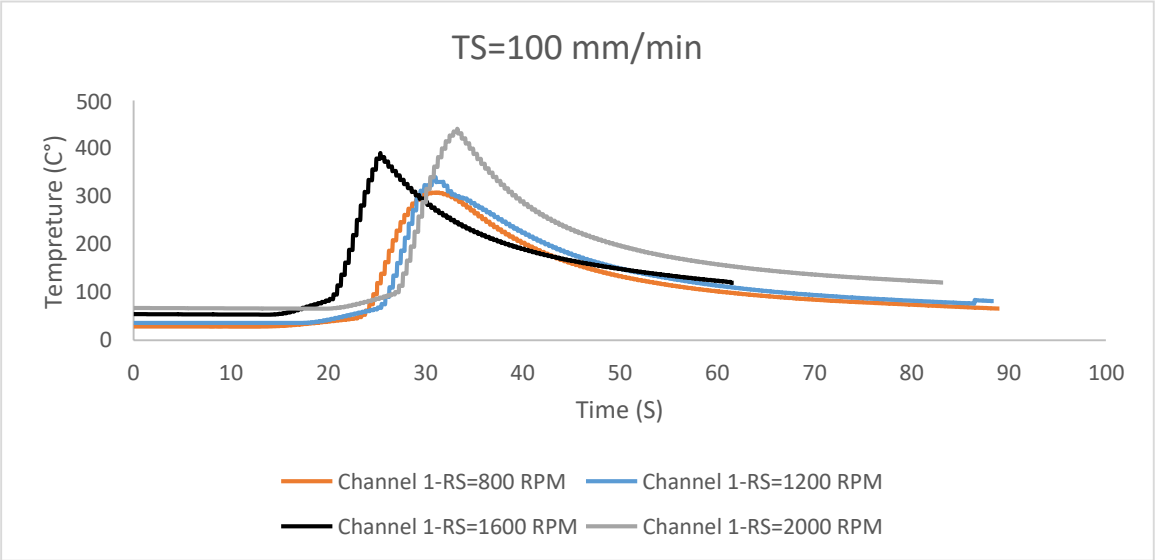

Figure 4.43: Effect of rotational speed @ TS=100 mm/min

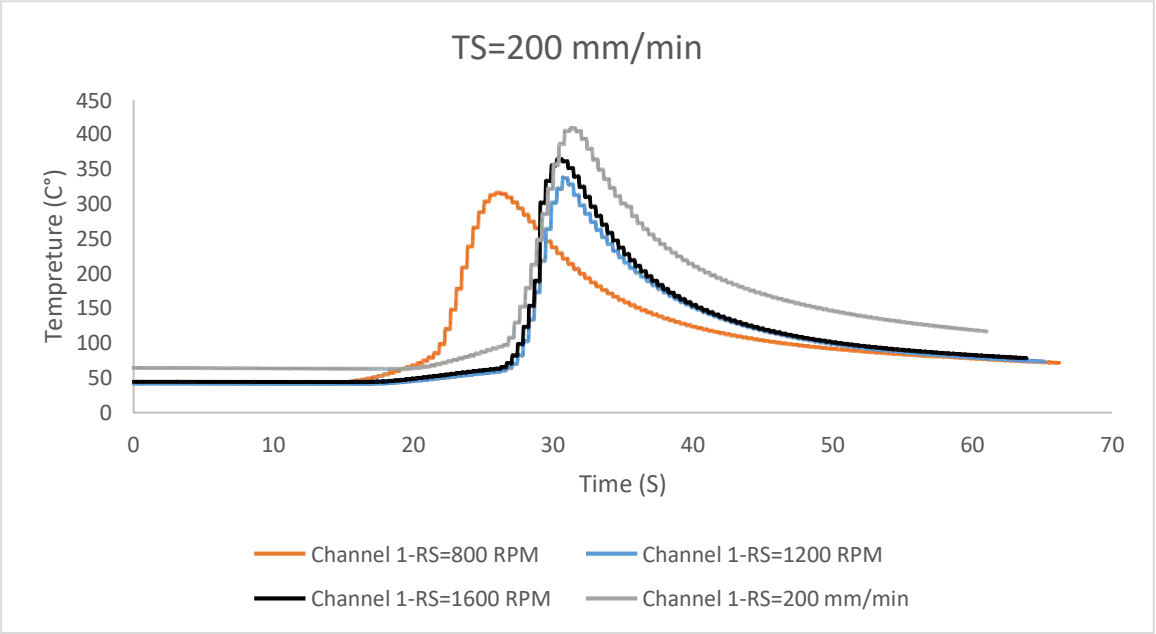

Figure 4.44: Effect of rotational speed @ TS=200 mm/min

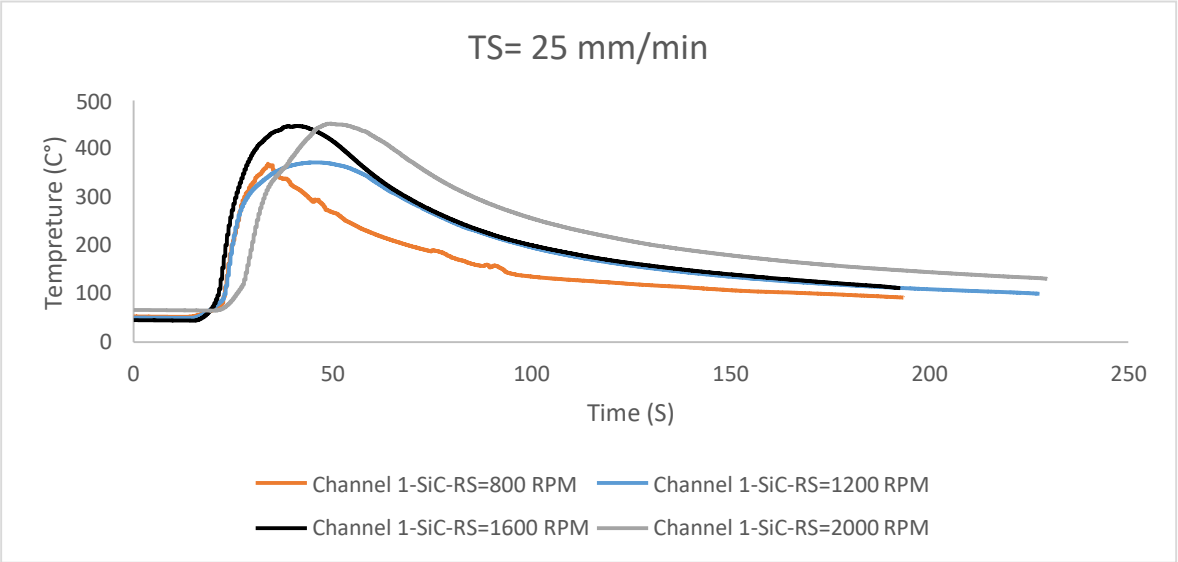

Figure 4.45: Effect of rotational speed @ TS=25 mm/min with SiC

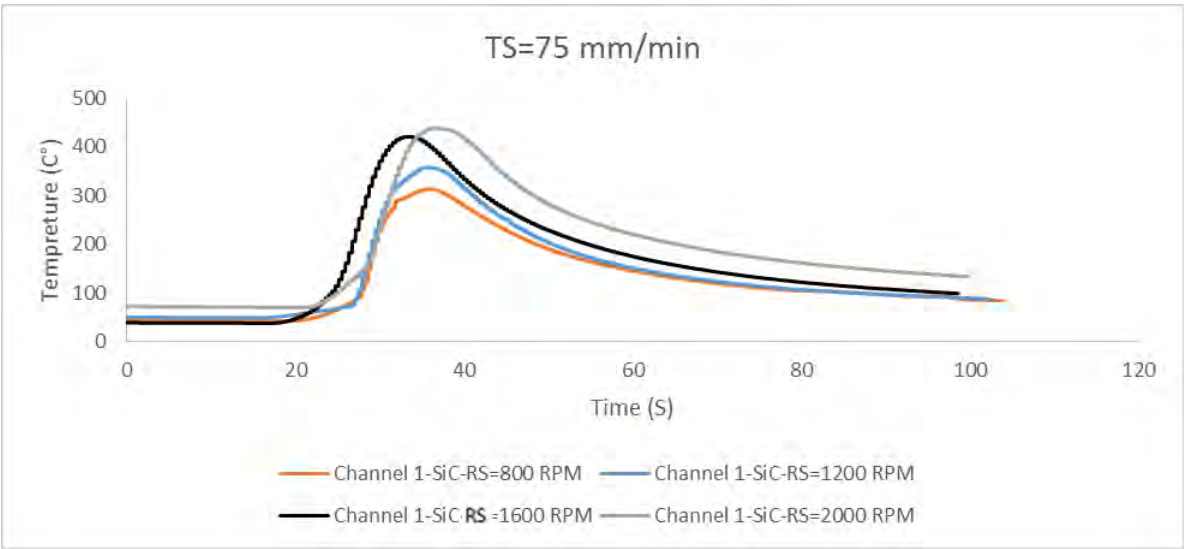

Figure 4.46: Effect of rotational speed @ TS=75 mm/min with SiC

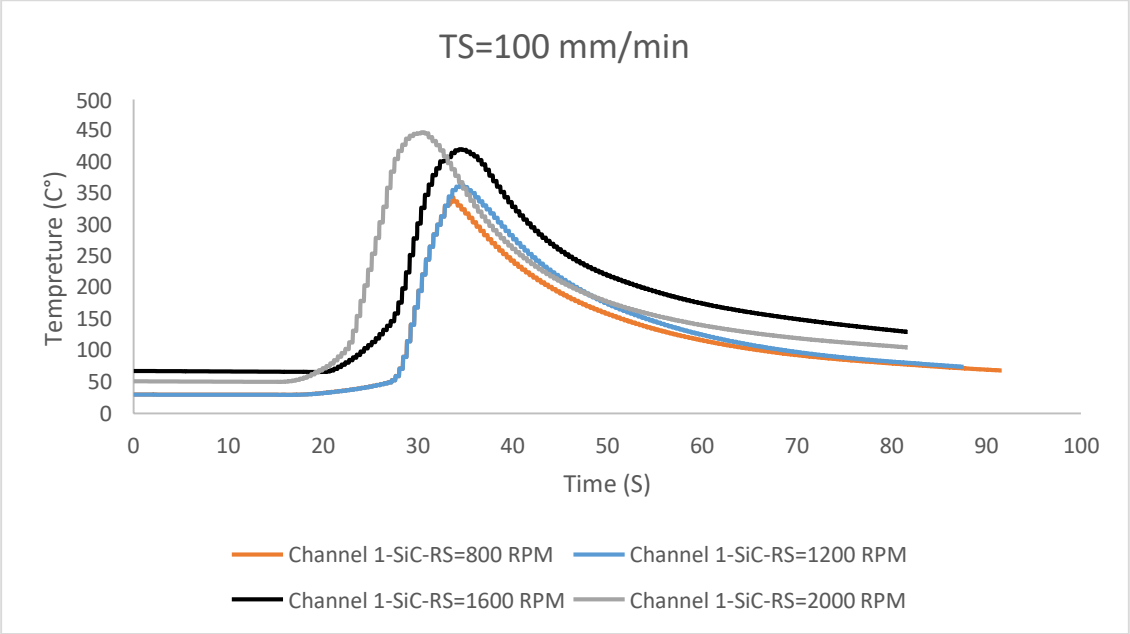

Figure 4.47: Effect of rotational speed @ TS=100 mm/min with SiC

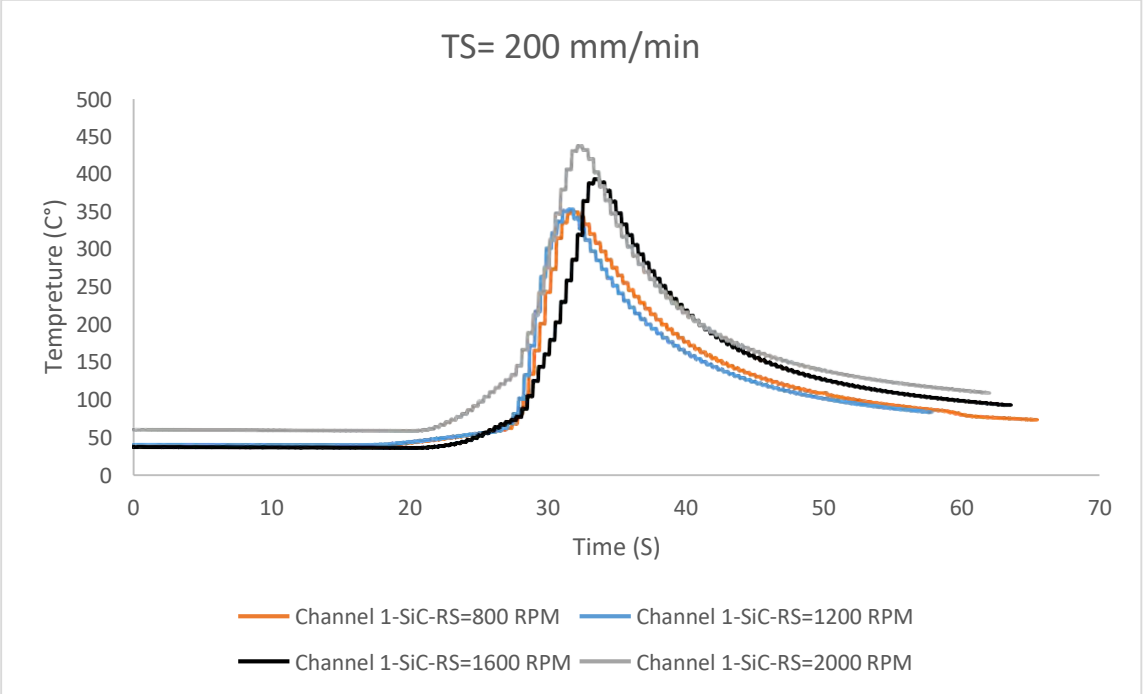

Figure 4.48: Effect of rotational speed @ TS=200 mm/min with SiC

Appendix C: Microstructural Results

Figure 1: Microstructure of FSP @ 800 rpm-75 mm/min

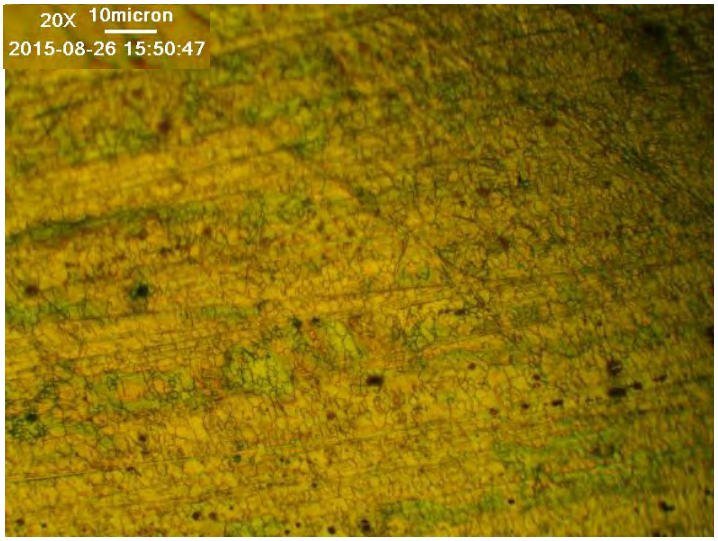

Figure 2: Microstructure of FSP @ 800 rpm-100 mm/min

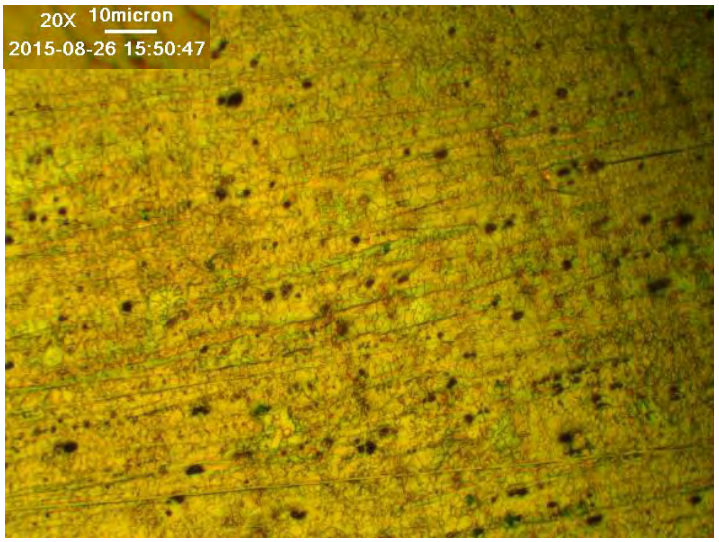

Figure 3: Microstructure of FSP @ 800 rpm-200 mm/min

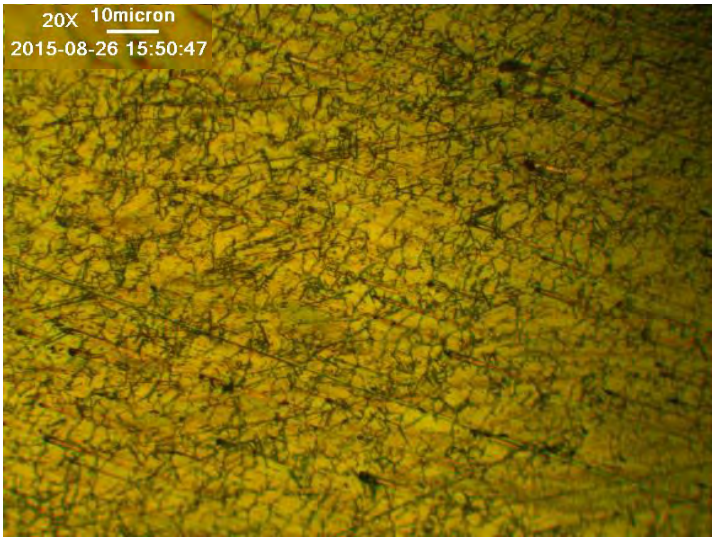

Figure 4: Microstructure of FSP @ 1200 rpm-75 mm/min

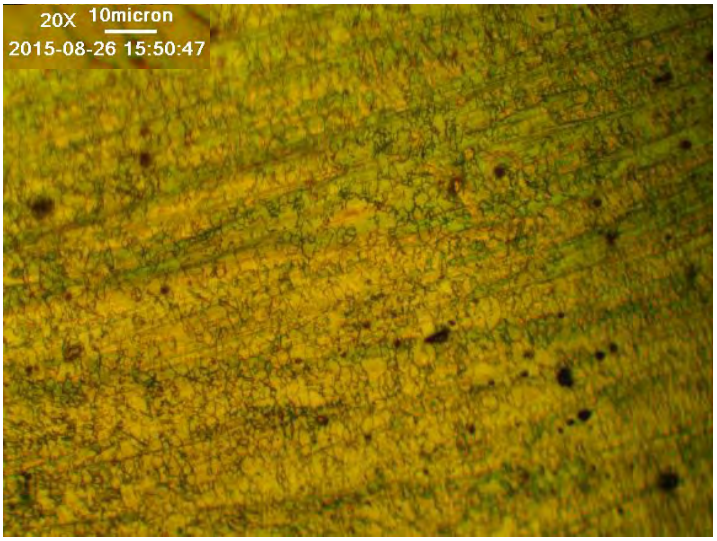

Figure 5: Microstructure of FSP @ 1200 rpm-200 mm/min

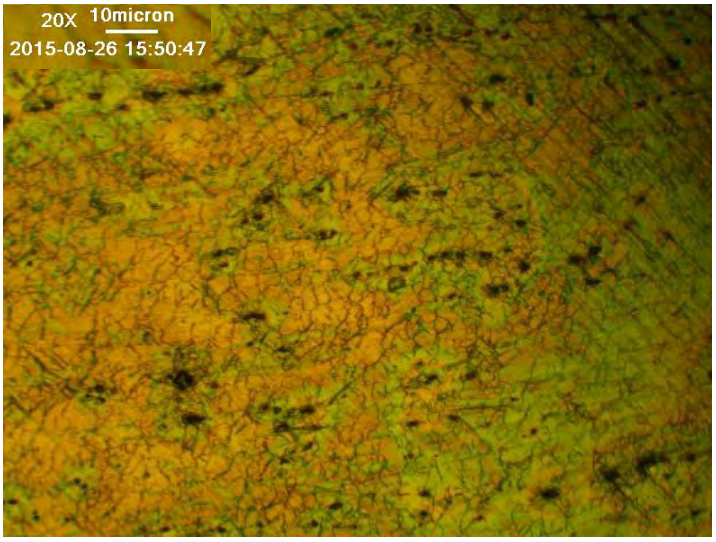

Figure 6: Microstructure of FSP @ 1600 rpm-25 mm/min

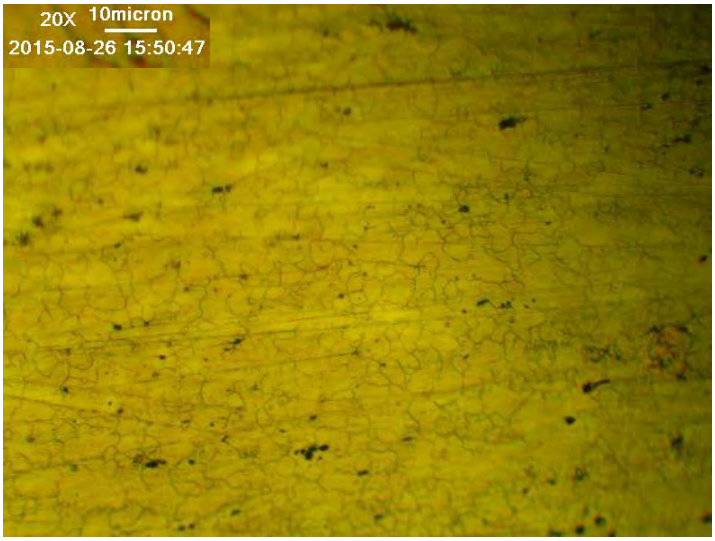

Figure 7: Microstructure of FSP @ 1600 rpm-75 mm/min

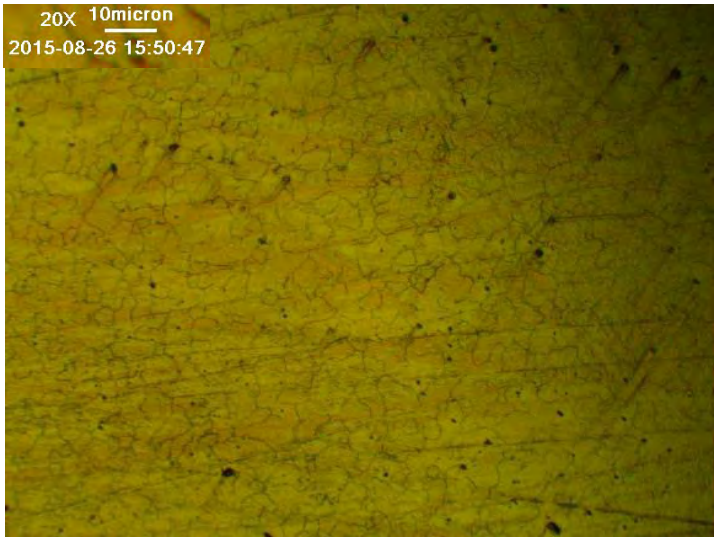

Figure 8: Microstructure of FSP @ 1600 rpm-200 mm/min

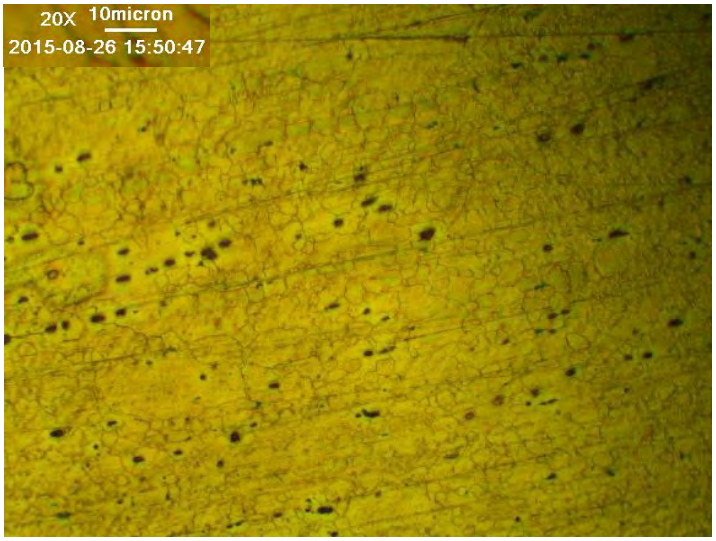

Figure 9: Microstructure of FSP @ 2000 rpm-25 mm/min

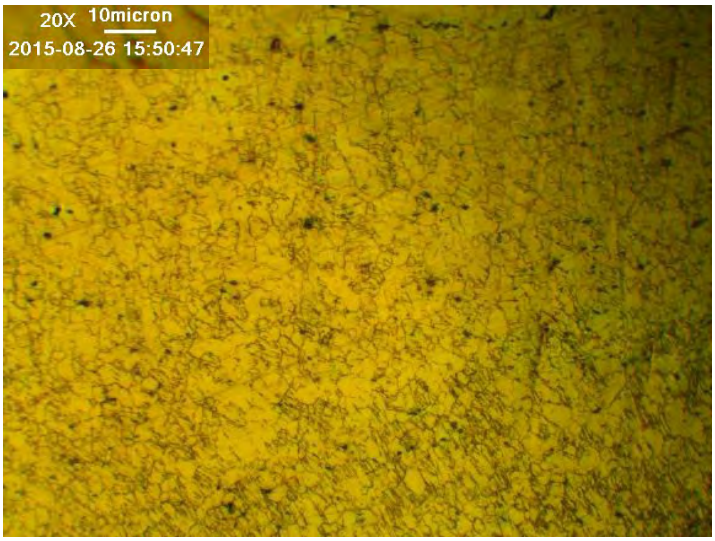

Figure 10: Microstructure of FSP @ 2000 rpm-75 mm/min

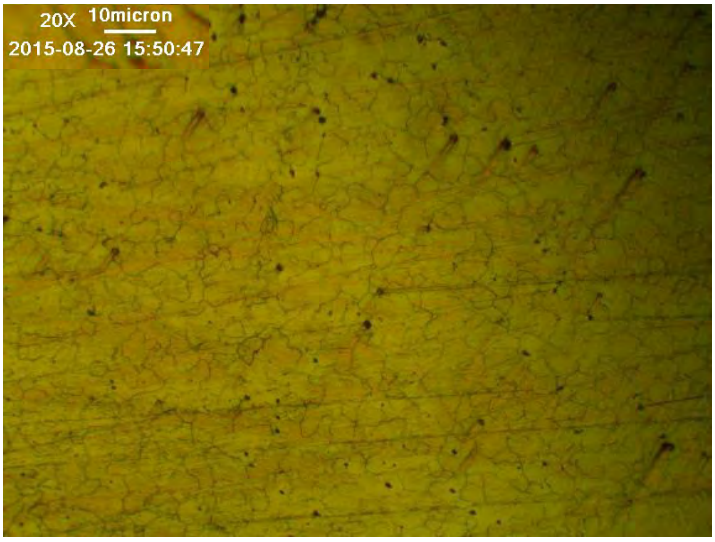

Figure 11: Microstructure of FSP @ 2000 rpm-100 mm/min

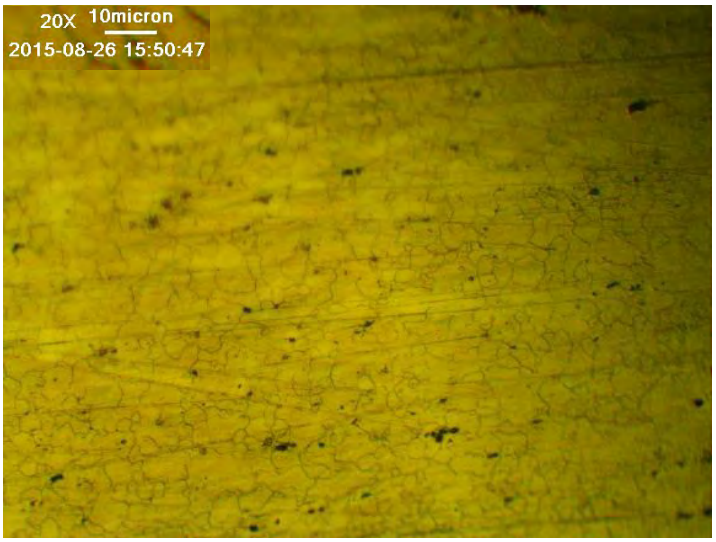

Figure 12: Microstructure of FSP @ 2000 rpm-200 mm/min

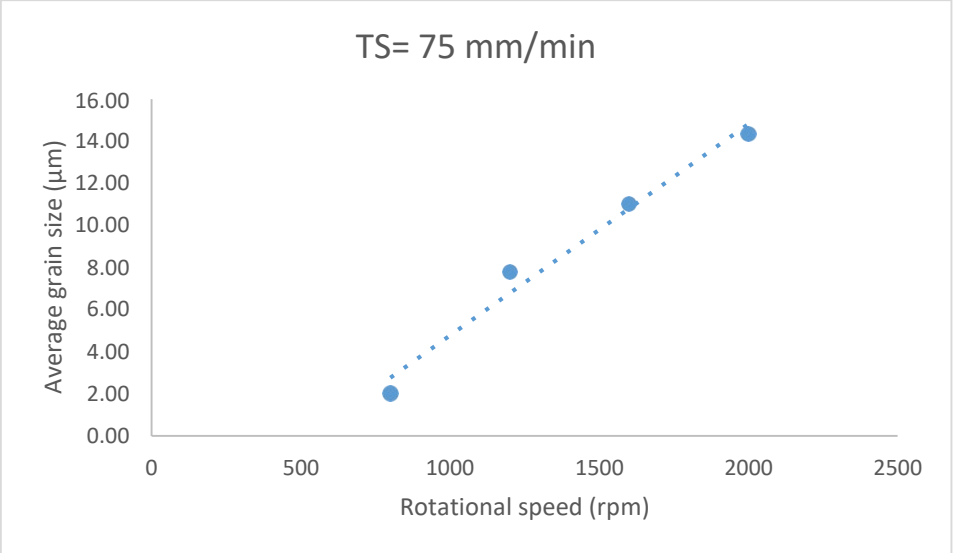

Figure 13: Avg. grain size @ TS=75 mm/min

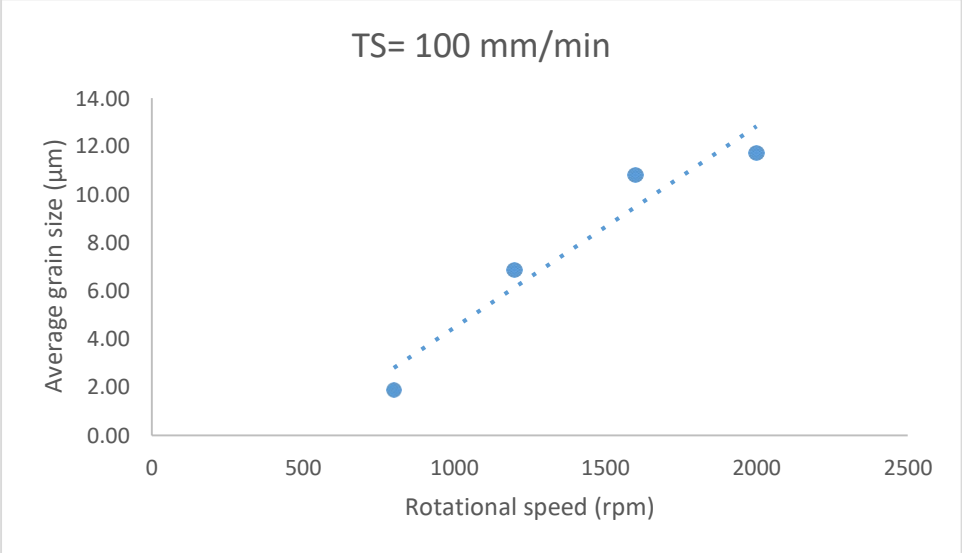

Figure 14: Avg. grain size @ TS=100 mm/min

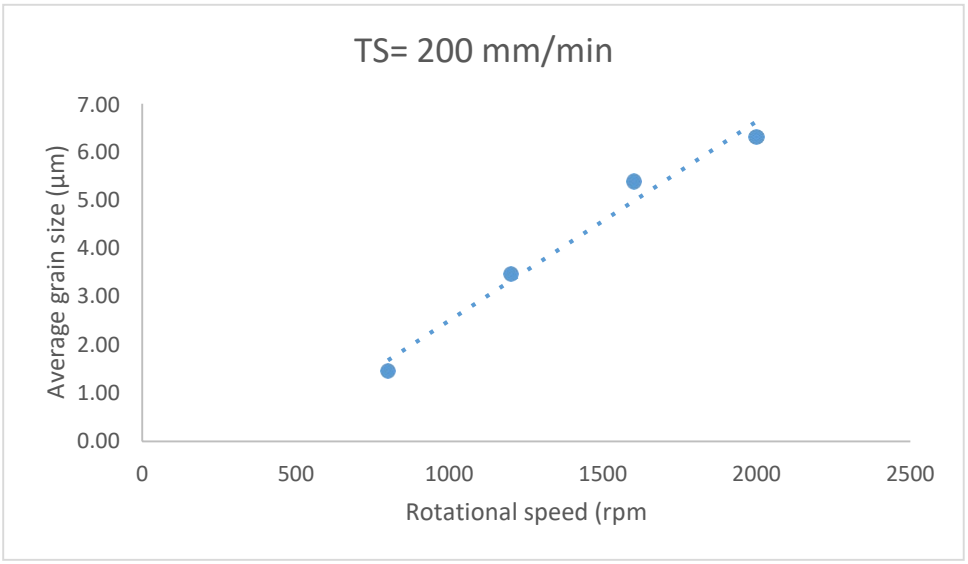

Figure 15: Avg. grain size @ TS=200 mm/min

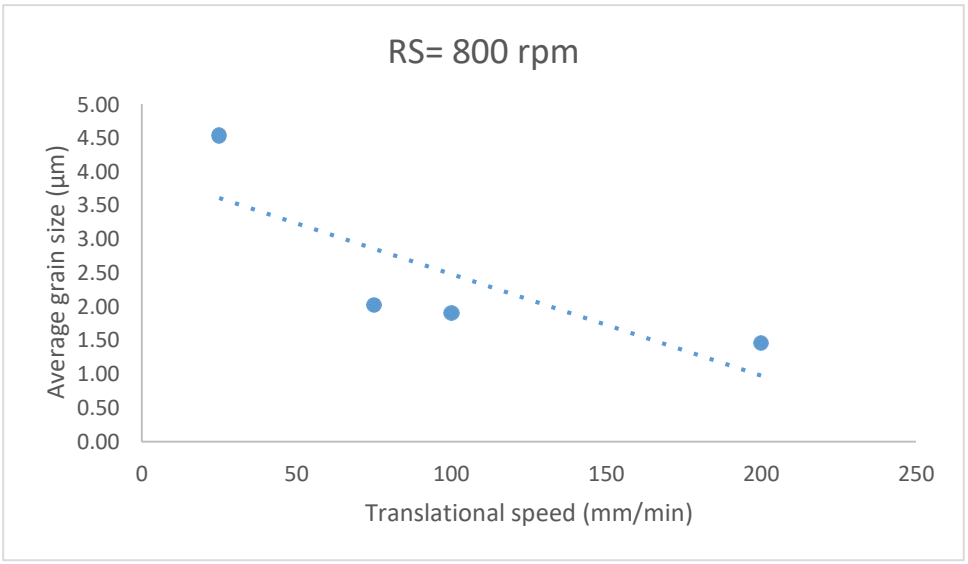

Figure 16: Avg. grain size @ RS=800 rpm

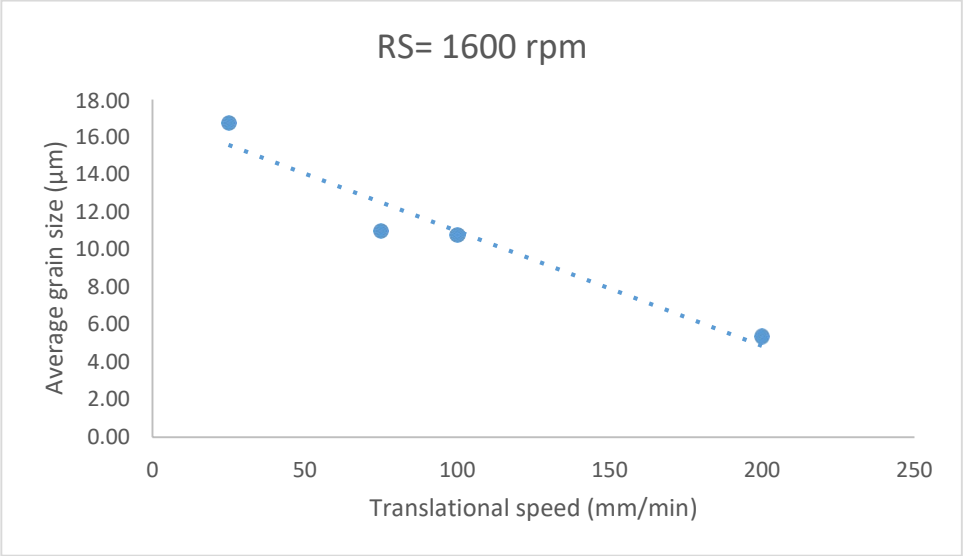

Figure 17: Avg. grain size @ RS=1600 rpm

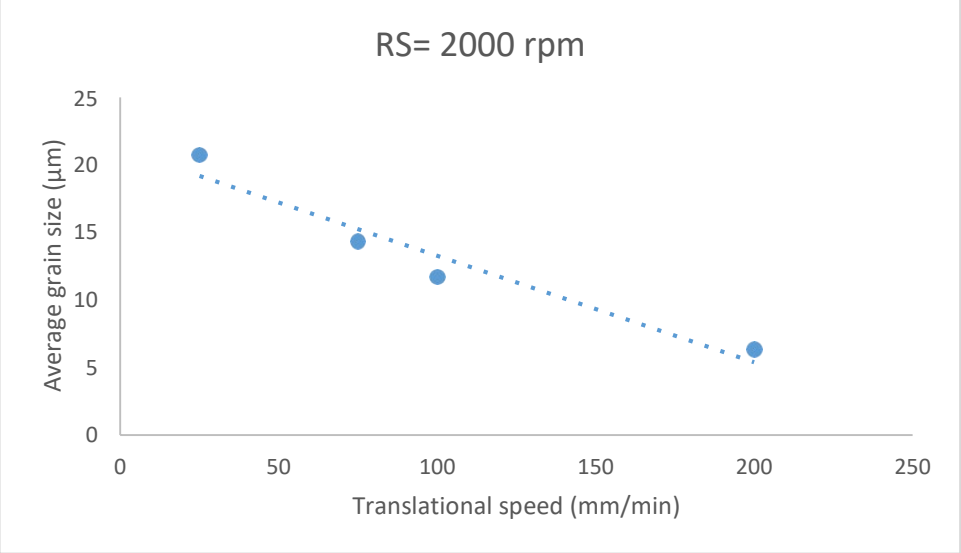

Figure 18: Avg. grain size @ RS=2000 rpm

Table 1: Average grain sizes for all FSP conditions

Tool rotational speed (rpm)	Translational speed (mm/min)	Average grain size (μm)
800	25	4.53
800	75	2.03
800	100	1.91
800	200	1.46
1200	25	7.88
1200	75	7.80
1200	100	6.87
1200	200	3.47
1600	25	16.78
1600	75	11.01
1600	100	10.81
1600	200	5.39
2000	25	20.73
2000	75	14.35
2000	100	11.73
2000	200	6.32

Appendix D: Micro-hardness Results

Table 1: Summarized micro-hardness results of FSP

Tool rotational speed (rpm)	Translational speed (mm/min)	Through-thickness distance (mm)	Average micro-hardness (HV)
800	25	1.25	68.1
800	25	2.5	70.9
800	25	3.75	73.2
800	75	1.25	73.3
800	75	2.5	74.9
800	75	3.75	76.3
800	100	1.25	75.5
800	100	2.5	77.3
800	100	3.75	78.4
800	200	1.25	76.6
800	200	2.5	78.5
800	200	3.75	79.6
1200	25	1.25	67.4
1200	25	2.5	69.3
1200	25	3.75	71.4
1200	75	1.25	67.6
1200	75	2.5	69.4
1200	75	3.75	72.2
1200	100	1.25	69.6
1200	100	2.5	71.7
1200	100	3.75	73.2
1200	200	1.25	70.8
1200	200	2.5	72.9
1200	200	3.75	75.4
1600	25	1.25	66.3
1600	25	2.5	68.7
1600	25	3.75	70.8

1600	75	1.25	66.3
1600	75	2.5	69.0
1600	75	3.75	70.8
1600	100	1.25	68.6
1600	100	2.5	69.7
1600	100	3.75	72.3
1600	200	1.25	69.1
1600	200	2.5	71.7
1600	200	3.75	72.7
2000	25	1.25	65.2
2000	25	2.5	67.3
2000	25	3.75	70.1
2000	75	1.25	65.2
2000	75	2.5	67.3
2000	75	3.75	70.1
2000	100	1.25	67.4
2000	100	2.5	68.8
2000	100	3.75	70.8
2000	200	1.25	68.2
2000	200	2.5	69.9
2000	200	3.75	71.3

Table2: Summarized micro-hardness results of FSP with SiC

Tool rotational speed (rpm)	Translational speed (mm/min)	Through-thickness distance (mm)	Average micro-hardness (HV)
800	25	0.5	94.6
800	25	0.8	74.5
800	25	2.5	70.8
800	25	3.75	73.2
800	75	0.5	89.9
800	75	0.8	78.2
800	75	2.5	74.5
800	75	3.75	76.1
800	100	0.5	93.7
800	100	0.8	79.7
800	100	2.5	77.0
800	100	3.75	77.6
800	200	0.5	91.3
800	200	0.8	81.4
800	200	2.5	78.0
800	200	3.75	79.1
1200	25	0.5	92.6
1200	25	0.8	73.7
1200	25	2.5	69.5
1200	25	3.75	71.5
1200	75	0.5	85.9
1200	75	0.8	74.5
1200	75	2.5	69.2
1200	75	3.75	72.0
1200	100	0.5	100.9
1200	100	0.8	85.1
1200	100	2.5	71.7
1200	100	3.75	73.3

1200	200	0.5	103.1
1200	200	0.8	87.3
1200	200	2.5	72.1
1200	200	3.75	75.0
1600	25	0.5	83.8
1600	25	0.8	71.6
1600	25	2.5	68.2
1600	25	3.75	70.3
1600	75	0.5	83.9
1600	75	0.8	73.4
1600	75	2.5	68.7
1600	75	3.75	70.3
1600	100	0.5	86.1
1600	100	0.8	75.4
1600	100	2.5	69.8
1600	100	3.75	72.0
1600	200	0.5	86.9
1600	200	0.8	76.3
1600	200	2.5	71.4
1600	200	3.75	72.4
2000	25	0.5	81.4
2000	25	0.8	71.3
2000	25	2.5	67.0
2000	25	3.75	70.2
2000	75	0.5	81.1
2000	75	0.8	72.4
2000	75	2.5	67.5
2000	75	3.75	70.0
2000	100	0.5	81.0
2000	100	0.8	73.5
2000	100	2.5	68.5
2000	100	3.75	70.4

2000	200	0.5	82.1
2000	200	0.8	73.7
2000	200	2.5	69.4
2000	200	3.75	71.3

Table 3: Micro-hardness values comparison between FSP with SiC and both FSP without SiC and as-processed

Tool rotational speed (rpm)	Translational speed (mm/min)	Through-thickness position (mm)	Maximum micro-hardness of FSP with SiC (without SiC)	% Increase With respect to FSP (With respect to as-received)
800	25	0.5	94.6	29.2
800	25	3.75	(73.2)	(39.7)
800	75	0.5	89.9	17.8
800	75	3.75	(76.3)	(32.8)
800	100	0.5	93.7	19.5
800	100	3.75	(78.4)	(38.4)
800	200	0.5	91.3	14.7
800	200	3.75	(79.6)	(34.9)
1200	25	0.5	92.6	29.5
1200	25	3.75	(71.5)	(36.8)
1200	75	0.5	85.9	18.9
1200	75	3.75	(72.2)	(26.9)
1200	100	0.5	100.9	37.7
1200	100	3.75	(73.3)	(49.0)
1200	200	0.5	103.1	36.9
1200	200	3.75	(75.3)	(52.3)
1600	25	0.5	83.8	18.4
1600	25	3.75	(70.8)	(23.8)
1600	75	0.5	83.9	18.5
1600	75	3.75	(70.8)	(23.9)
1600	100	0.5	86.1	19.6
1600	100	3.75	(72)	(27.2)
1600	200	0.5	86.9	20.0
1600	200	3.75	(72.4)	(28.4)
2000	25	0.5	81.4	15.9

2000	25	3.75	(70.2)	(20.2)
2000	75	0.5	81.1	15.7
2000	75	3.75	(70.1)	(19.8)
2000	100	0.5	81.0	14.4
2000	100	3.75	(70.8)	(19.6)
2000	200	0.5	82.1	15.1
2000	200	3.75	(71.3)	(21.3)

Vita

Ahmad Zeyad Naser was born on September 21, 1990, in Abu Dhabi, in the United Arab Emirates. He was educated in local public schools and graduated from high school as class valedictorian in 2008. He graduated from the American University of Sharjah in 2013 with a Bachelor degree in Mechanical Engineering and a minor in Aerospace Engineering. In 2013, Ahmad began a Master's program in Mechanical Engineering at the American University of Sharjah. He received a full scholarship and worked as a graduate research and teaching assistant.

Publication

- Basil M. Darras, Ibrahim M. Deiab, Ahmed Naser. (2014) Prediction of Friction Stir Processed AZ31 Magnesium Alloy Micro-hardness Using Artificial Neural Networks. Advanced Materials Research. 1043, 91–95.